INVESTIGATION INTO THE DOSIMETRIC CHARACTERISTICS OF MOSFETs FOR USE FOR *IN VIVO* DOSIMETRY DURING EXTERNAL BEAM RADIOTHERAPY

by

Raelene Ann Nelligan, B.Sc

Associate Member ACPSEM

Member APESMA

School of Chemistry and Physics

The University of Adelaide

South Australia

Thesis submitted for the degree of
Master of Science (Medical Physics)

May 2009

This thesis is dedicated to my parents,
both of whom passed away during this work.

CONTENTS

Page

INDEX

Appendices

References

ABBREVIATIONS AND SYMBOLS

Symbol	Physical Constant / description	Value / unit
C_e	Concentration of electrons in conduction band	cm^{-2}
CF	Calibration factor	
C_h	Concentration of holes in valence band	cm^{-2}
CMRP	Centre for Medical Radiation Physics, University of Wollongong, New South Wales, Australia	
C_{ox}	Oxide capacitance per unit area	F/cm^2
D	Absorbed dose	$J\ kg^{-1}$
D_{max}	Depth of maximum dose	
D_{ref}	Reference absorbed dose	Gy
E	Energy level	J
$\bar{E}_{ab}$	Average energy absorbed per interaction	eV
E_c	Minimum energy of conduction band	eV
E_F	Fermi energy	eV
E_{gap}	Energy difference between conduction and valence bands in a semiconductor	eV
E_{tr}	Energy transferred by ionising radiation	eV
eV	Electron-Volt	
E_v	Maximum energy of valence band	eV
f	Frequency of radiation	s^{-1}
f(E)	Charge yield	coulomb
F(E)	Fermi-Dirac distribution function	
$F(E)_e$	Fermi-Dirac distribution function for electrons	
$F(E)_h$	Fermi-Dirac distribution function for holes	
F_{corr}	Correction factor	
g	Hole generation rate	$7.9 \times 10^{12}\ cm^3/cGy$
$G_{\square}$	Number of electron-hole pairs per second	s^{-1}
Gy	Absorbed dose	$1\ Gy = 1\ J\ kg^{-1}$
h	Planck's constant	6.62617×10^{-34} J.s
I	Current	ampere
IC	Ion chamber	
IVD	*In vivo* dosimetry	
k	Boltzmann's constant	8.617×10^{-5} eV/K
m_e*	Density-of-states effective mass of electron	$1.08m_o^{-1}$
m_h*	Density-of-states effective mass of hole	$0.811m_o^{-1}$
min	Minute	
m_o	Free electron mass	9.1095×10^{-31} kg
MOS	Metal-oxide-semiconductor	
MOSFET	Metal Oxide Semiconductor Field Effect Transistor	
n	Density of electrons or holes	cm^{-3}
N	Number of electron-hole pairs	
N(E)	Density of quantum states per unit volume per unit energy	$cm^{-3}\ J^{-1}$
$N(E)_e$	Density of electron quantum states per unit volume per unit energy	$cm^{-3}\ J^{-1}$
$N(E)_h$	Density of hole quantum states per unit volume per unit energy	$cm^{-3}\ J^{-1}$
n_d	Density of donors	cm^{-3}
$n_e(t)$	Density of electrons at time *t* after irradiation	cm^{-3}
$n_h(t)$	Density of holes at time *t* after irradiation	cm^{-3}
N_{ss}	Density of interface states	cm^{-3}
$\Delta N_{ss}(t)$	Density of interface states with time after irradiation	cm^{-3}

N_T	Area density of available traps in trapping sheet	cm^{-2}
q	Electronic charge	1.60218×10^{-19} C
Q_i	Interface charge density per unit area	Cm^{-2}
s	Second	
SD	Standard deviation	
Si	Silicon	
SiO_2	Silicon dioxide	
SSD	Source-to-surface distance	cm
T	Temperature	kelvin
t	Time	s
$T\&N$	Thomson Nielsen Electronics Ltd, Canada	
t_h	Time of travel for holes across SiO_2	s
t_o	Time of termination of irradiation	s
t_{ox}	Oxide thickness	cm
t_{sat}	Time of MOSFET saturation	s
v	Velocity	$cm\ s^{-1}$
V	Voltage	
V_{FB}	Flatband voltage	V
V_g	Gate voltage	V
V_{ss}	Voltage between source and substrate	V
V_{th}	Threshold voltage	V
$\Delta V_{th\ FB}$	Flatband threshold voltage shift	V or mV
ΔV_{th}	Threshold shift	V or mV
$\Delta V_{th\ i}$	Threshold shift for the first exposure of a new MOSFET	V or mV
$\Delta V_{th\ ox}$	Threshold shift due to oxide trapped charge	V or mV
$\Delta V_{th\ ref}$	Reference Threshold shift	V or mV
$\Delta V_{th\ sat}$	Threshold shift at saturation	V or mV
W	Energy to produce one electron-hole pair	> 17±1 eV in SiO_2
Wollongong MOSFETs	MOSFETs provided by University of Wollongong, New South Wales, Australia	
x	Distance travelled by holes or electrons in SiO_2	cm
x_h	Distance travelled by holes in SiO_2	cm
$\angle$	Angle	degree

Greek symbols

ε	Electric field strength of oxide	$V\ cm^{-1}$
ε_o	Permittivity in free space	8.854×10^{-14} F/cm
ε_s	Permittivity in silicon	11.9 F/cm
ε_{ox}	Permittivity in silicon dioxide	3.9 F/cm
□	Activation energy for annealing process	eV
μ	Coefficient of mobility	cm^2 / V.s
μ_{en}/ρ	Mass energy absorption coefficient	cm^2/g
ρ	Density of material	cm^{-3}
ρ_{ox}	Density of oxide charge	Cm^{-3}
τ	Timescale of charge build-up, or time constant	s
τ_e	Lifetime of electrons	s
τ_h	Lifetime of holes	s
□$_F$	Bulk potential of silicon	V
□$_M$	Work function of metal	V
□$_S$	Work function of semiconductor	V
□	Electron affinity for semiconductor	4.05 V

LIST OF FIGURES AND TABLES

THESIS ABSTRACT

This thesis investigates the response to ionising radiation, of p-type Metal Oxide Semiconductor Field Effect Transistors (MOSFETs) (REM Oxford (UK)) and a reader system developed by the Centre for Medical Radiation Physics, The University of Wollongong, to determine their feasibility for measurements of dose during radiotherapy treatment (in vivo dosimetry (IVD)). Two types of MOSFET probes were used – "single sensitivity", for measuring low doses, and "dual sensitivity", to measure both high and lose doses. Sensitivity, linearity of response with dose, and response changes with accumulated dose and direction of incident radiation (angular dependence) were investigated.

The average sensitivity reduction over the lifetime of the probes was 22.37% with a standard deviation of 0.63%. This reduction in sensitivity can be corrected for by the use of "drift equations". MOSFETs have a limited "lifetime" due to saturation effects with increasing accumulated dose. Saturation occurred at an average of 40 Gray (Gy) accumulated dose, for the high sensitivity probes investigated.

The high sensitivity probes were linear within 1.6% for doses between 5 and 140 cGy, and 3.8% for the high sensitivity probes for doses between 50 and 500 cGy.

Drift (changes in readings with time since irradiation due to electronic processes) over the long-term (from hours to weeks following irradiation) has been previously well characterised in the literature. This work focuses on short-term drift, within the first few seconds or minutes following irradiation, being the most clinically relevant for in vivo measurements. Drift is investigated for various reading methods, such as reading frequency, and delays between irradiation and readings. It is shown that sensitivity, and consequently dose determination, is significantly influenced by the reading methodology.

During the first five minutes following an irradiation, drift increased inversely with delivered dose, and was greater for probes having accumulated dose of > 20 Gy (2.0 – 16.2% compared with 1.2 – 7.4% for < 20 Gy probes).

When two post-irradiation readings were taken following an irradiation, the difference between them generally increased as the time interval between the two readings increased, by up to 8.8%.

Delays in taking pre- and post-irradiation readings resulted in drift of up to 5.7% or 9.3% respectively, compared with readings without a delay.

These results emphasise the necessity for consistent methodologies between calibration and measurement in the clinical situation.

Greater sensitivity was measured with the epoxy bubble, rather than the substrate side, facing the beam. The greatest variation, for orientations other than the bubble side facing directly towards the beam, was 10%, or 5% uncertainty in dose. The variations with angle were found to be reproducible, so that appropriate correction factors could be applied to correct measurements at angles other than with the sensitive area of the probes facing directly towards the radiation beam.

AUTHOR'S STATEMENT

I hereby certify that this thesis contains no material which has been accepted for the award of any other degree or diploma in any university or other tertiary institution and, to the best of my knowledge and belief, contains no material previously published or written by another person, except where due reference has been made in the text.

I give consent to this copy of my thesis, when deposited in the University Library, being available for loan and photocopying.

Raelene Nelligan 9 October 2008

ACKNOWLEDGEMENTS

I firstly thank my supervisors, Dr Sergei Zavgorodni and Mr Madhava Bhat, for sharing their vast experience with me, and their support and helpful advice with this work. I will try to keep in mind Mr Bhat's "story of Ramaayan".

I especially thank my husband and family for their encouragement and pride in my endeavours, and my colleague and office-mate, Dr Lotte Fog, for her forbearance throughout the throes of the thesis write-up.

Thanks also go to Dr John Patterson, who assisted me during the early experimental stage, and whose understanding during the very trying times following the deaths of my parents encouraged me to continue my studies when I was inclined to discontinue them.

The assistance of Professor Anatoly Rosenfeld, Director for Centre for Medical Radiation Physics, University of Wollongong, was greatly appreciated, as was the support provided through the Peter MacCallum Cancer Centre's Robert Sephton Educational Fellowship.

1. INTRODUCTION

Accurate dosimetry is critical in delivering high quality radiotherapy treatments to patients. The aim of radiotherapy treatment is to deliver the prescribed radiation dose to the target volume of the patient, whilst minimising the dose to the surrounding healthy tissues and organs. The delivered dose should be within ± 5% of the dose prescribed, as recommended by the International Commission on Radiation Units and Measurements [ICRU 24]. Deviations from prescribed dose can occur due to random and systematic errors including patient set-up and radiation beam output. Measurement of absorbed dose during radiotherapy treatment can identify such errors, and is therefore an important quality assurance tool for verification of accurate dose delivery [1-3].

With appropriately calibrated instrumentation, small dosimeters placed on the patient's skin function as *in vivo* dosimeters, which can measure entrance and/or exit dose, from which the dose to the midline can be estimated. Entrance dose measurements verify patient set-up and beam delivery, whilst exit dose measurements provide information on any inhomogeneities and verify treatment planning [4].

Thermoluminescent detectors (TLDs) and semiconductor diodes have traditionally been used as *in vivo* dosimeters, however they have certain disadvantages. TLDs do not provide real-time monitoring of dose, but require post-irradiation processing, which destroys their dose history. Semiconductor diodes are electronic devices which can measure in real-time, but many correction factors must be applied to their readings due to their dependence on radiation energy, dose-rate and angle of incidence, as well as ambient temperature, size of the radiation field, distance between the detector and the source, and beam modifiers which alter the quality of the beam, such as wedges and shielding block trays. MOSFETs are gaining in popularity for many dose measurement applications in radiation therapy, since their response to irradiation is also proportional to dose (see Ch. 3). Their extremely small sensitive volume (typically 4×10^{-5} mm^3) enables measurement in very small radiation fields where larger volume dosimeters are unsuitable, and excellent spatial resolution (1 μm) can be achieved for microbeam dosimetry and in regions with high dose gradients [5, 6]. Like diodes, they can measure in real-

time and store dose information after readout, however they are dose-rate and energy-independent [7-9], except for very low energies (<~100 keV), and some MOSFETs are isotropic and temperature-independent. They can measure low radiation doses (< 10 cGy) [10], and their sensitivity can be adjusted by altering characteristics during the manufacturing process, such as the oxide thickness, as well as the irradiation bias. These attributes make MOSFETs promising candidates for use clinically as *in vivo* dosimeters, requiring fewer correction factors than semiconductor diodes.

However, a disadvantage of electronic detectors like diodes and MOSFETs is response drift (variation in response with time since irradiation) which impacts on their use as clinical radiation dosimeters. It depends on many factors, and can result in uncertainties in dose determinations, depending on readout methodology.

The intrinsic drift of MOSFETs over the long-term (hours-weeks following irradiation) has been previously well characterised [11-14], however, little work has been published on short-term drift (within the first few seconds or minutes following irradiation), which period is clinically appropriate for routine *in vivo* dosimetry (IVD). While the principal emphasis of this thesis is on drift effects, certain other characteristics of MOSFETs have also been investigated, such as linearity with dose and angular dependence, to investigate the feasibility of their use for clinical IVD for external beam radiotherapy at the Royal Adelaide Hospital.

Most published work on the characteristics of MOSFETs as radiation dosimeters relates to the MOSFETs and reader systems developed by Thomson Nielsen Electronics Ltd of Canada, referred to as “T&N” throughout this thesis. The current work reports on results using the MOSFETs and reader system developed by the Centre for Medical Radiation Physics (CMRP), University of Wollongong, New South Wales, Australia (“Wollongong MOSFETs”). It should be noted that the reader system used for this work (as described in section 4.1) has both automatic and manual readout facilities, and that the present work utilises only the manual method, and hence the results presented apply only to that mode of operation.

2. GENERAL DESCRIPTION AND OPERATION OF MOSFETs

2.1 Introduction

It is now approximately 40 years since the effect of radiation exposure on MOSFET performance was first observed. Early developments of metal-oxide-semiconductor (MOS) technology for space and military applications had shown that radiation caused a detrimental affect on properties of electronic circuits, due to a build-up of trapped charge in the silicon dioxide (SiO_2) of MOS devices [15]. Ionising radiation passing through a medium may deposit some or all of its energy in that medium by various processes as described in section 3.2. This deposition of energy may result in changes to the lattice structure or the release of electrons from atoms (ionisation). The extent of lattice change or ionisation is therefore proportional to energy absorbed by the medium, i.e. dose. The amount of energy, *dE*, deposited in a small mass, *dm*, at a point, *p*, in a medium is the absorbed dose, *D*:

$$D(p) = \frac{dE}{dm} \quad \text{.....(2.1)}$$

The International System of Units (SI) unit for absorbed dose is the Gray (Gy), where 1 Gy = 1 joule/kg. The absorbed dose to the medium may be measured indirectly using MOSFETs, by measuring one of their electrical characteristics, the "threshold voltage" (V_{th}), as described below.

2.2 General Semiconductor Structure and Operation

The MOSFETs used for this work incorporate silicon (Si) semiconductors. Silicon has an atomic number of 14. In the ground state, its 14 electrons are distributed in three shells:

Shell:	K	L	M
Configuration:	1s	2s, 2p	2s, 2p
No. of electrons in shell:	2	8	4

The 4 valence electrons in the M-shell join with 4 surrounding Si atoms through covalent bonds comprising 2 electrons with opposite spins (according to Pauli's exclusion principle) to form a diamond lattice structure.

The pure or "intrinsic" Si bulk structure can be considered in terms of quantum physics, whereby electrons behave as travelling waves. These waves can undergo constructive or destructive interference by interaction with the Si ion core, and create an energy difference between electrons which are "bound" and those which are "free" to carry charge. The "bound" electrons occupy the "valence band" and the "free" electrons occupy the "conduction band". The difference in energies in these two bands is the "bandgap" or "forbidden gap" or "energy barrier" (E_{gap}). For intrinsic Si at room temperature, the bandgap energy is 1.107 eV (*CRC Handbook of Chemistry and Physics, 55th ed., pE103*), and for an interface of Si with silicon dioxide, it is 8.8 eV. The energy bands are formed of large numbers of energy levels (quantum states). There are 5 x 10^{22} energy levels in each band per cm^3 [16]. According to Pauli's exclusion principle, each level can accommodate 2 electrons of opposite spin, therefore each band may have up to 1 x 10^{23} electrons.

Under normal circumstances, electrons in the valence band are unable to surmount the energy barrier, however, given certain conditions (for example, heating) they may gain energy sufficient to enable them to enter the conduction band and carry negative charge throughout the lattice structure. The vacancy, or "hole", left in the valence band can similarly carry positive charge. For intrinsic Si, the numbers of electrons equals the number of holes, and the semiconductor has a neutral charge. The effectiveness of a semiconductor to carry charge is a function of the number density of charge carriers. The density of charge carriers depends on the density of quantum states, and the probability of carriers occupying those states. At thermal equilibrium for intrinsic Si, the density of charge carriers depends on the distribution of available states, and the probability of occupancy of those states by electrons or holes.

The total electron or hole concentration per unit volume, *n*, in the conduction or valence band is a function of energy [17]:

$$n = \int_{E_{gap}}^{\infty} N(E).F(E)dE \quad \text{.....(2.2)}$$

where E = energy level (J)

$N(E)$ = density of quantum states per unit volume per unit energy ($cm^{-3}\ J^{-1}$)

$F(E)$ = Fermi-Dirac distribution function.

The Fermi-Dirac distribution functions, $F(E)_e$ and $F(E)_h$ give the probabilities of occupancy of energy level E by electrons and holes respectively. At room temperature and thermal equilibrium, the probability that an electron occupies level E is given by [17]:

$$F(E)_e = \frac{1}{1 + exp\left[\frac{E - E_F}{kT}\right]} \quad \text{.....(2.3)}$$

where E_F = is the Fermi energy, the level for which the probability of occupancy is ½

k = Boltzmann's constant (eV/K)

T = temperature (K)

and $1 - F(E)_e$ is the probability that level E is empty (i.e. probability of a hole, $F(E)_h$). The Fermi level is the energy level for which there are equal densities of filled shells above and below it.

The density of states $N(E)$ is also a function of energy, as well as of density-of-states effective mass m^* of the electron or hole. (The density-of-states effective mass differs from the free-space mass due to the influence of the periodic force field of the lattice atoms.) The density of quantum states equations for electrons ($N(E)_e$ and holes $N(E)_h$ are [17]:

$$N(E)_e = \left(\frac{8\pi\sqrt{2}}{h^3}\right)\left(m_e^*\right)^{\frac{3}{2}}\sqrt{(E - E_c)} \quad \text{.....(2.4)}$$

$$N(E)_h = \left(\frac{8\pi\sqrt{2}}{h^3}\right)\left(m_h^*\right)^{\frac{3}{2}}\sqrt{(E_v - E)} \quad \text{.....(2.5)}$$

where h = Planck's constant (J.s)

E_c = Minimum energy of conduction band (eV)

E_v = Maximum energy of valence band (eV)

m_e^* = 1.08(free electron mass, m_o)$^{-1}$

m_h^* = $0.811m_o^{-1}$.

Figure 2.1 shows the convolution of functions *N(E)* and *F(E)*, to give the carrier density at equilibrium and for T > 0 K.

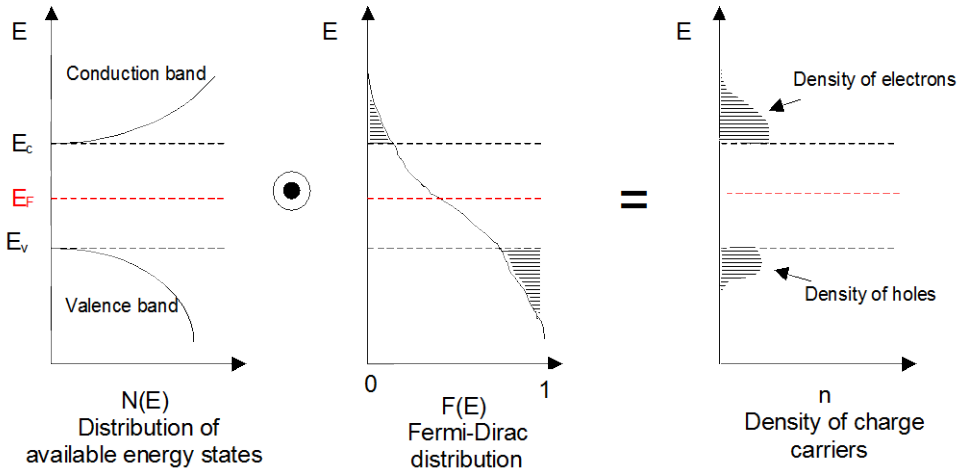

Figure 2.1 Density of charge carriers in the valence and conduction bands of a pure semiconductor

Semiconductors can be “doped” by replacement of a percentage of the Si atoms in the lattice by atoms of other materials. These materials may have either extra negative charge carriers (e.g. phosphorus with 5 valence electrons), or extra positive charge carriers, (e.g. boron with 3 valence electrons). Semiconductors doped with extra electrons are called “donors” or “n-type”, whilst those with extra holes are called “acceptors” or “p-type”.

Donors introduce extra energy levels close to the conduction band edge, and acceptors introduce energy levels close to the valence band edge. This reduces the bandgap energy between the valence and conduction bands in the semiconductor, and makes it easier for electrons to jump from the valence to the conduction band. The Fermi level is adjusted accordingly – up closer or into the conduction band for n-type, and down closer or into the valence band for p-type. Figure 2.2 is an example of how the electron density in the conduction band is increased in an n-type semiconductor. Similarly, the hole density increases in a p-type semiconductor.

When n-type and p-type semiconductors are placed in contact with each other, there will be a diffusion of majority electrons and holes between them (figure 2.3(a)), leaving a narrow layer of ionised minority carriers.

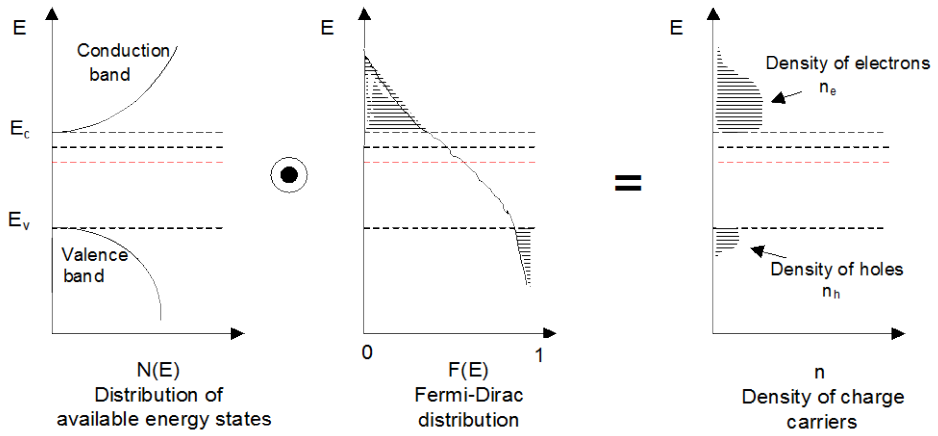

Figure 2.2 Density of charge carriers in an n-doped semiconductor

This produces an electric field across the junction (figure 2.3(b)). The narrow layer is called the "depletion region", as it is depleted of majority carriers, since the electric field prevents their further diffusion. The Fermi levels of the two types of material will adjust until there is one continuous Fermi level between them, as shown. This forms a p-n junction.

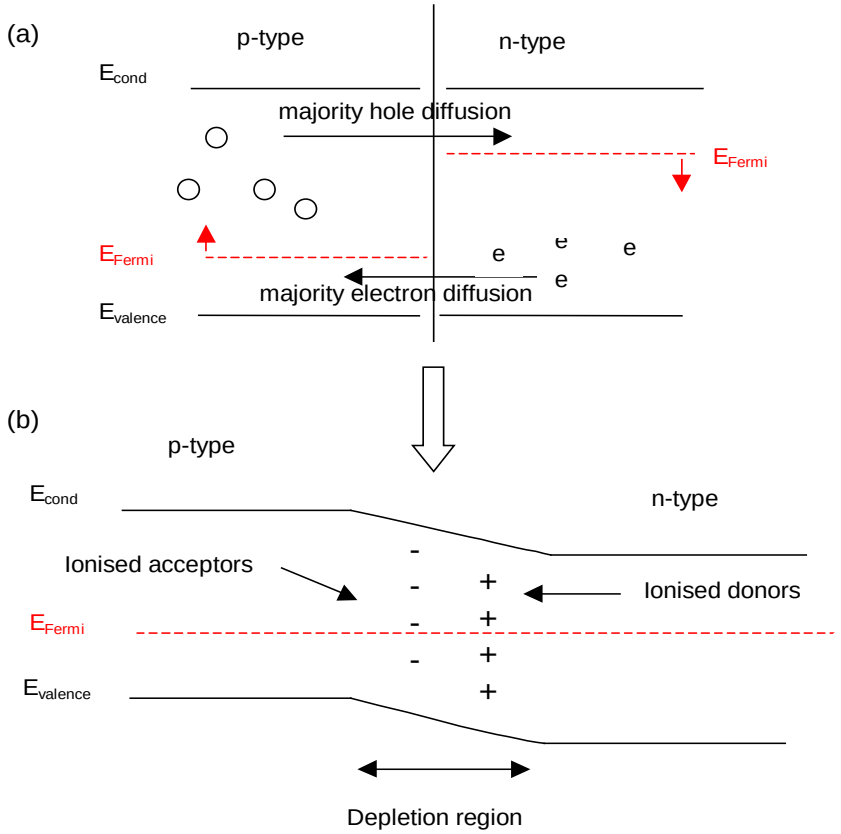

Figure 2.3 Typical p-n junction

The next section describes the use of two p-n junctions in a MOSFET.

2.3 MOSFET Description and Threshold Shift

The MOSFET used for this work consists of an n-type silicon substrate in which are embedded two p-type areas. The substrate is separated from an aluminium gate by an SiO_2 insulator, and the whole MOSFET is covered with about 0.3 mm epoxy. The oxide is a passivator, thermally grown (through oxidation at elevated temperatures) onto the Si, which insulates it from the metal gate electrode. The MOSFET comprises two p-n junctions, denoted the "source" and the "drain" (see figure 2.4).

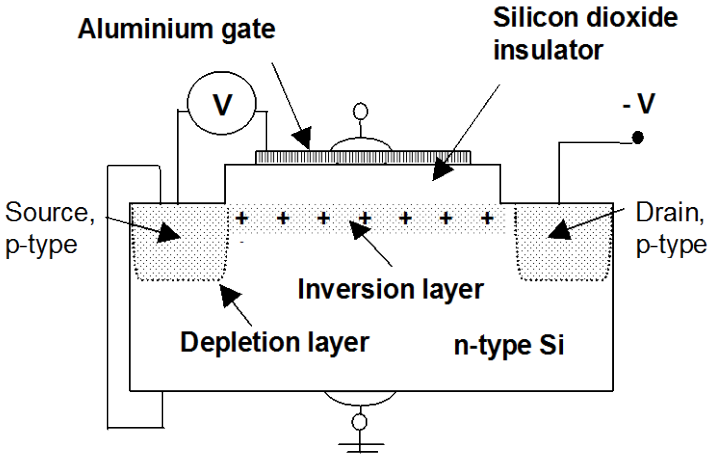

Figure 2.4 Schematic of a typical p-MOSFET

MOSFETs may be operated in several modes - flatband, accumulation, depletion or inversion - depending on bias voltage between the substrate and gate, called "gate voltage" (V_g). When there is no charge in the semiconductor, the energy levels of the Si in an energy band diagram are flat, hence this is called the flatband mode. The V_g required to maintain this condition is called "flatband voltage", V_{FB}. For n-type Si, accumulation mode occurs by applying a positive gate bias ($V_g > V_{FB}$) which attracts electrons towards the Si/SiO_2 interface. Depletion or inversion occurs when a negative gate bias ($V_g < V_{FB}$) is applied. When a large negative voltage is applied to the gate with respect to the substrate, an electrostatic field is set up between the gate and the rest of the device. This voltage repels electrons from the interface between the substrate and insulator, and also attracts holes (minority carriers) to the interface, thus producing a positively charged channel. This region of the substrate, having been "inverted" from n-type to p-type, is called an "inversion layer". This layer is a p-type channel in the silicon close to the insulator, through which holes can move and carry charge from the

source to the drain. The gate voltage which induces inversion and first permits a current to flow between source and drain is V_{th}. The V_{th} necessary to cause this inversion depends on:

- the thickness, capacitance and charge of the oxide
- the doping density
- temperature
- the electron and hole concentrations
- electric potential between the gate and the Si.

The MOSFET used for the current work is operated in inversion mode and is called a "p-type MOSFET". For a p-type MOSFET, V_{th} is given by [17]:

$$V_{th} = V_{FB} - |2\phi_F| - \frac{\sqrt{2\,\varepsilon_s q n_d (|2\phi_F| - V_{SS})}}{C_{ox}} \quad \text{.....(2.6)}$$

where ϕ_F = bulk potential (V)

ε_S = permittivity in Si (F/cm)

q = electron charge (C)

n_d = density of donors (m^{-3})

V_{SS} = voltage between source and substrate (V)

C_{ox} = oxide capacitance per unit area (F/m^2).

The flatband voltage is the applied gate voltage which yields a flat energy band in the semiconductor. It equals the difference between the work-functions of the metal, ϕ_M, and the semiconductor, ϕ_S, minus terms expressing the voltage across the oxide due to charge at the oxide-Si interface, and in the oxide. The work function is the voltage required to extract an electron from the Fermi level to the vacuum level (i.e. outside the atom). Flatband voltage is given by:

$$V_{FB} = \phi_M - \left(\chi + \frac{E_{gap}}{2q} - |\phi_F| \right) - \frac{Q_i}{C_{ox}} - \frac{1}{\varepsilon_{ox}} \int_0^{t_{ox}} x\ \rho_{ox}(x)\, dx \quad \text{.....(2.7)}$$

where χ = electron affinity for semiconductor (V)

Q_i = interface charge density per unit area (C/m^2)

ε_{ox} = permittivity of the oxide (F/cm)

ρ_{ox} = oxide charge density (C/m^3)

t_{ox} = oxide thickness (m)

In investigating charge yield and effects of oxide thickness and applied bias on flatband voltage in MOS capacitors, Boesch and McGarrity [18] determined that, for a uniform radiation-produced oxide hole charge density, ρ_{ox}, the shift in flatband voltage was proportional to radiation dose, oxide thickness and the applied electric field across the oxide:

$$\Delta V_{th\,FB} = \frac{-\rho_{ox}\, t_{ox}^{\,2}}{2\varepsilon_{ox}} \quad \text{.....(2.8)}$$

$$\propto \frac{f(E)\, D\, t_{ox}^{\,2}}{W} \quad \text{.....(2.9).}$$

where $\Delta V_{th\,FB}$ is the flatband threshold voltage shift (V).

From this, they confirmed that the radiation energy required to produce one electron-hole pair in SiO_2 was 18 ± 3 eV. Later work [19] achieved greater accuracy of 17 ± 1 eV.

For the use of MOSFETs as dosimeters, the V_{th} is slightly differently defined – it does not relate to the *inversion* V_g which first permits a current to flow, but to a certain *specified constant* current, as shown in figure 2.5 which depicts the shift in V_{th} produced by irradiation. It shows the current-voltage (I-V) curves of a p-MOSFET prior to and following irradiation in passive mode (no applied gate bias). In this example, the shift is 2V to maintain a constant source-drain current of 160 μA.

It can be seen that the curve is translated as well as "stretched out" as a result of the exposure. The translation is due to charge trapped in the oxide, whilst the distortion is due to interface charge.

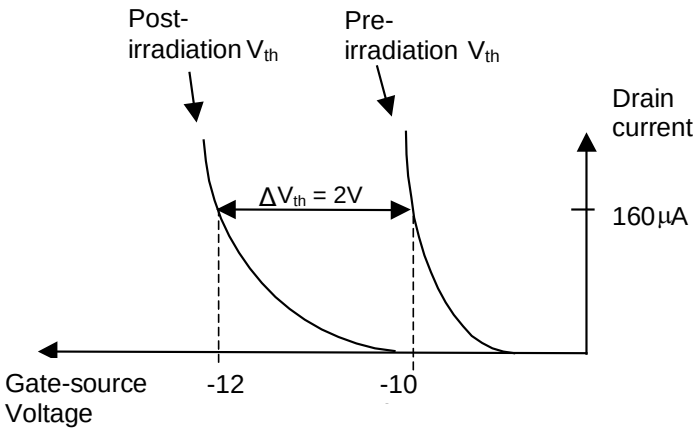

Figure 2.5 I-V curves prior to and following irradiation, displaying the shift in V_{th} to maintain a 160 μA current

The measurement of the V_{th} before and after irradiation, *viz*. “threshold shift”, ΔV_{th}, is the basis of MOSFET dosimetry, as will be described in the next chapter.

3. THE MOSFET AS A RADIATION DOSIMETER

3.1 Background

Most early work into radiation effects on MOS devices had been directed at minimising degradation of circuits containing them, particularly for their use for the defence and space industries [20-22]. The use of MOSFETs for radiation dosimetry was first suggested in 1974 by Andrew Holmes-Siedle [23], who developed a space-charge dosimeter for radiation monitoring and safety applications. In 1978, Adams and Holmes-Siedle [24] suggested that, since radiation damage was proportional to radiation dose, dose absorbed by MOSFETs could be determined by measurement of its properties, such as inversion voltage, and thus they could be used as radiation detectors. They realised the potential of controlling certain parameters of MOS transistors, such as oxide thickness and density of traps through fabrication processes, to optimise, rather than to minimise, the space-charge density, to produce useful radiation dosimeters.

Since the late 1980s, MOSFETs have been investigated extensively for use for many medical dosimetry applications, including diagnostic radiology [7], skin surface dosimetry [25, 26], dose distributions of small fields such as used for stereotactic radiosurgery [5], microbeam dosimetry [6, 27, 28], image-guided radiotherapy [29] and quality assurance of Intensity Modulated Radiotherapy equipment [30, 31]. An understanding of the characteristics and response of MOSFETs to irradiation is necessary prior to their use for medical dose determination.

3.2 The processes subsequent to interaction of ionising radiation with a MOSFET

Radiation exposure damages the structure of the SiO_2 with the result that charge traps are created in the bulk oxide and at the interface with the silicon, as will be explained hereunder. Most charge traps are located in the SiO_2 within 20 nm of the interface with the silicon, although some traps exist in the bulk oxide and at the interface. Figure 3.1 shows the identified trapping zones. SiO_x indicates an unknown oxygen species.

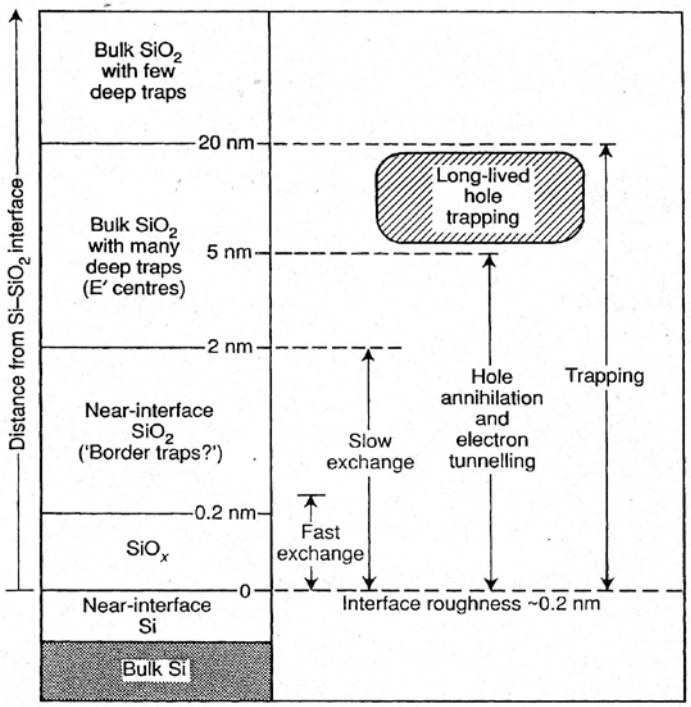

Figure 3.1 Bulk oxide, border and interface traps in a MOSFET [89, p87]
(with permission from Oxford University Press)

When a MOSFET is exposed to radiation of sufficient energy, W, (>17±1 eV in SiO_2), electron-hole pairs may be produced. The number of pairs produced, N, is proportional to the energy transferred, E_{tr}, and therefore on dose:

$$N \propto \frac{E_{tr}}{W} \quad \text{.....(3.1)}$$

The main processes involved as a result of the interaction with ionising radiation with a MOSFET are:

1. Creation of electron-hole pairs in the SiO_2 by ionising radiation;
2. Separation of electrons from holes by application of an external electric field across the oxide, and the movement of electrons towards the gate;
3. Hole transport through the oxide towards the Si/SiO_2 interface;
4. Trapping of holes and electrons in the oxide;
5. Build-up of interface and border traps in the Si bandgap; and
6. Electron-hole recombination.

These are described in greater detail below, and illustrated in figure 3.2.

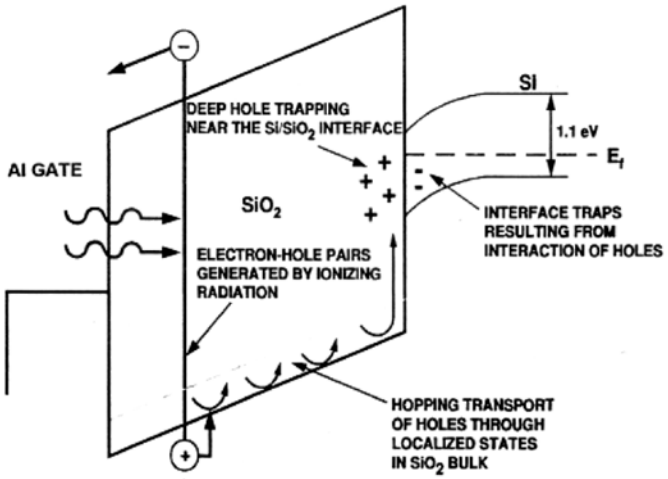

Figure 3.2 Band diagram of a MOS device with a positive gate bias, illustrating the main processes subsequent to irradiation [90, p333]
(with permission from Elsevier)

3.2.1 Electron-hole pair creation

When energy is transferred to electrons by ionising radiation, they are excited from the valence band into the conduction band in solid state material such as SiO_2. They leave behind holes in the valence band, thus forming electron-hole pairs. (Electron-hole pairs are also produced in the gate and the substrate, however these pairs quickly recombine and do not contribute to ΔV_{th}, so will be disregarded for the purposes of this study).

3.2.2 Electron-hole separation by an applied electric field

Both the holes and electrons can carry charge and, although SiO_2 is an insulator, it does allow the movement of electrons and holes under certain circumstances. Some electrons and holes will recombine immediately, but with an applied positive gate-substrate bias, the electrons are attracted to the gate, while the holes move by so-called “hopping transport” through the oxide towards the Si/SiO_2 interface. The rate of transport of the electrons and holes is a function of the oxide thickness and electric field, and their coefficients of mobility. Hole velocity is much less than electron velocity [16] (see section 3.5.1). The mobility of holes in SiO_2 at room temperature is about 10^{-4} – 10^{-11} $cm^2/V.s$, while typical electron mobility is of the order of 20 $cm^2/V.s$.

3.2.3 Hopping transport of holes through SiO2

The continuous-time-random-walk model [32] of transport phenomena in solids has been used to describe the movement of holes in SiO_2. Essentially, it involves quantum tunnelling of holes via lattice distortions. A strong polarization interaction between the hole and the lattice creates a local distortion of the lattice, an increase in the effective mass of the hole and lowering of the local potential. In effect, the hole is "self-trapped", and is called a "small polaron" (see figure 3.3(a)). The small polaron is able to "hop" through the lattice via thermally activated quantum tunnelling. Thermal fluctuations in the lattice may lead to conditions where the potentials of the hole trap and an adjacent empty trap coincide such that the wave functions of the two traps overlap, and the hole can tunnel into the adjacent trap (3.3(b)).

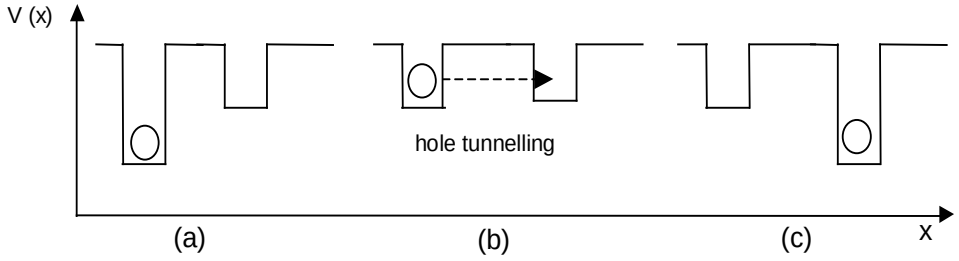

Figure 3.3 Small polaron hopping model for hole transport through SiO_2. (a) polaron trapped in a potential well; (b) quantum tunnelling to an adjacent well; (c) polaron trapped in the next well

The potential of that trap is then lowered, and the process is continued (3.3(c)). Polaron hopping may continue for up to several seconds following irradiation, at room temperature.

3.2.4 Oxide electron and hole trapping

The holes and electrons may be trapped either in the oxide or at the interface with the Si. The exact nature of these oxide and interface traps is not yet entirely understood, but much work has been done on their chemical characterisation [33-38]. Certain radiation-produced defects in the oxide structure or at the interface with the Si have been identified as possible traps, including the E' centre (of the form $\bullet Si{\equiv}O_3$) believed to be inherent in the oxide,

and the P_b centre at the interface. Figure 3.4 shows some of the identified E' and P_b centres in the oxide and at the interface.

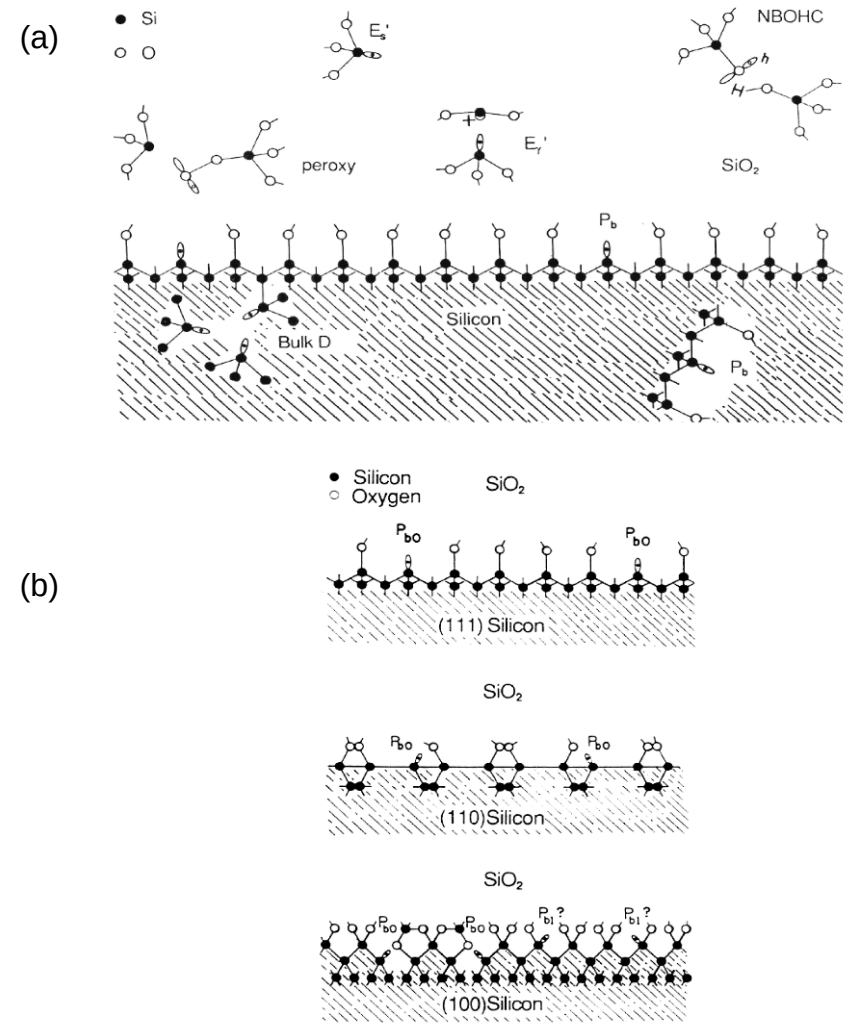

Figure 3.4 Examples of chemical species believed to be involved in the formation of oxide and interface traps. (a) oxide species; (b) interface species in 3 types of Si. [33, pp230, 237]
(with permission from Institute of Physics Publishing)

3.2.4.1 Hole trapping in the oxide near the Si/SiO_2 interface

H^+ and oxygen have been suggested to be involved in the formation of hole traps [33]. It is believed that these species are produced as a result of lattice displacement and are attracted towards the Si/SiO_2 interface in the presence of an electric field. Most of the oxide traps exist between 2 and 20 nm of the Si/SiO_2 interface, but small numbers can be found in the bulk oxide. More than 10 of these centres have been identified.

3.2.4.2 *Electron Traps in the oxide*

Although the majority of electrons are drawn out of the oxide through the gate, some are trapped in the oxide. It is believed that the build-up of these electron traps can form a conduction path across the oxide, which eventually leads to saturation. However, the generation mechanism is not clear. At least three models have been proposed to describe the build-up of electron traps in SiO_2 [39]:

- *Anode hole injection model*

  Holes injected from the anode can recombine with electrons, and the energy released by this recombination generates electron traps.

- *Hydrogen model*

  Hydrogenous species, released by holes, can travel through the oxide and generate electron traps.

- *Electric field energy model*

  The high oxide field itself can induce sufficient energy directly into the oxide to create electron traps.

3.2.5 *Interface and border traps*

3.2.5.1 *Interface traps*

As well as oxide traps, interface traps (P_b centres) are caused by ionising radiation. These are defects at < 0.2 nm of the Si/SiO_2 interface which increase the density of energy levels within the bandgap, close to the valence or conduction band. These defects can exchange charge, by capturing or emitting electrons or holes from the conduction and valence bands respectively [16]. Therefore, interface traps store and release both positive and negative charge, depending

on MOSFET type and bias conditions. The P_b centres may be triggered by irradiation or charge injection. Most interface defects have been found to contain either dangling •Si≡ orbitals or hydrogenous species, especially H^+ [33].

3.2.5.2 Border traps

Hybrid traps, having properties between the E' and P_b centres called "border traps", have been found to exist in the oxide, between 0.2 - 2 nm from the Si/SiO_2 interface. Border traps can also exchange charge with the Si, and their effective density depends on the timescale and bias conditions of measurements. Border trap densities of ~ 10^{10} – $10^{11}/cm^3$ have been suggested [40]. They may be donor-like or amphoteric as shown in figure 3.5. The donor-like traps have electrons associated with trapped holes which neutralise charge.

Figure 3.5 Three types of border traps. (1) & (2) donor-like; (3) amphoteric. [40]
(with permission from American Institute of Physics)

In the first type of donor-like trap, the electron may exist in a transitional region of the oxide, (SiO_x indicates unknown oxygen species), whereas in type 2, the electron is believed to exist in the oxide bulk, perhaps at

the same site as the trapped hole (E' centre). From the amphoteric trap, a hole or electron may be exchanged with the Si, depending on bias conditions at the interface. In p-MOSFETs, the border traps may exchange holes with the Si.

3.2.6 Recombination of electrons and holes

Following irradiation, some electron-hole pairs will recombine, and free electrons may form covalent bonds with other atoms. Recombination therefore reduces the density of electron-hole pairs. It has been shown [41] that the densities of holes and electrons decrease in an exponential fashion whilst the following equations show the densities taking into account the production of electron-hole pairs:

for n-type Si,

$$n_h(t) = C_h + G_v \tau_h \left(1 - e^{(-t/\tau_h)}\right) \quad \text{.....(3.2)}$$

and for p-type Si,

$$n_e(t) = C_e + G_v \tau_e \left(1 - e^{(-t/\tau_e)}\right) \quad \text{.....(3.3)}$$

where
- $n_h(t)$ = hole density at time t after irradiation (cm^{-3})
- $n_e(t)$ = electron density at time t after irradiation (cm^{-3})
- C_h = concentration of holes in valence band (cm^{-2})
- C_e = concentration of electrons in conduction band (cm^{-2})
- G_v = no. of electron-hole pairs generated by irradiation per sec (s^{-1})
- τ_h = lifetime of holes (s)
- τ_e = lifetime of electrons (s).

In addition to recombination, electrons may tunnel or be injected from the silicon (for example by a reader system). Figure 3.6 shows the sites of hole traps and recombinations, and the resulting variation of oxide electric field. The field strength increases close to the Si interface (between d1 and d2) where holes are trapped, then is stabilised by recombination of the holes with electrons injected from the Si.

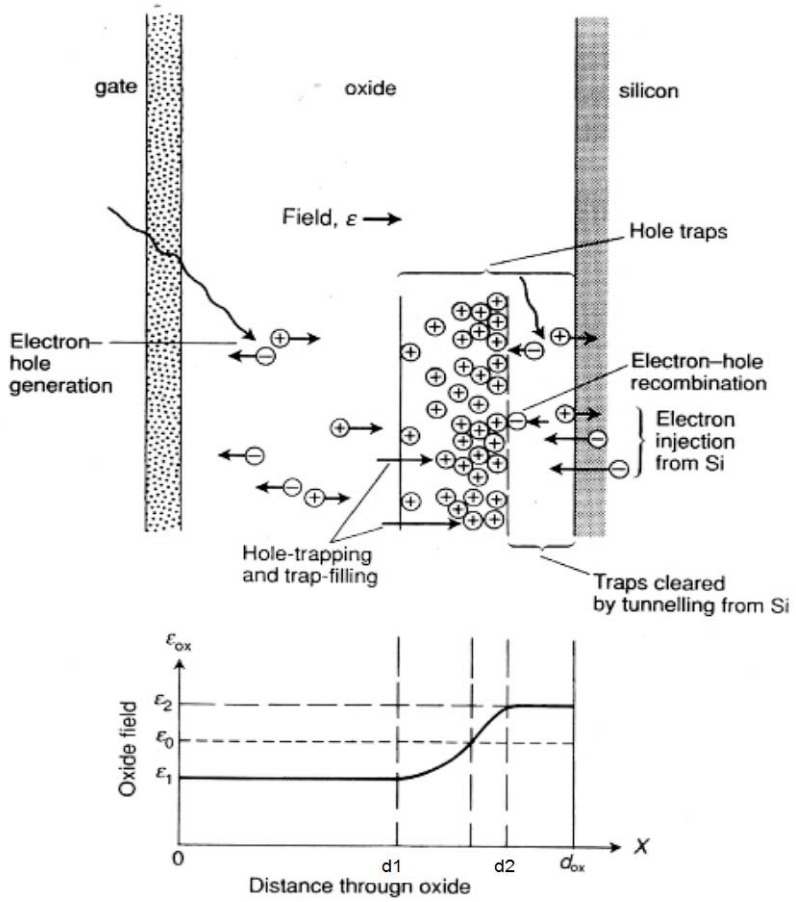

Figure 3.6 Sites of hole trapping and electron-hole recombination, and electric field across SiO_2 [89, p139]
(with permission from Oxford University Press)

3.3 Dose determination by measurement of Threshold Shift

As previously mentioned, a positive gate-substrate bias during irradiation attracts electrons towards the gate, whilst the holes migrate towards the Si/SiO_2 interface where some are trapped, either in the oxide itself, or at the interface. In p-channel MOSFETs, the interface states also trap positive charge. These trapped holes repel the positively charged carriers in the channel, hence a greater negative voltage must be applied between the gate and source to maintain the specified source-drain current. The reduced concentration of positive charge carriers in the channel thus results in a "shift" of the threshold voltage to a greater negative value.

Threshold shift is measured by taking readings of V_{th} (mV) prior to, and following, irradiation. However, due to various electronic effects such as carrier drift, recombination of electrons with holes, build-up of interface traps, thermal emission of holes from the traps and interface defects with accumulated dose, readings of ΔV_{th} for the same given dose may vary (drift) with time since irradiation. This thesis investigates some of these drift effects, particularly their influence on the use of MOSFETs for IVD.

3.4 Calibration and use of MOSFETs as Radiation Dosimeters

Sensitivity is a measure of the response of the dosimeter to radiation. It is defined as:

$$\frac{\Delta V_{th}}{D} \quad \text{.....(3.4)}$$

where ΔV_{th} is ($V_{th\ post\text{-}irradiation}$ - $V_{th\ pre\text{-}irradiation}$) (mV) and D is absorbed dose (cGy).

In order to be used as *in vivo* dosimeters, MOSFETs must first be calibrated to determine their response to radiation. Once the response to a specified radiation dose under "reference conditions" is known, an unknown radiation dose can be determined using the ΔV_{th}, a "calibration factor" *CF*, and "correction factors" F_{corr}, which are necessary when the irradiation conditions differ from the reference conditions. For example, reference conditions could be 100 cm source-to-surface distance (SSD) and 10 cm x 10 cm field size at the isocentre, at depth at which maximum dose is deposited, D_{max}, with the sensitive side of the MOSFET facing directly towards the beam. The *CF* is determined by:

$$CF = \frac{\Delta V_{th,ref}}{dose_{ref}} \quad \text{.....(3.5)}$$

Then, following exposure to an unknown dose in other than reference conditions, resulting in a threshold shift of ΔV_{th}, dose is given by [42]:

$$D = \Delta V_{th}\, CF \prod^{i} F_{corr,i} \quad \text{.....(3.6)}$$

where $F_{corr,i}$ are obtained by cross-calibration with an ionisation chamber having a calibration factor traceable to a National Standards Dosimetry Laboratory (in Australia, Australian Radiation Protection and Nuclear Safety Agency). The MOSFET and the calibrated ion chamber (IC) are placed on the central axis of the radiation beam – the MOSFET on the surface and the IC at D_{max} of a water-equivalent phantom:

$$F_{corr,i} = \frac{\frac{M_{IC}}{M_{IC,ref}}}{\frac{M_{MOS}}{M_{MOS,ref}}} \quad \text{.....(3.7)}$$

where M_{IC} and $M_{IC,ref}$ are the IC measurements, and M_{MOS} and $M_{MOS,ref}$ are the readings of ΔV_{th}.

As will be discussed in section 3.5, the sensitivity to radiation of MOSFETs decreases with accumulated dose, therefore dose is determined using a *CF* to compensate for this effect As will be shown in section 5.1, this *CF* is given by a quadratic equation called a "sensitivity drift equation", where the constant is the initial ΔV_{th} of the unirradiated probe.

The characteristics which influence the use of MOSFETs as dosimeters are discussed in the following sections.

3.5 Sensitivity and measurement reproducibility

Sensitivity can be controlled by varying certain parameters, as described hereunder, and several models of MOSFET have been developed specifically to measure low doses ("high sensitivity"), or high doses ("low sensitivity"), or both ranges on the one detector ("dual sensitivity"). The high sensitivity detector purportedly is capable of measuring as low as 5 cGy doses (commonly called R-type), whilst the low sensitivity detector can be used to measure doses of several 10^4 Gy (K-type). The dual sensitivity probes, based on R- and K-type MOSFETs on the same chip, allow measurement of a wide range of radiation doses.

In early 1995, T&N introduced the TN-RD-50 system, with reported sensitivity of 1 mV/cGy and reproducibility of dose of about 1.5% [43] using a standard TN-RD-20 bias box. Later that year, sensitivity of 2.7 mV/cGy was obtainable by the introduction of a high sensitivity bias supply, the TN-RD-19 [44]. They have since developed dual sensitivity dual bias MOSFETs, on which a different bias is applied to two identical detectors on one chip during irradiation to reduce temperature effects, in addition to an isotropic model, MT-TN-502RDI, to minimise angular response (see section 3.9).

The Wollongong reader system used for the current work supports up to 5 MOSFETs (up to 10 detectors), simultaneously (REM Oxford Ltd (UK)). The claimed sensitivity at D_{max} is about 5 mV/cGy [6]. CMRP has also developed other models of probe, including a quadruple chip containing 2 each of high and low sensitivity detectors, biased at different voltages during irradiation, which it claims improves linearity of ΔV_{th} with dose [27].

MOSFET sensitivity can vary depending on:

- applied bias during and following irradiation
- oxide production method and thickness
- radiation energy
- accumulated dose
- angle of incidence of radiation, and
- ambient temperature,

as will be discussed hereunder.

3.5.1 Applied bias during and following irradiation

As mentioned in section 3.2, following the production of electron-hole pairs by radiation, a positive applied gate bias will attract the electrons rapidly to the gate where they leave the system, while the holes will drift slowly towards the Si/SiO_2 interface. The velocity of holes and electrons in SiO_2 is given by [45]:

$$v = \frac{x}{t} = \frac{\mu}{\varepsilon} \qquad \text{.....(3.8)}$$

where x = distance travelled (cm)

μ = coefficient of mobility (cm^2 / V.s)

ε = electric field strength of the oxide (V/cm)

t = time of travel across oxide (s).

For a typical electric field strength of 10^6 V/cm, the time of travel of electrons across a 10 nm thick oxide is of the order of picoseconds, while for holes, it can last up to several seconds, and is a function of the oxide thickness, temperature and oxide electric field strength. The time of travel for holes, t_h, across SiO_2 in the direction of the electric field is [16]:

$$t_h \propto \left(\frac{t_{ox}}{x_h}\right)^4 exp\left(\frac{A - qx_h\frac{\varepsilon}{2}}{kT}\right) \qquad \text{.....(3.9)}$$

where x_h = average hopping distance travelled by holes (cm)

A = constant.

Sensitivity decreases with accumulated dose, due to the diminishing number of available traps, as well as the reduction of the electric field across the charge collection regions, and

increases with applied gate bias [22, 28, 46-48]. A positive bias applied to the gate during irradiation inhibits electron-hole recombination, so that a greater proportion of holes reach the interface to become trapped. Sensitivity has been found to vary with positive gate bias as $V_g^{2/3}$ [49], and to be approximately 5V/Gy for a +100V bias, and to vary logarithmically with bias potential from 1.5 – 9 V [11].

The sensitivity of T&N single bias MOSFETs has been found to decrease by 23% after 46 Gy accumulated dose when biased at +5V, and only by 16% when biased at +10V and +15V [46].

As well as bias *during* irradiation, the post-irradiation bias conditions can also substantially influence response (section 3.8).

3.5.2 Oxide production method and thickness

The oxides used for semiconductors can be produced, or "grown", by different methods, including thermal and deposited oxides. Thermal oxides are produced by heating (850-1100^{o}C) in an oxidising atmosphere by "dry" or "wet" oxidation, given by [50]:

Dry: $Si + 0_2 \rightarrow SiO_2$

Wet: $Si + 2\ H_2O \rightarrow SiO_2 + 2\ H_2$

Alternatively, deposited oxides are produced with chemical reactions which create free product species which condense to form a thin deposit film on a substrate.

Sensitivity of a MOSFET is oxide growth method-dependent, with greater reproducibility being obtained for wet oxides rather than dry-grown oxides [20].

Thicker oxides have greater sensitivity than thin oxides [12, 51] since they have a greater number of atoms with which radiation can interact, hence the greater the probability of electron-hole pairs being created and subsequently holes being trapped. Ensell *et al* [52] showed variations in response of p-MOSFET dosimeters of varying thicknesses of oxide between 0.69 and 2.3 microns, to

different types of radiation (Cobalt-60 and x-rays from medical linear accelerators) exposed with either no bias, or an applied bias of 20 V/μm during irradiation. Variations in response were found due to different oxide processing methods which influenced the balance between oxide trapped and interface trapped charge. For unbiased dosimeters, ΔV_{th} was found to be due to trapped oxide charge only, while for biased dosimeters (20 V/μm during irradiation), it was dependent on the method of oxide growth. For deposited oxides, shift was due to trapped oxide charge predominantly, but for thermal oxides, both oxide traps and interface states contributed. They found the threshold shift due to oxide traps, $\Delta V_{th\,ox}$, depended on the square of oxide thickness (up to 1.45 μm) for both biased and unbiased dosimeters:

$\Delta V_{th\,ox} \propto D\, t_{ox}^2$ for biased dosimeters .....*(3.10)*

$\Delta V_{th\,ox} \propto D^{0.9}\, t_{ox}^2$ for unbiased dosimeters.....*(3.11).*

Others have found the time of interface trap formation to increase as $t_{ox}^{2.6}$ for a negative V_g during irradiation, followed by a positive V_g immediately afterwards [53].

3.5.3 Energy of radiation

As previously mentioned, MOSFETs over-respond at low energies (<100 keV) due to the predominance of the photoelectric effect in this energy range [54-56]. The greater photoelectric cross-section for Si than for SiO_2 means that secondary electrons produced in the Si will cross into the SiO_2, and contribute to the absorbed dose. Variations in the microscopic structure of each individual MOSFET could also vary each detector's response. The result is that, with decreasing energy of radiation, response increases by up to 440% compared with 6MV x-rays [56], necessitating calibration of each individual MOSFET detector at the relevant clinical energy to be used at these low energies. However, good reproducibility of 3.6% (2 standard deviations (SD) of the mean) has been found for 50 consecutive measurements of 100 cGy doses with superficial and orthovoltage beams [56], so this increase in response can be accounted for in dose determination.

T&N have reported no energy dependence for their MOSFETs for high energy radiation, claiming response within 5% for 1-20 MeV photons and 6-20 MeV electrons [57]. Edwards *et al* [58], using two T&N MOSFETs (TN-502RD), found their maximum relative sensitivities with 33 keV X-rays, compared to response to 6MV X-rays, to be 4.19 ± 0.25 mV/cGy and 4.44 ± 0.26 mV/cGy.

Kron *et al* [47] developed a model to evaluate MOSFET response to monoenergetic synchrotron radiation with photon energies between 10 and 99.5 keV. They assumed response at low energies to reduce exponentially, and to vary at medium energies with the energy dependence of the photoelectric effect. They used a similar MOSFET system to that used for the current work. Their response model was given as:

$$R(E)=\{1-\exp[-\alpha_1(E-E_1)]\}\quad\frac{1+\alpha_2}{(E-E_2)^3} \qquad \textit{.....3.12)}$$

where α_1, α_2 are fitting parameters relating to the exponential fall-off towards low energies and inverse cubic fall-off towards higher energies, and E_1 and E_2 allow for an energy shift for the two components. They found over-response to low energy X-rays by up to a factor of 7.

3.5.4 Accumulated dose

A comparison of the responses of the Wollongong and T&N systems has been reported by Kron *et al* [47]. Gate biases of +5V and +7V were applied to the Wollongong and T&N MOSFETs respectively during irradiation from a 4MV linac. Dose response was found to be a decreasing linear function of total accumulated dose in the range ~ 8 Gy to 42 Gy. The Wollongong detector response reduced by approximately 3% for a gate voltage change of 1V, compared with less than 1% for T&N. This was due to the different bias conditions for the two systems. Dose response of both systems diminished with accumulated dose.

3.5.5 Angle of incidence of radiation

The epoxy “bubble” which covers the active MOSFET chip filters low-energy photons from the spectrum [47]. Also, since the

sensitive region of MOSFETs is extremely small, many secondary electrons are backscattered into the active volume from the substrate. Therefore, the response of the MOSFET to radiation will depend on the incident direction of the radiation beam, and whether or not it passes through the substrate. This will be discussed at some length in section 3.9.

3.5.6 Ambient temperature

MOSFETs are temperature-sensitive, since thermal fluctuations will affect the rate of hole transport across the oxide, and electron-hole recombinations. An increase in ambient temperature of 1^{o}C can result in a reduction of 7mV in ΔV_{th} [11] or 0.3%/^{o}C for temperatures 22 – 40^{o}C [59]. The T&N dual bias dual sensitivity MOSFET alleviates this problem. Since both detectors are exposed at the same temperature, any temperature influence is minimised by using the *difference* between the threshold shifts measured by each detector as the output signal. These dual bias MOSFETs have achieved sensitivity reproducibility better than ± 3% for doses 20 cGy – 100 Gy, with a temperature coefficient of 0 – 0.015 cGy/^{o}C for temperatures between 0^{o} and 80^{o}C [46].

3.6 MOSFET saturation

MOSFETs have a limited useful lifetime as dosimeters due to saturation. Saturation occurs when all available traps have been filled, and the gate charge density equals the trapped charge density – there will be no nett voltage across the oxide to allow transport of holes through the oxide. In addition to trap filling, recombination of trapped holes with radiation-generated free electrons, and annealing through electron tunnelling from Si contribute to saturation [18, 60]. Boesch *et al* [60] found the dominant process for low oxide electric fields (< 2 MV/cm) to be recombination, while for fields larger than this, trap filling predominates. Freeman and Holmes-Siedle [22] created a simple model (figure 3.7) to explain saturation dependency on gate bias, oxide thickness and hole trapping probability. They assumed that holes occupy a thin layer in the oxide, a variable distance x_1 from the Si and x_2 from the gate, where x_2 is the variable “charge collection region” for a positive gate bias.

NOTE:
This figure is included on page 28 of the print copy of the thesis held in the University of Adelaide Library.

Figure 3.7 Simple model of charge density in a SiO_2 MOSFET [22]
(IEEE © 1978, with permission from IEEE)

Using the rate of generation of holes in SiO_2, they determined that threshold shift for a positive gate bias was given by:

$$\Delta V_{th} = -\frac{qg}{\varepsilon_{ox}\,\varepsilon_o} x_2^2 f(E).A.D \quad \text{.....(3.13)}$$

where g = hole generation rate (= 7.9 x 10^{12} cm^3/cGy (derived from the density of the oxide (2.27 g/cm^3) and the work function, W)

$f(E)$ = charge yield (C)

ε_o = permittivity of free space (F/cm)

A = probability of hole trapping (0 – 1).

This indicates that ΔV_{th} is linear with dose for low charge build-up, but the probability of hole trapping, A, will decrease with accumulated dose as traps fill up, as too will the electric field across the oxide, and saturation will occur at large accumulated doses. The saturation value, $\Delta V_{th\,sat}$ due to the filling of all available traps is given by [22]:

$$\Delta V_{th\,sat} = -\frac{qx_2 N_T}{\varepsilon_{ox}\varepsilon_o} \quad \text{.....(3.14)}$$

where N_T = density of available traps in the trapping layer. Expressed in terms of the reduction of the electric field across the charge collection region, it is:

$$\Delta V_{th\,sat} = -V_g\left(\frac{t_{ox}}{x_1} - 1\right) \quad \text{.....(3.15)}.$$

The build-up of interface states does not saturate with accumulated dose [51].

Responses for the T&N low sensitivity detector have been reported to be about 0.5 - 1.0 mV/cGy [7, 58, 61, 62] and about 3.0 – 3.5 mV/cGy [55, 63] for the high sensitivity detectors.

Reproducibility of ±3% has been reported for T&N MOSFETs for doses >20 cGy [1, 9, 31, 46, 64] and using Wollongong MOSFETs, Cheung, Butson and Yu [56] found reproducibility of response of 2.6% to 250 kV_p radiation for 50 consecutive irradiations of 1 Gy.

Dose measurement with MOSFETs has been found to be comparable to other dosimetry methods. Butson *et al* [65] reported agreement better than 1% between a Wollongong n-MOSFET with a gate bias of +5V, an Attix ion chamber and a TLD for measurements of depth dose for electron and photon beams. Ramani *et al* reported a standard deviation of 3.9% between planned and measured dose by MOSFET compared to 5.1% for TLDs [62]. Scalchi and Francescon found agreement within 2% of an ion chamber, and within 5% of TLDs [1].

3.7 Linearity

An important requisite for any direct-reading radiation dosimeter such as the MOSFET system used for this work, is linearity with dose. As dose increases, the dosimeter response should increase proportionally.

During the 1970s, Adams and Holmes-Siedle [23, 24] first used specially-made MOS transistors as radiation dosimeters. By exposure to Co-60 under a constant applied bias, they found ΔV_{th} as a function of dose to be linear in the range $10^3 – 10^4$ cGy, then sub-linear. This was because the build-up of space charge is initially proportional to the number of electron-hole pairs created, and hence to dose, but then proportionality is gradually lost due to the space-charge produced electric field which reduces the applied electric field. Similar results were found by Boesch and McGarrity [18] who explained the non-linearity with greater accumulated dose by:

- charge recombination in low field regions in the oxide
- electron injection at high interface fields
- accelerated hole transport
- collapse of applied field due to electron transport
- dielectric breakdown.

They also found that saturation of hole yield occurred for applied electric fields above 10^6 V/cm, and showed that an applied positive bias during irradiation extended the range over which linearity existed.

The response of a MOSFET operated in passive mode is similar to its response when operated in bias mode. In this mode, it is initially linear, but becomes non-linear with increasing accumulated dose [46, 66], due to the decreasing electric field strength across the oxide with accumulated positive trapped charge, and the finite number of oxide traps. Response in passive mode is given by [47]:

$$\Delta V_{th} = \Delta V_{th,i}\left[1 - A\exp(-BD)\right] \quad \text{.....} \textit{(3.16)}$$

where the ΔV_{th} for the first exposure of a new MOSFET, $\Delta V_{th,i}$ is a function of trap concentration, and *A* and *B* are parameters of oxide thickness and location of the space-charge, and are complicated functions of the local area density of the oxide trapping species and mobility and lifetime of electrons in the oxide [23].

In active mode, the charge trapped as a result of the incident radiation up to ~ 10^5 cGy is linearly proportional to the dose deposited [8], and has been shown to be energy-independent, except for energies less than 100 kV where the photoelectric effect dominates [47, 58, 67]. The range of linearity (and sensitivity) can be increased by increasing the gate bias during irradiation [66].

Winokur, *et al* [48] linked response of $D^{0.65}$ to the interface state density, N_{ss}, in the range 10^5 – 10^7 cGy, prior to sublinearity and subsequent saturation.

Users of the T&N MOSFETs have reported linearity within ± 2-3% over a range of radiation doses and energies [61, 64, 67-69] from 60 kV to 20 MeV.

Chuang *et al* [31] also found good linearity for a range of 6 MV doses from 5 cGy to 420 cGy with a linearity coefficient of 0.998. However a greater standard deviation was found for doses lower than 30 cGy (about

20% for 5 cGy to 6% for 25 cGy), while standard deviation was 2-3% for doses higher than 30 cGy.

CMRP has developed radiation detectors on which there are two pairs of p-channel MOSFETs with different gate oxide thicknesses (0.13 and 1 micron). Two of the detectors are R-type (high sensitivity) and the other two are K-type (low sensitivity) and are irradiated with +5 V and +12 V gate bias respectively. They have reported that this combination of oxide thickness and applied bias improves linearity of ΔV_{th} with dose [27]. These probes were unavailable for the current work.

For the single bias MOSFETS similar to those being investigated in the current work, the system's developers have claimed linearity to within 1% up to accumulated doses of 50 Gy, with an applied bias of +6V, but this was for a MOSFET from which the nickel casing was removed [65].

Therefore, the linearity of MOSFETs with accumulated dose is not constant, but reduces with accumulated radiation exposure due to the abovementioned effects, and must be taken into account for IVD measurements.

3.8 Response drift

There are many complex processes simultaneously occurring during and following irradiation of a MOSFET, as shown in figure 3.8. As a result, measurements of ΔV_{th} may "drift" with time following irradiation, that is, a reading taken at some time after a radiation exposure will differ from that taken immediately following irradiation.

As a result of these processes, although the dosimetric information is "stored" in the MOSFET until the next exposure, that information may drift with time since irradiation. This drift therefore has an impact on dose determination, and requires characterisation.

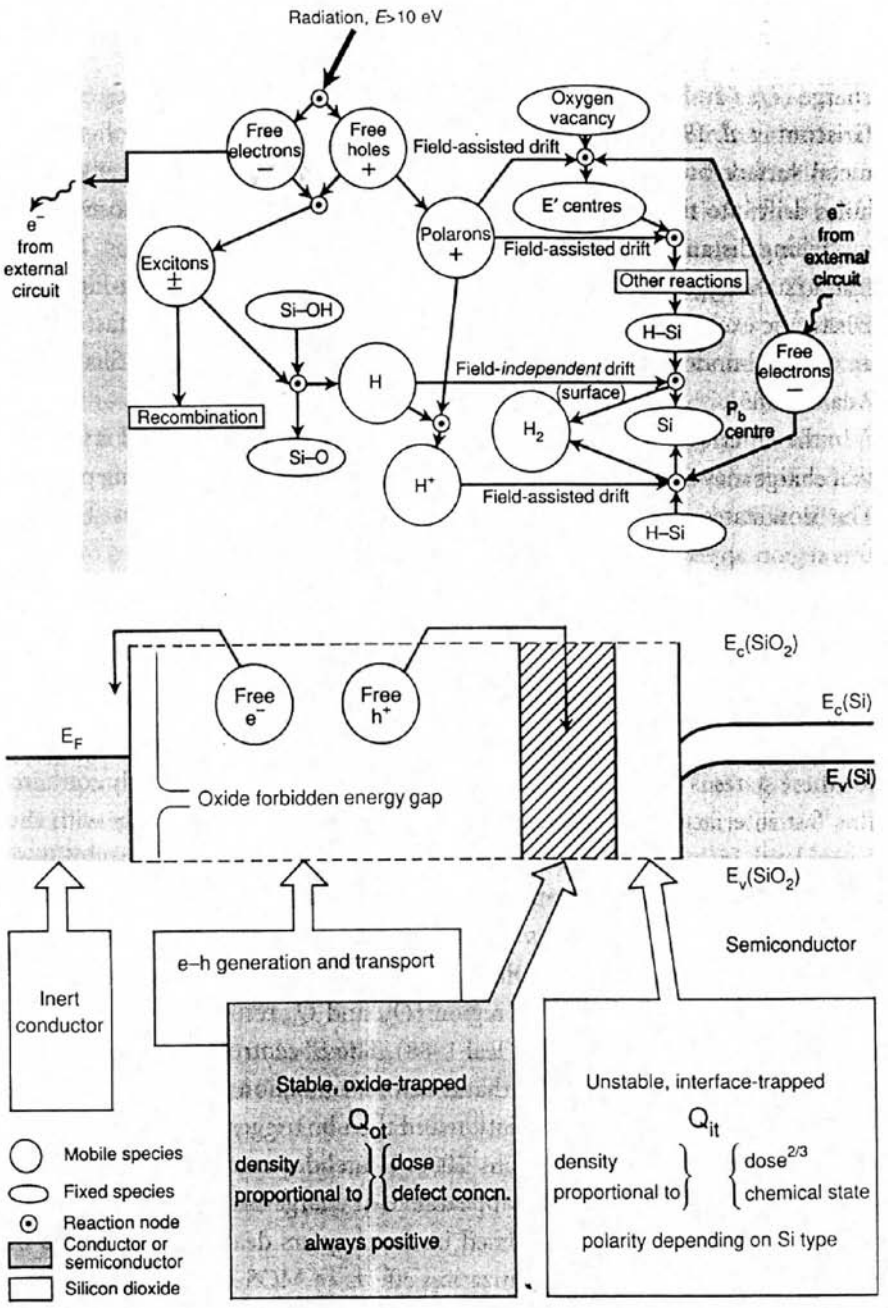

Figure 3.8 Processes set in motion by ionising radiation [89]
(with permission from Oxford University Press)
(Polarons are electronic charge which is stabilised by the relaxation of the lattice around it, whilst excitons are electron-hole pairs which are able to move together without instantly recombining)

Drift phenomena have been referred to in the literature as “creep-up”, “fade”, “annealing” and “drift” effects of MOSFETs. The long-term drift effects (from hours to years) following irradiation have been well investigated [7, 8, 12, 13, 46, 61, 70-72], however, little has been published on the short-term drift effects (seconds to hours), which period is particularly relevant for the use of MOSFETs for IVD, since real-time measurement results are required.

Many reasons have been suggested for post-irradiation drift. It is now generally believed to be mainly caused by the build-up and relaxation of charge traps in the oxide and the charge and discharge of interface states at the junction of the Si/SiO_2. At room temperature post-irradiation anneal under positive bias, the interface trap charge usually continues to build up whilst the (net) positive oxide trap charge density usually decays exponentially with time [72].

Holmes-Siedle and Adams [73] reported that contributing factors to drift included:

- intrinsic density of interface states at manufacture
- interface states caused by injection of electrons during reading
- rearrangement of ions or dipoles under an applied electric field
- deep oxide charge trap relaxation.

The bias conditions, and hence the electric field across the oxide, during and following irradiation play an important role in the build-up of interface states. Winokur and Boesch Jnr [48] reported an increased interface build-up with applied positive bias, with the density of interface states being given by:

$$N_{ss} = \frac{\Delta V_{th}\ \varepsilon_{ox}}{q\ t_{ox}} \qquad \textit{(3.17)}$$

They proposed that the build-up of interface states under a positive applied bias was a two-stage process – the first stage (< 1 sec) involved the holes moving towards the Si/SiO_2 interface, and this determined the final (saturation) value. This stage was electric field dependent but temperature independent. The second stage continued for several thousands of seconds, and involved the generation of interface states, and was dependent both on electric field and temperature.

Figure 3.9 shows the effects of applied bias on the build-up of interface states. A logarithmic build-up of density of interface states, N_{ss}, with time following irradiation is evident when a positive gate bias is applied both during and after irradiation (Curve A). Curves B, C and D were irradiated under a positive bias, with the bias changed to negative at 1s, then

switched back to positive at 20, 200 and 2000s respectively. Curve E was the result of a negative gate bias throughout the trial.

Figure 3.9 Effect of gate bias on build-up of interface states [75], p1654

The saturation time of the build-up could be directly correlated with the number of "hops" required for an ion at a further distance from the interface to travel across the whole width of the oxide, compared to the shorter times (less hops) for those ions formed close to the interface.

Pejović, Jakšić and Ristić (1997) [38] performed a detailed study of post-irradiation effects, in which they investigated oxide-trapped and interface-trapped charge effects separately. They found that during annealing, oxide-trapped charge was typically neutralised, however the density of interface traps could either increase, decrease or remain unchanged, and that an initial increase in interface trap density may be followed by a decrease at subsequent times. They showed that a negative bias during irradiation suppressed the formation of oxide defects, and a negative post-irradiation bias suppressed the decrease in oxide trap density as well as the increase in interface trap density.

The build-up and annealing of interface states was also characterised by Fischetti *et al* [74] who investigated the kinetics of the formation of "fast" and "slow" states during electron avalanche injection*. ("Fast" states are those which quickly respond to an applied field, by capture or relaxation,

* injection of high energy electrons into the SiO_2 by applying a high voltage (15-20V) between the source and drain

whereas “slow” states take a longer time to change their occupancy, through tunnelling or hopping transport.) They found that N_{ss} increased with injected charge until saturation was reached. Annealing was alleged to follow first-order kinetics, was temperature-dependent, and controlled by a time constant, τ, where:

$$\tau \quad \propto \quad exp\left(\frac{\Lambda}{kT}\right) \qquad \text{.....(3.18)}$$

where □ = activation energy for the annealing process. They also found an annealing rate dependence on the position of interface traps in the bandgap, *viz.* a faster annealing rate existed for deeper traps.

McLean [75] modelled the build-up of interface states, and its dependence on time, electric field, temperature and dose. He produced an expression for the interface state density with time after irradiation, $\Delta N_{ss}(t)$ as a product of expressions for two stages:

$$\Delta N_{ss}(t) \quad = \quad \underbrace{A\, D^{(2/3)} \quad \exp\left(B\sqrt{E_1}\right)}_{\text{first stage}} \quad \underbrace{f(t/\tau)}_{\text{second stage}} \qquad \text{.....(3.19)}$$

where $f(t/\tau) = b \ln (1 + t/\tau)$ $(V_g > 0)$ $(0 < t < t_{sat})$ .....(3.20)
$= 0$ $(V_g < 0)$

and E_1 = applied electric field during stage 1

$b = [\ln (1 + t_{sat} / \tau)]^{-1}$

t_{sat} = time of MOSFET saturation (s)

A and *B* are constants, depending on whether the oxide is wet or dry grown, and the time-scale of build-up, τ, was defined as:

$$\tau \quad = \quad \tau_o \exp\left(\frac{\Lambda}{kT - \alpha E_2}\right) \qquad \text{.....(3.21)}$$

where τ_o and α are constants and E_2 is the applied electric field during stage 2.

The first stage not only involved the movement of *holes* through the oxide, but also the release of *ions* via interactions with the holes. Whilst the first stage solely determined the saturation value of interface states,

the second stage involved electric field-assisted ion diffusion through the oxide.

By electron avalanche into the oxide from the Si, Aslam [76] concluded that there is a distribution of trapping centres of different energies in the bandgap of SiO_2. He showed that electrons can transfer from shallow interface traps with capture cross section ≈ 10^{-16} cm^2 to deeper traps (with cross-section ≈ 10^{-19} cm^2), which lie about 10 nm from the interface. Shallow traps near the interface exhibited the highest probability of charge transfer. Aslam suggested that trapping centres located in the interfacial region where bonds of molecules undergo strain, may relax after electron capture, causing electrons to move into more stable, deeper, energy levels. He concluded that the initial capture process occurs only through shallow centres, and whether or not the captured electron is transferred to deeper energy levels depends upon the probability of lattice relaxation after the capture.

Figure 3.10 Effects of electron injection at different temperatures on flatband Threshold Shift, (a) 100 K, (b) 400 K [76]
(with permission from American Institute of Physics)

Figure 3.10 (a) and (b) show the effects on $\Delta V_{th\,FB}$ with time after electron injection at different temperatures, followed by annealing for 30 min at 725K (annealing not to scale on the time axis). Both graphs show that some charge is not annealed out, but increases with the number of injection-anneal cycles, as reflected by the increasing $\Delta V_{th\,FB}$ (lower dashed curve), due to electrons transferring to deeper traps which do not anneal at 725K.

However, Savić, Radjenović and Pejović [77] excluded interface traps as the sole cause of ΔV_{th} drift because if this were so, the drift would be less than the maximum contribution of interface traps to the conventionally defined ΔV_{th}, of 10%, whereas they found drift voltages of 10-20% of ΔV_{th}. They concluded that only the oxide border traps were involved in the drift process, which presumption was borne out by good agreement between experimental results and their model based on that assumption.

Hence, due to the many complicated interactions and movements of electrons, holes and ions in the MOSFET, together with temperature, bias conditions during and following irradiation and associated changing electric fields, ΔV_{th} will drift with time. In view of the possible repercussions on dose determination *in vivo*, four aspects of drift were explored in some detail for this work, as described below:

(1) Drift following a single irradiation (i.e. repeated random readings of V_{th} taken up to 2½ hours after one exposure), to characterise the medium-term post-irradiation behaviour;

(2) Creep-up (as defined by Ramani et al [62]), being drift between two post-irradiation readings to determine a suitable time to allow for system relaxation between consecutive readings;

(3) Reading interval effect (single irradiation followed by repeated readings made at varying set intervals), in order to investigate the short-term effect on ΔV_{th} of repeated enquiries of the system, and how often readings should be taken, for example, during a total body irradiation IVD measurement ; and

(4) Reading delay in taking a pre-, a post- or both pre- and post-irradiation reading. This was to investigate effects on MOSFET response due to possible reading delays in the clinical situation.

3.8.1 Drift following a single irradiation

Long-term response drift following irradiation is a well-known effect in MOSFETs. It has been characterised during work on predicting CMOS inverter charging and annealing behaviour in nuclear (high dose-rate) or space (low dose-rate) environments. "Transient annealing curves" were derived for different types of inverters (n- and p-channel) for various dose-rate irradiations by monitoring drift after irradiation for up to 20 years [8]. For all devices, the "drift curve", ΔV_{th} vs ln(t) was found to be linear, so linear system theory was applied to derive drift functions which could be used to estimate ΔV_{th} at any time following irradiation, taking drift with time into account. The slope of the drift function, A, as shown in figure 3.11, was determined from different dose-rate irradiations [13] to be:

$$A = \frac{\Delta V(t_2) - \Delta V(t_1)}{\ln (t_2 / t_1)} \quad \text{.....(3.22)}$$

This was then used to obtain the drift function per unit dose, $\Delta V_{th}(t)$ to estimate ΔV_{th} at any later time:

$$-\Delta V_{th}(t) = \frac{-A \ln (t / t_0) + C}{D_0} \quad \text{.....(3.23)}$$

where D_o = total dose used to obtain the drift function (Gy)
A = slope of the drift function
C = intercept at $t = t_o$ (V)
t_o = time of termination of irradiation (s).

NOTE:
This figure is included on page 39 of the print copy of the thesis held in the University of Adelaide Library.

Figure 3.11 Determination of slope of drift function, A, and intercept, C, at t_o = 1 min, used to determine drift function with time after irradiation [13]

A similar method was used by Gladstone & Chin [70] who monitored signal drift up to seven days following Cs-137 exposure whilst maintaining a gate bias of +5V (see figure 3.12).

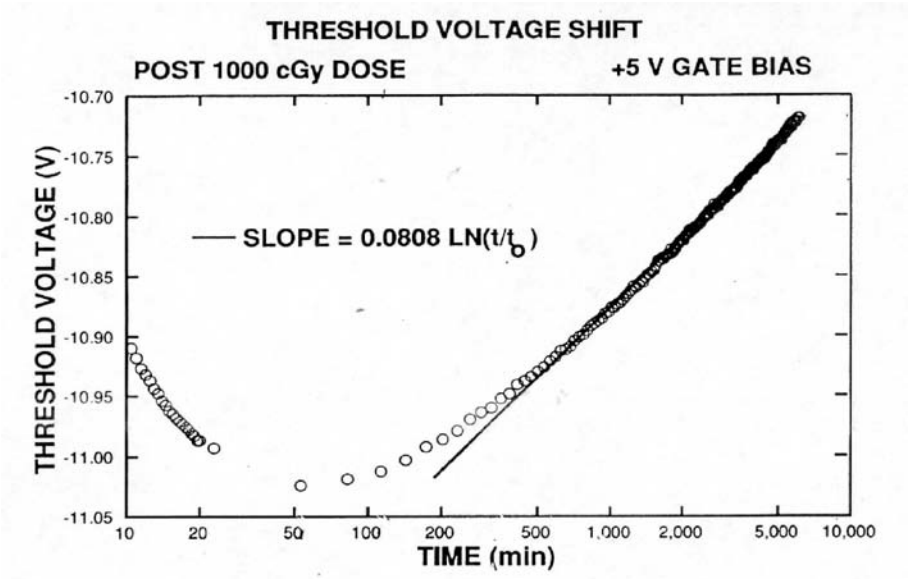

Figure 3.12 Drift in V_{th} at long times after irradiation of 10 Gy under a +5V gate bias [70] *(with permission from AAPM)*

Although these methods are useful for estimating ΔV_{th} for times greater than 8 hours following an irradiation, short-term drift (during the first seconds, minutes and hours) following irradiation has not been extensively characterised, and is of more importance for the use of MOSFETs for IVD, hence this time period was the focus of the current work.

3.8.2 *Creep-up*

The term “creep-up” has been loosely used in the literature to describe any drift effect, however, in this thesis, it is used to describe the phenomenon investigated by Ramani *et al* [62] as the drift between two post-irradiation readings – one taken immediately after irradiation, and a second after a time delay. They described creep-up as:

> *“a sharp initial increase of 4 mV when a second reading was taken 5 seconds after an immediate reading following exposure, followed by a gradual decline until the second reading was similar to the initial reading if the interval between the two readings was at least 1 minute”* (see figure 3.13).

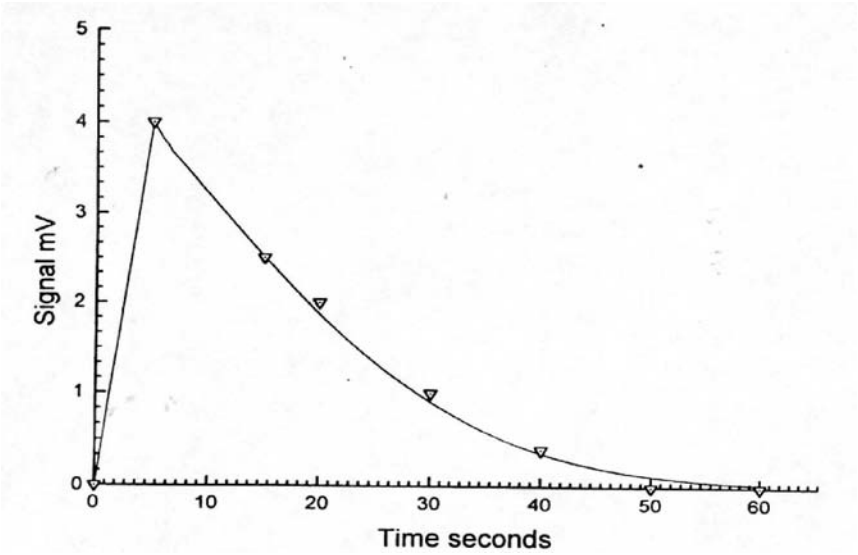

***Figure 3.13 Creep-up as found by Ramani* et al [62]**

(with permission from Elsevier)

They reported this effect for MOSFETs having accumulated dose ≥ 20 Gy and it has been found to be important during low-dose-rate, long-time-scale measurements [11].

3.8.3 *Reading interval*

Very little has been reported in the literature regarding reading interval response, i.e. how often repeated ‘read’ cycles are performed, and that reported has related to T&N MOSFETs only. Bower and Hintenlang [78] found an increase in ΔV_{th} following an irradiation of 7 MV X-rays when 27 readings were taken in 15 minutes, compared to 6 readings in 15 minutes. As will be described in section 5.3.1, the data obtained for measurements of

drift following a single irradiation during the current work indicated the need for further investigation of drift effects due to taking frequent readings.

3.8.4 Reading delay

In the clinical situation, there could be delays between taking a pre-irradiation reading and the actual irradiations, due to, for example, the radiation therapist needing to adjust the patient set-up, or being interrupted in some other way. As is the case for reading interval response, very few workers have reported investigations of reading delay response of MOSFETs, and none using Wollongong MOSFETs. Peet and Pryor [7] found an increase of 0.2 mV/cGy in sensitivity when a MOSFET was exposed every 15 minutes, but the post-irradiation readings were delayed for 2½ hours, compared with another MOSFET which was similarly exposed, but read-out immediately after each irradiation. Dong *et al* [55] investigated drift up to 15 minutes after irradiation exposure, with different read-out intervals between zero and 15 minutes, and found a slight tendency for ΔV_{th} to increase with time, but results were within 3% of initial ΔV_{th}.

3.9 Angular dependence

Since 1988, it has been known that MOSFETs were anisotropic, due to the different beam attenuation properties of their components, such as the metallic leads, substrate, gate and insulating covering [61]. Many reports have been made of variations in response for different orientations of MOSFETs to the incident radiation beam [5, 25, 78-81]. Many of these relate to model T&N MOSFET (TN-RD-502 with the TN-RD-50 dosimetry system), prior to 1999, when an isotropic version was introduced. Variations in response with angle of radiation incidence of up to 17% over 360^o [82], 28% for $0–180^o$ [61, 62] and 7% for $0\text{-}90^o$ [1] have been reported for the standard version MOSFET, but variations within 3% over the full 360^o range have been reported for the isotropic version [69, 83, 84]. Using Wollongong MOSFETs, Quach *et al* [25] reported angular response within 3% inside a 10 cm cylindrical phantom for 0^o – 180^o for 6MV linac irradiation.

4. EQUIPMENT AND METHOD

4.1 MOSFET system description

The commercially-available "*Clinical MOSFET Semiconductor Dosimetry System"* used for this work comprises a 5-socket reader unit, an Interface Unit, an Active Bias Unit and associated auxiliary cabling, and is battery-operated (figure 4.1).

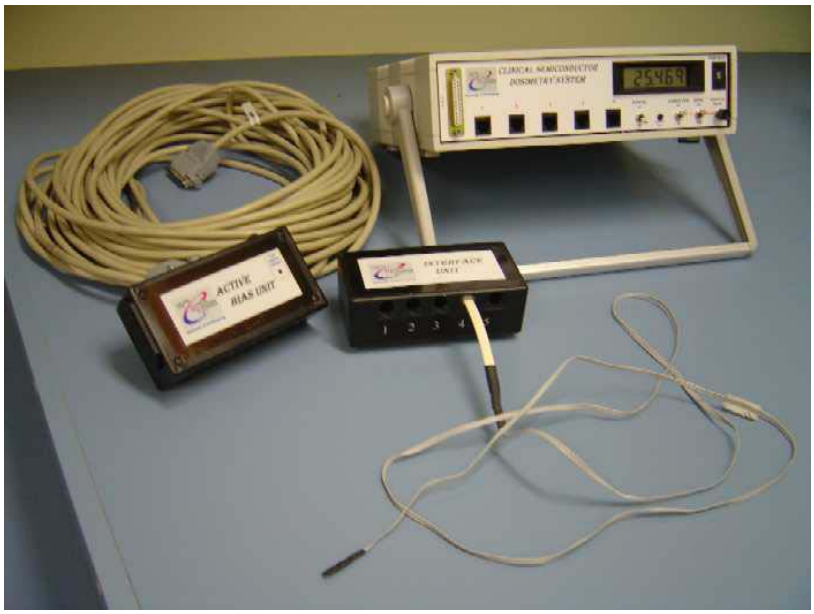

Figure 4.1 MOSFET reader unit with associated hardware. Readings can either be taken on-line via the cable and Interface Unit, or the Active Bias Unit can be used off-line

The reading indicated by the unit is the source-gate voltage (-V) which will allow a specified source-drain current to flow (see section 2.3). The specific current is commercially-confidential to CMRP, and cannot be disclosed herein.

The system is capable of providing "on-line" readings either manually or automatically, as well as "off-line" readings. In automatic mode, readings can be viewed in real-time and saved directly to computer via an RS232 connection, using MosPlot™ software also developed by the CMRP. In "off-line" mode, the probes are connected to the Active Bias Unit during irradiation and connected to the reader for readout at a later time. For the current work, the readings were taken "on-line" with manual readings, with the probes being connected via the Interface Unit located inside the bunker to the reader in the console area via auxiliary cable. Future work

is proposed to investigate any difference in response of the system using the automatic and off-line modes.

The MOSFETs used in this work have a sensitive volume of typically 1 x 200 x 200 microns, or 4 x 10^{-5} mm^3, with a thick gate oxide (about 1 micron). As mentioned in section 3.5, single high sensitivity (low dose) and dual sensitivity (high or low dose) MOSFETs were used for the current work. In this thesis, the dual sensitivity probes will be denoted with the particular sensitivity option used, e.g. #D12 (low) or #D12 (high) for high and low sensitivity types R and K respectively. The system is operated with applied gate bias of +5V and +12V for the R- and K-type MOSFETs respectively [85] and their respective operating voltage ranges are 9 – 24V and 3 – 16V [86]. A +5V operating bias corresponds to sensitivity of about 5 mV/cGy for measurements in a solid water® phantom under a 6MV linear accelerator (linac) beam at D_{max} [6].

Preliminary readings during familiarisation of the system had shown quite large variations in ΔV_{th} for the same delivered dose. Advice from CMRP was that the reader could be subject to electrical interference from other electrical equipment such as computers, console and Visual Display Units, as well as slight temperature fluctuations. Henceforth, an earth cable was attached to the reader, and all readings were taken with the unit at least 1 metre away from other electrical equipment.

4.2 Measurement setup

The reader unit was given warm-up time of at least 30 minutes (min) before measurements began, and the linear accelerators were warmed up by beaming-on to deliver at least a 10 Gy dose. All measurements were taken at ambient temperature of 22 – 23^{o}C. Prior to each set of measurements, repeated readings were taken until the system had stabilised, to ensure thermal equilibrium of the probe-reader-system had been reached. Unless otherwise stated, readings were taken immediately prior to, and following, irradiation, and at least one minute was allowed between reading sets, as recommended by CMRP. Throughout this thesis, reference to “immediate” readings means readings of V_{th} were made within 1 second (s) of beam on (pre-irradiation) or beam off (post-irradiation).

Twenty-three single and 15 dual sensitivity probes were used for this work. Measurements were taken for exposures to 4MV and 6MV X-ray beams from radiotherapy linear accelerators (Varian Clinac® 4/100 and 6/100) with doses per fraction between 5 and 140 cGy for the high sensitivity probes, and between 50 and 500 cGy for the low sensitivity probes. The system's developers recommend calibration doses of 10 and 20-30 cGy for the high and low sensitivity probes respectively. The initial V_{th} varies for each individual probe due to processing variations, so each probe was calibrated individually to determine its initial sensitivity.

For measurements other than for investigation of response variation with angle of incidence of the beam with respect to the sensitive volume ("angular dependence"), the probes were placed between sheets of solid water® (Gamma RMI). To minimise air gaps, the probes were laid in dental wax channels conforming to their shape, either singly or side by side if two probes were irradiated together, with the sensitive volume (commonly called "bubble side" or "epoxy bubble") facing towards the beam, at the isocentre. Solid water® "build-up sheets" were placed on top of the dental wax to provide electronic equilibrium, so that the effective point of measurement of the probe was at D_{max}. (For IVD use, electronic equilibrium could be achieved by using appropriate bolus or build-up caps.) In all cases (except for angular dependence investigations), the set-up was as follows:

Source to phantom surface distance	:	100 cm
Field Size	:	10 cm x 10 cm
Phantom thickness for backscatter	:	≥ 5 cm
Phantom thickness for buildup	:	1.0 cm for 4MV and 1.5 cm for 6MV beam

The standard equipment set-up is shown in figure 4.2, with the build-up sheets removed.

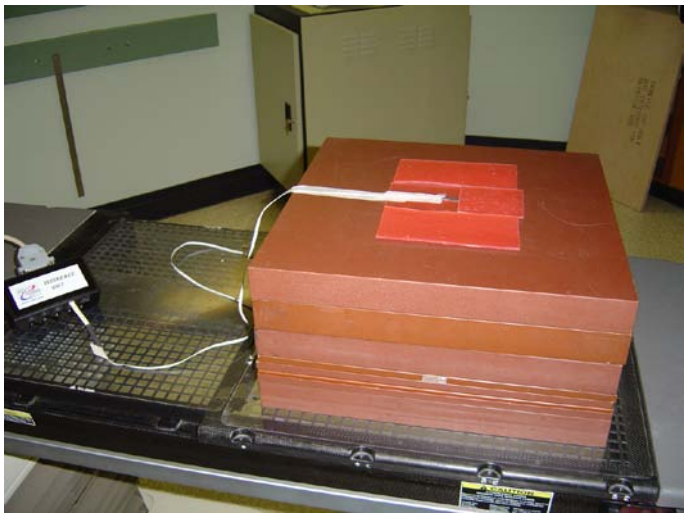

Figure 4.2 Probe in dental wax channel on solid water®, connected via the Interface Unit to the reader in the console area. (Build-up sheets removed to show the probe placement)

For angular dependence measurements, each probe was placed in a channel inside a custom-built cylindrical perspex phantom measuring 10 cm long with a diameter of 9 cm (figure 4.3). This phantom was placed vertically inside a custom-built circular stand, so that the cylinder could be easily rotated about its axis by hand (a non-slip mat was placed on the couch top under the holder, to alleviate slipping during phantom rotation). The stand was marked at intervals of 15 degrees. The cable between the probe and the Interface Unit exited the top of the phantom.

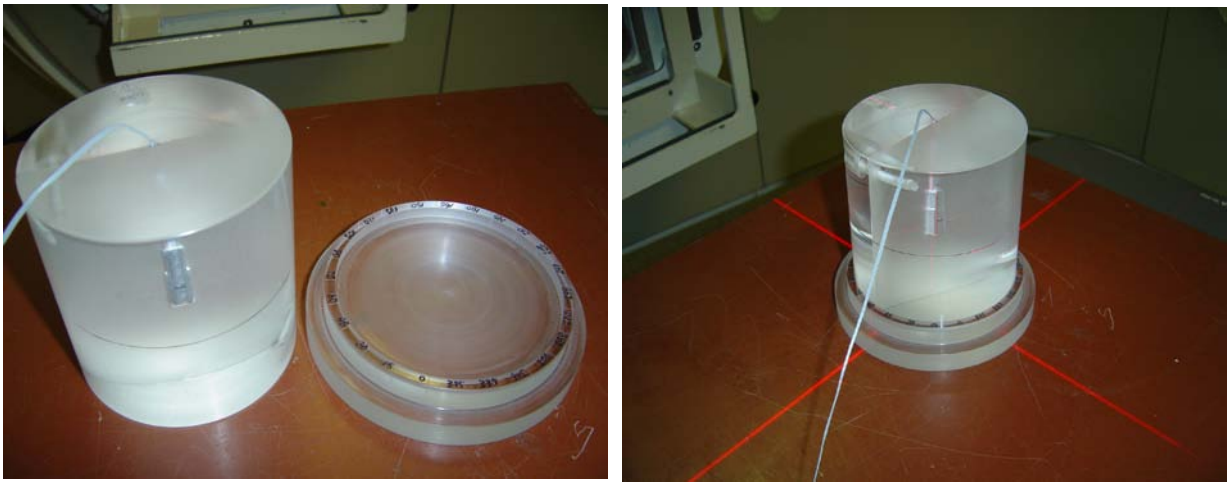

Figure 4.3 Custom-build perspex phantom and stand used for angular dependence measurements

The channel in the phantom was made such that the probe's sensitive volume could be easily seen. Its location was marked externally with a line around the phantom's circumference, to assist with placement.

Each probe was positioned with its sensitive volume at the isocentre, initially with the epoxy bubble facing towards the beam with the gantry set at 270^o. While the gantry was fixed at 270^o throughout the experiment, the phantom was rotated manually in its stand in 30^o increments. The 0^o/360^o position was defined as the epoxy bubble facing towards the gantry. A field size of 12 cm x 12 cm was used so that the entire phantom was within the radiation field. Threshold Shift was determined for each position from readings immediately prior to and following irradiation at each position.

4.3 Error analysis

The factors contributing to errors in this work are the precision of the reader system, temperature fluctuations and setup errors. The precision of the system for each reading of V_{th} is given by CMRP as ± 1 mV, therefore, throughout this work, each stated value of V_{th} should be understood as being ± 1 mV, and of ΔV_{th} as being ± 2 mV. This uncertainty becomes important for low delivered doses for statistical reasons, for example, uncertainty for ΔV_{th} of 100 mV will be 4%. The epoxy covering acts as an insulator to the sensitive area of the MOSFETs and ambient temperature, T, fluctuated during short measurement sets by≤ 0.5 ^{o}C, corresponding to variations in V_{th} of ±1 mV [59]. Uncertainty in ΔV_{th} due to temperature variations during extended measurement sets (several hours) is estimated at ± 2 mV. Setup errors for the angular dependence, $\angle$, are estimated at ± 2^o. Total uncertainty in measurements of dose, *D*, is therefore:

$$\sigma D = \sqrt{\left(\frac{\partial D}{\partial \Delta V_{th}}\right)^2 \sigma^2 \Delta V_{th} + \left(\frac{\partial D}{\partial \Delta V_{th,ref}}\right)^2 \sigma^2 \Delta V_{th,ref} + \left(\frac{\partial D}{\partial D_{ref}}\right)^2 \sigma^2 D_{ref} + \left(\frac{\partial D}{\partial T}\right)^2 \sigma^2 T + \left(\frac{\partial D}{\partial \angle}\right)^2 \sigma^2 \angle}$$

4.4 Measurement Methods

The MOSFETs were characterised in terms of their sensitivity (defined as ΔV_{th}/cGy), useful lifetime, linearity with delivered dose, drift effects and angular dependence. Although it was intended to investigate other influences on MOSFET response, such as energy, temperature and field size dependence and any impact of beam modifiers such as photon wedges or shielding blocks, variations in response with different reading methodologies prompted the greatest emphasis to be on drift response.

4.4.1 ΔV_{th}, sensitivity and saturation

Characterisation of the Wollongong MOSFETs with regard to sensitivity reduction with accumulated dose was carried out by using six single and four dual (low) sensitivity probes. These were characterised for ΔV_{th} vs V_{th} and sensitivity over their lifetime.

Each probe was repeatedly exposed to the same dose of 20 cGy or 50 cGy of 4MV or 6MV X-rays. Between 1 and 1½ min were allowed between a post-irradiation reading and the next pre-irradiation reading. Readings were taken immediately prior to, and following, irradiation. Appendix A1 describes the methods of correction for sensitivity reduction with accumulated dose. To determine the useful lifetime of the MOSFETs, ten single sensitivity and 5 dual sensitivity (low) probes were used during these and other tests until they saturated.

4.4.2 Linearity

Dose response linearity testing was carried out for doses up to 5 Gy. This dose limit was chosen because most external radiotherapy treatments are prescribed at less than 5 Gy per fraction.

Linearity was measured by comparison of ΔV_{th} vs delivered dose using four single and two dual sensitivity (low dose) probes. Various doses were delivered of 4MV radiation ranging between 5 cGy and 140 cGy (single probes) or 50 cGy and 500 cGy (dual probes). Very low doses (5 and 10 cGy) were included in order to determine the "cut-off" dose below which measurements should not be made due to large statistical uncertainties. Six trials were performed, with 1 – 1½ min allowed between post- and next pre-irradiation readings, unless otherwise indicated below. Appendix A2 describes the methods of correction for sensitivity reduction with accumulated dose. Different reading methodologies were trialled, as outlined below, to investigate any influence of:

- different waiting periods between readings (Trials 1 and 2) to determine an appropriate time to allow between consecutive exposures;

- the order of taking readings in respect to the delivered dose, i.e. any hysteresis effect depending on whether delivered doses were increasing or decreasing during the trial;

and to compare the responses of the single and dual sensitivity (low) probes (Trials 3-6).

(Note: During familiarisation with the MOSFETs, when two probes had been irradiated together, it was noticed that the order of taking pre- and post-irradiation readings had influenced the ΔV_{th} measured (see section 4.4.3.4). Therefore, for Trials 1 and 2, readings were taken in the same order pre- and post-irradiation, to avoid this effect, i.e. probe 1 was read before probe 2, both before and after irradiation.)

Trial 1

Two single sensitivity probes irradiated together, with 1 - 1½ min between a post- and the next pre-irradiation reading. Measurements were made in one set, with consecutive irradiations from 5 to 100 cGy.

Trial 2

The same two probes and method as in Trial 1, but with 2 - 2½ min between readings.

Trial 3

Using a single sensitivity probe, two reading sets were taken consecutively (from 5 to 120 cGy, then vice versa), and the equivalent readings of each set for each dose were averaged.

Trial 4

Using a single sensitivity probe, two reading sets were taken consecutively (both from 5 to 140 cGy), and the equivalent readings of each set for each dose were averaged.

Trials 5 and 6

Using two dual (low dose) probes, two reading sets were taken consecutively (from 50 to 500 cGy, then vice versa), and the equivalent readings of each set for each dose were averaged.

4.4.3 Response drift

4.4.3.1 Drift following an irradiation

As previously mentioned, MOSFETs "store" dosimetric information, in the sense that the V_{th} for the most recent exposure is not erased through readout, and therefore dose may be verified, if necessary, at some later time, however, the inherent post-irradiation drift in V_{th} must be accounted for in any later reading. This drift can be characterised by exposing a MOSFET and taking subsequent periodic readings to obtain "drift curves" of V_{th} or sensitivity vs time after irradiation. However, the usefulness of these drift curves is limited to estimating ΔV_{th} for times greater than approximately 8 hours, when the drift is linear with ln (t/t_o) (see section 3.8.1).

As well as long-term drift, the current work was aimed at characterising short-term drift, particularly during the first seconds-minutes of irradiation. Three probes were used in eight trials. In each trial, a MOSFET was irradiated to a known dose of 4MV X-rays, after which random intermittent readings were taken for periods of up to 93 hours, without further irradiation. Post-irradiation readings were taken at intervals between 1 s and 30 min, as shown in table 1.

Set #	Date	Probe #	Accumulated Dose (Gy)	Delivered Dose (cGy)	Time after irradiation during which readings were taken	Reading intervals
1	3/5/02	1	13.3	50	1 m to 74.5 hrs	1 s – 5 m
2	3/5/02	1	13.8	50	30 s to 35.25 hrs	1 – 40 s
3	3/5/02	1	14.1	30	30 s to 19 m	1 – 30 s
4	3/5/02	1	14.4	30	30 s to 10 m	1 – 30 s
5	26/6/02	1	24.9	20	5 s to 24.1 hrs	5 s – 30 m
6	15/7/02	5	37.7	100	0 s to 93 hrs	5 s – 30 m
7	20/10/03	D12 *	27.7	100	0 s to 49.25 hrs	10 s – 15 m
8	23/10/03	D12 *	28.7	100	0 s – 30 hrs	15 m

* low dose

Table 1 Readings taken to investigate drift following single exposures

The reading timeline is shown below.

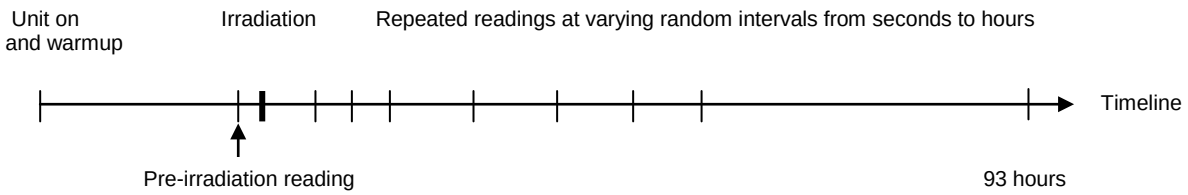

Various doses (20, 30, 50 and 100 cGy) were given to investigate any delivered dose effects. Probes having different accumulated doses at the commencement of the trials were used to examine any accumulated dose effects on drift. Differing reading intervals were chosen to investigate how reading frequency may affect post-irradiation drift.

Table 2 shows the reading intervals for each of the 8 sets, up to 20 min after irradiation, which period was investigated in depth.

4.4.3.2 Creep-up

Creep-up is defined as:

$$\left(\frac{\Delta V_{th}(t) \quad - \Delta V_{th}(0)}{\Delta V_{th}(0)} \right) * 100 \quad \text{.....} \textit{(4.1)}$$

where $\Delta V_{th}(0)$ is the shift measured immediately following irradiation, and $\Delta V_{th}(t)$ is the shift measured at some later time, t, where t is between 2 and 500 s. Creep-up has been reported to affect MOSFETs with > 20 Gy accumulated dose.

It was important to characterise creep-up for the Wollongong MOSFETs in order to determine an appropriate read-out methodology to use clinically, in particular, the minimum time between repeated irradiations to allow for “relaxation” of the system, that is, for the V_{th} drift from the previous irradiation not to influence subsequent exposures, in which case ΔV_{th} would not only reflect the shift caused by the irradiation, but also include drift, and lead to inaccurate dose determination.

Set #	Probe and Dose	Minutes after irradiation
		1 2 3 4 5 6 7 8 9 10 11 12 13 14 15 16 17 18 19 20
1	#1, 50 cGy	1 2 3 4 5 6 7 8 9 10
2	#1, 50 cGy	1 2 3 4 5 6 7 8 9 10 11 12
3	#1, 30 cGy	1 2 3 4 5 6 7 8 10 12 20 30
4	#1, 30 cGy	1 2 3 4 6 8 10 12 20 30
5	#1, 20 cGy	5 10 15 30
6	#5, 100 cGy (1)	5 10 15
7	#D12(low) 100 cGy (2)	10 30
8	#D12(low) 100 cGy (3)	900

Table 2 Reading intervals (s) up to 20 min for investigation of short-term drift following a single irradiation

To investigate this effect, three single sensitivity MOSFETs having accumulated dose greater than 20 Gy (20.8, 24.8 and 26.3 Gy respectively) were studied. Each detector was exposed to a dose of either 20, 50 or 100 cGy, to investigate whether creep-up was influenced by delivered dose. The pre-irradiation readings were taken immediately prior to exposure. Two post-irradiation readings were taken following each exposure – the first reading immediately, then a second reading after a time interval, similar to the method of Ramani *et al* [62]. This process was repeated, expanding the time intervals between the two post-irradiation readings from 1 s up to 5 min. Three extra reading sets were taken in reverse time order, (from 5 min down to 2 s), to investigate hysteresis effects. The reading timeline is shown below.

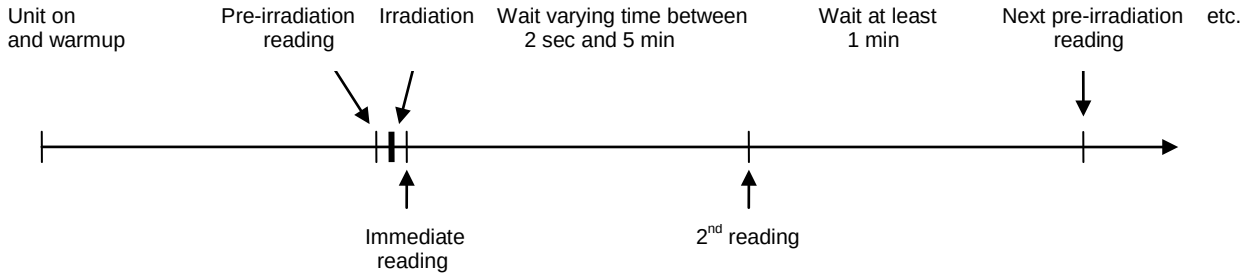

4.4.3.3 Reading interval

The results from the investigation of drift following a single irradiation (see section 5.3.1) indicated a "reading interval effect", that is, ΔV_{th} drift with time was greater when readings were taken more often. It was important to further investigate this effect, including whether it was related to accumulated dose and/or delivered dose, since the reading interval would be an important factor in characterising and correcting for short-term drift. It was also important in order to determine an optimum time interval to allow between a series of consecutive readings, for example to monitor dose during total body irradiations.

With this aim, two probes were used - one probe having no accumulated dose, and the other with accumulated

dose > 28 Gy, termed “new” and “old” MOSFET respectively. To investigate any delivered dose effect, each probe was exposed to separate doses of 20, 30, 50 and 100 cGy. Each probe was irradiated in five measurement sets A to E, as shown in table 3.

Set	Minutes after irradiation				
	1	2	3	4	5
A	5s	10s	15s	30s	
B	10s				
C	5s	10s			
D	1s	2s	3s	4s	6s	8s	10s
E	1s	2s	3s	4s	5s

Table 3 Reading interval measurement sets

Each irradiation was followed by repeated readings at different set intervals up to 5 min after the exposure. For example, for set A, readings were taken every 5 s during the first minute, then every 10 s for the next minute, then every 15 s for the next 2 min, ending with every 30 s during the 5th minute after irradiation. This method was repeated for each delivered dose for each probe. The reading timeline is shown below for set A.

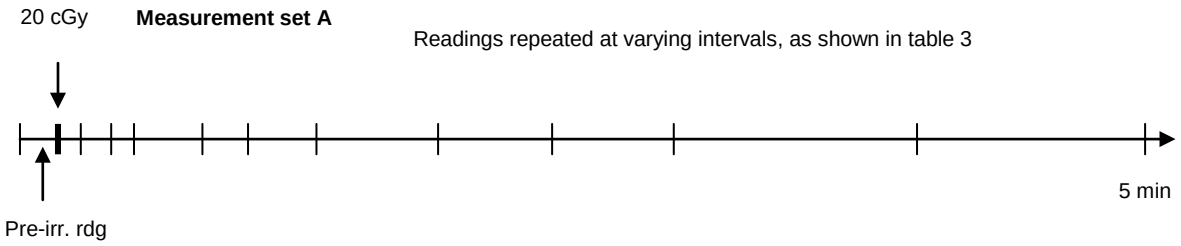

After waiting at least 1 minute, measurement set B was performed, followed by sets C, D and E for 20 cGy doses. This procedure was repeated for doses of 30, 50 and 100 cGy. The 5 measurement sets for each of the 4 doses were performed for both the "new" and "old" probe. The data were corrected for sensitivity reduction with accumulated dose during the measurement period as described in Appendix A1.

In analysing the results of these data sets, a comparison was made of the percentage drift in ΔV_{th} between readings taken immediately, and those taken at 5 min following each irradiation, for each reading interval set and delivered dose, for the new and old probe. The reading interval data sets were analysed using equation 4.2:

$$\left(\frac{\Delta V_{th}(5\min) - \Delta V_{th}(0)}{\Delta V_{th}(0)} \right) * 100 \quad \text{.....} \textit{(4.2)}$$

4.4.3.4 Reading delay

The results of measurements taken to investigate reading interval effect (section 5.3.3) also indicated a "reading delay effect" (increased ΔV_{th} when there was a delay between irradiation and readings). Also, during familiarisation with the system, two "new" (unexposed, V_{th} ~10V) probes had been exposed simultaneously with 11 irradiations between 5 and 100 cGy dose. Pre- and post-irradiation readings were taken immediately. When one probe was read out first pre-, but second post-irradiation, i.e.

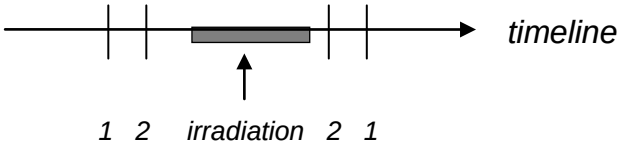

it was observed that probe 1 consistently measured greater ΔV_{th} than for probe 2, by up to a maximum of 13 mV (2.6%) for the 100 cGy dose. The average difference between the two probes was 6 mV (1.9%). This was although the time difference between reading the probes was only of the order of a second. To confirm this apparent effect, measurements were repeated with the probes read in the *same* order pre- and post-irradiation, with the result that the average difference in ΔV_{th} between the two probes was reduced to 0.3%.

These results suggested that the drift during even a delay of a few seconds could be significant, and required further investigation of the reading delay response. This response could be significant in practical situations where there was a delay between reading and irradiation. Similarly, if the system was used off-line via the Active Bias Unit, there would be a delay between irradiation and post-irradiation reading, due to the disconnection of the probe from the Bias Unit and its placement into the reader. In this situation the accuracy of ΔV_{th} measurements, and consequently dose determination, will be less due to drift during the delay period, as compared to calibration measurements taken with no delay between irradiation and readings. There could be delays between readings before or after irradiation, or both.

The reading delay response was investigated by making repeated exposures, and delaying the time between irradiation and pre- or post-irradiation reading by a variable time interval between immediate (< 1 s) and 120 s, and comparing the ΔV_{th} to that obtained for the immediate reading. Measurements were obtained for delays between (i) pre-irradiation reading and irradiation; (ii) irradiation and post-irradiation reading; and (iii) the same time delay both pre- and post-irradiation (see hereunder for reading timelines).

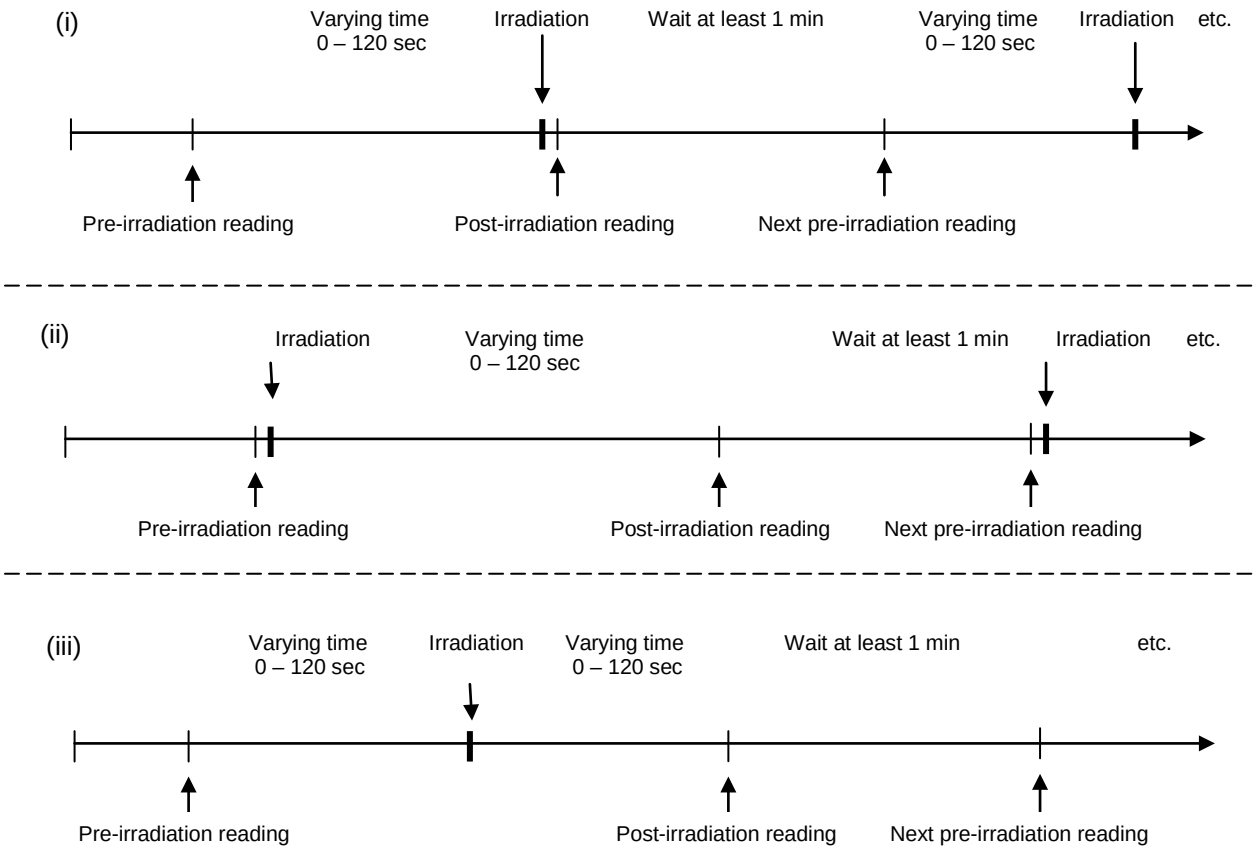

In trial (i), the post-irradiation reading was taken immediately after irradiation, whilst in trial (ii), the pre-irradiation reading was taken immediately prior to irradiation. For one of the MOSFETs (#9), delays of the same period both pre- and post-exposure were allowed (trial (iii)).

Read-out delay response was defined as:

$$\left(\frac{\Delta V_{th,delay} - \Delta V_{th}(0)}{\Delta V_{th}(0)} \right) * 100 \quad \text{.....} \textit{(4.3)}$$

Six single sensitivity probes and two dual (low) sensitivity probes were used, with delivered doses of 20 or 50 cGy, in thirteen trials using 4MV x-rays. A dependence of the drift on the accumulated dose to the probes was also explored by exposures of two probes (#9 and #10) at different stages of their lifetime. Appendix A1 describes the correction method for accumulated dose sensitivity reduction during the measurement period.

4.4.4 Angular dependence

For measurements of angular dependence, two single and one dual (low) sensitivity probes were used. For each set of measurements, repeated irradiations were made with different angles of beam incidence to the probe, by manual rotation of the phantom (section 4.2) in its holder. A set-up error of ± 2^o is estimated.

Two probes were exposed to 4 MV x-rays and one probe to 6MV x-rays with 50 cGy doses. In each trial, two consecutive sets of readings were taken, and an average of the two sets was obtained. In two of the trials, rotations were made clockwise, and in the third, rotations were anti-clockwise for comparison.

The data were corrected for sensitivity reduction with accumulated dose as described in Appendix A3. Variation in ΔV_{th} due to angle of incidence of radiation is defined as:

$$\left(\frac{\Delta V_{th,\Phi} - \Delta V_{th,0}}{\Delta V_{th,0}} \right) * 100 \quad \text{.....} \textit{(4.4)}$$

where $\Delta V_{th,0}$ is the shift for incident beam angle of 0^o/360^o, and $\Delta V_{th,\Phi}$ is the shift measured at other angles.

5. RESULTS AND DISCUSSION

5.1 ΔV_{th} and sensitivity

The results of the measurements of ΔV_{th} and sensitivity with accumulated dose for each probe over its lifetime were graphed to obtain "drift equations". Figure 5.1 shows the changes in (a) ΔV_{th} and (b) sensitivity for four probes exposed to repeated irradiations of 50 cGy (#7 and #8) or 20 cGy (#13 and #14).

Figure 5.2 shows characteristic ΔV_{th} drift for delivered doses of 20 and 50 cGy. This response drift is comparable with that reported in the literature for MOSFETs with similar bias [46, 47], and is due to increasing positive charge trapping in the SiO_2 with increasing irradiation, which leads to a reduction of the electrical field in the gate oxide. Also, the density of (positive) interface states increases with accumulated dose [87]. The relative drift was independent of x-ray energy (4 MV or 6 MV).

(a)

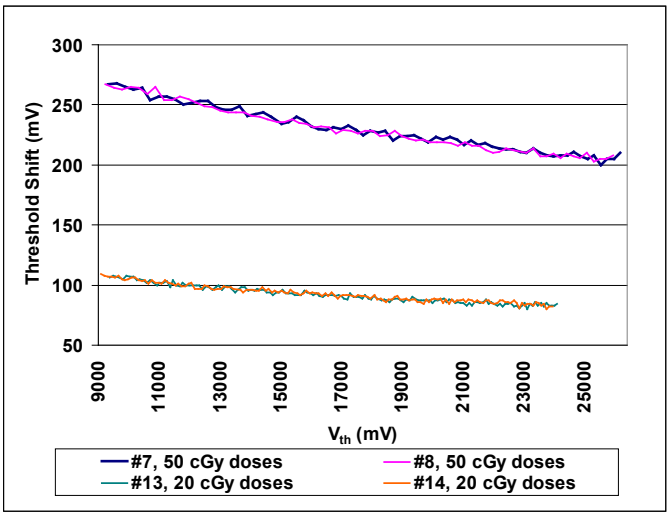

(b)

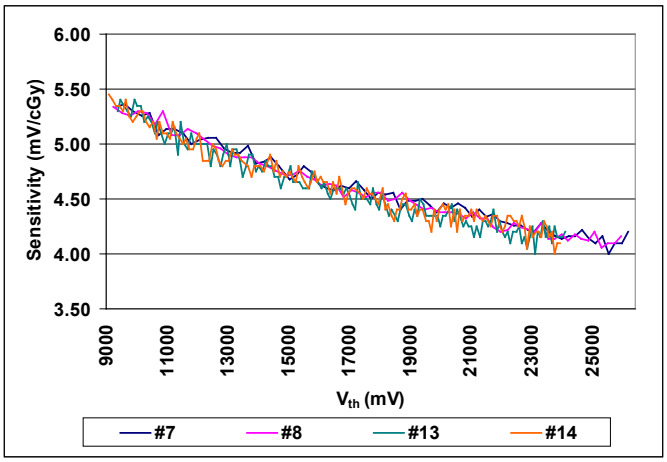

Figure 5.1 (a) ΔV_{th} and (b) sensitivity over lifetime of four probes for repeated exposures of 50 cGy (#7, #8) or 20 cGy (#13, #14)

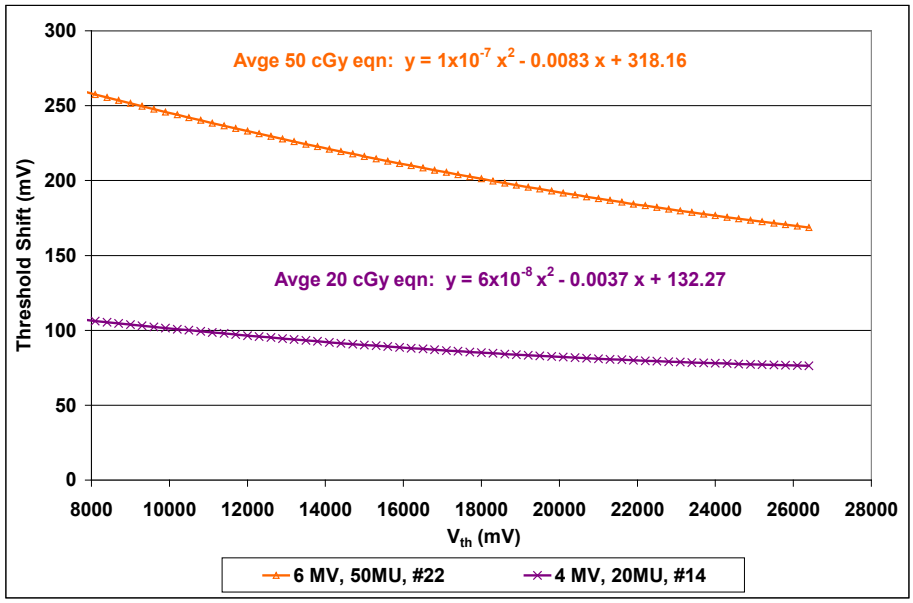

Figure 5.2 Average ΔV_{th} drift equations for 20 and 50 cGy doses

All the probes tested exhibited almost the same sensitivity drift with accumulated dose, regardless of energy of the radiation, or whether the probe was single or dual sensitivity. This may not be the case for kV energies where the photoelectric effect has a greater role in x-ray interactions with matter. The sensitivity over the lifetimes of the probes decreased by an average of 22.37% with a standard deviation of 0.63%, or 1.3% per change of 1V in V_{th}. It was found that quadratic equations provided the best fit over the lifetime of the probes, however, over a 4-5 V range, the sensitivity decrease can be approximated by a linear reduction in response within the uncertainty of measurements made, as shown in figure 5.3. The sensitivity drift equations for the probes are tabulated at Appendix C. An average sensitivity drift equation for the probes tested can be given by:

$$y = 3 \times 10^{-9} x^2 - 0.0002 x + C \quad \text{.....(5.1)}$$

where y = sensitivity (mV/cGy) and x = V_{th} (mV) and C is the initial threshold voltage prior to any exposure of a probe (figure 5.3). This sensitivity can be used to determine dose (CF in equation 3.5).

These results indicate a reproducible reduction in ΔV_{th} and sensitivity over the lifetime of the probes, provided measurements are taken in a way which is consistent with the calibration procedure from which the drift equation was obtained.

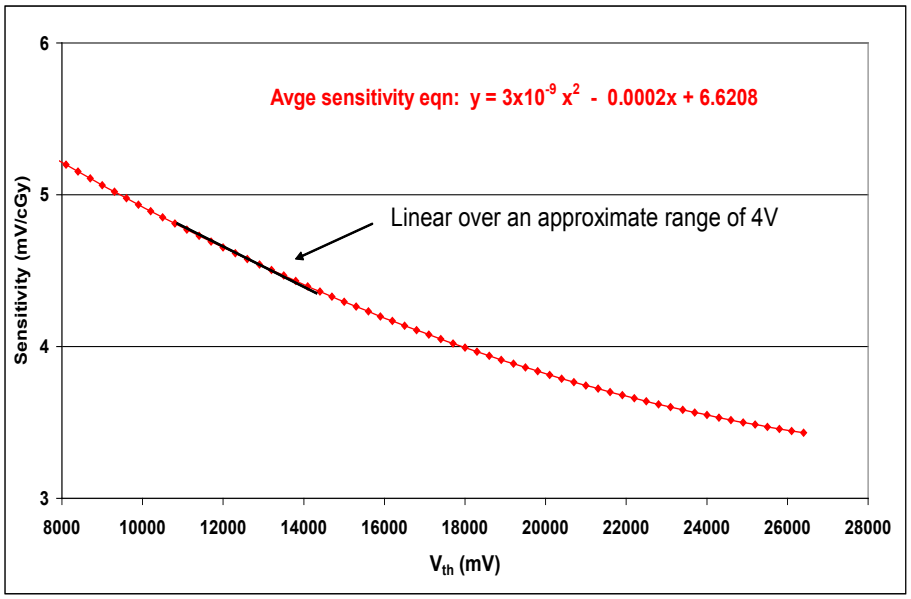

Figure 5.3 Average sensitivity drift equation for ten probes tested

5.1.1 Saturation

As described in section 3.6, saturation will occur when all available traps have been filled, and the oxide electric field vanishes when the charge density on the gate equals the trapped oxide and interface charge density, so that transport of holes through the oxide ceases. The saturation electric field has been determined as 10^6 V/cm [22]. In the current work, saturation was observed as a sudden decrease in ΔV_{th} for a given dose, compared to previous shifts for that dose (see figure 5.4). This figure is representative of the effect for all probes tested.

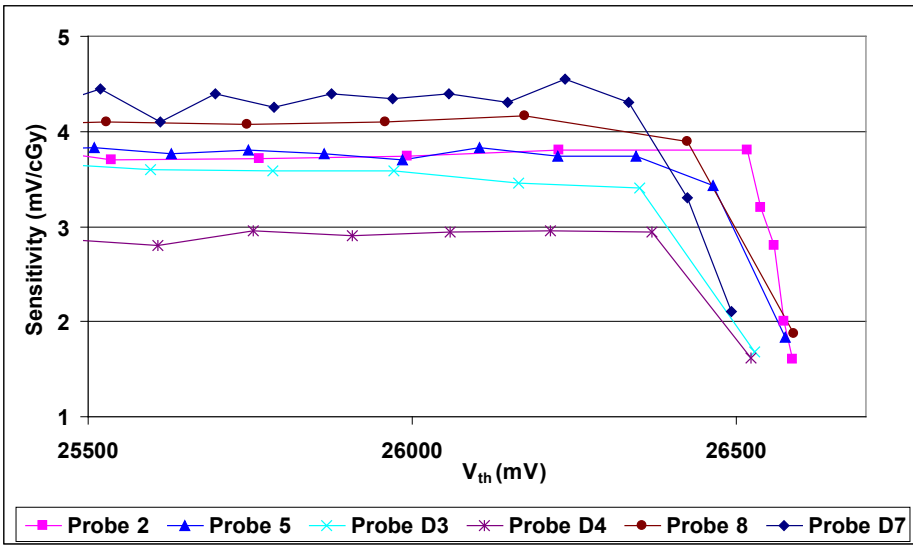

Figure 5.4 MOSFET saturation

Saturation occurred for the probes tested as shown in Table 4:

Single sensitivity probes			Dual sensitivity probes (low)		
Probe No.	**Reading (± 2mV)**	**Accum. Dose Gy**	**Probe No.**	**Reading (± 2mV)**	**Accum. Dose Gy**
1	26830	41.9	D3	26613	40.5
2	26596	39.5	D4	26604	49.0
4	26571	37.7	D7	26535	35.0
5	26630	47.0	D8	26332	35.8
6	26618	37.7	D9	26550	36.6
7	26608	36.5	D11	26499	37.0
8	26683	36.5			
20	26500	40.5			
22	26599	37.5			
Avge:	26626	39.4		26522	39.0
Std. Dev:	90	3.38		100	5.26

Table 4 Probe saturation V_{th}

These results indicate that the useful lifetime of single sensitivity MOSFET probes or dual MOSFETs used only in high sensitivity mode is approximately 39 Gy or V_{th} of approximately 26.5 V. The accumulated dose to reach saturation varies since each individual probe has a different initial V_{th}. None of the low sensitivity probes were used to saturation during this work, and an investigation of their lifetime is proposed in future.

5.2 Linearity

The raw data were corrected for sensitivity reduction with accumulated dose as outlined in Appendix A 2, and a constant temperature was maintained throughout these tests. A summary table of results is included at Appendix D. The deviations from proportionality were normalised to the results for doses of 50 or 250 cGy for the single and dual (high) probes respectively. Figure 5.5 shows the measured deviations from proportionality.

The range of deviations from proportionality for all probes over all doses was ± 7.6%, although these figures included the lowest doses (5, 10 and 20 cGy for the single probes, and 50 c Gy for the dual (high) probes), where a change of 1 or 2 mV statistically leads to a greater percentage variation due to the small shifts. Disregarding these lowest doses, the overall linearity for all probes was within 1.2%.

The single sensitivity probes were linear within 1.6% for doses between 5 and 140 cGy, and of the dual (high) probes, for doses between 50 and 500 cGy, was within 3.8%. Disregarding the lowest doses as abovementioned, the respective linearities are within 1.4% and 1.5%.

(a)

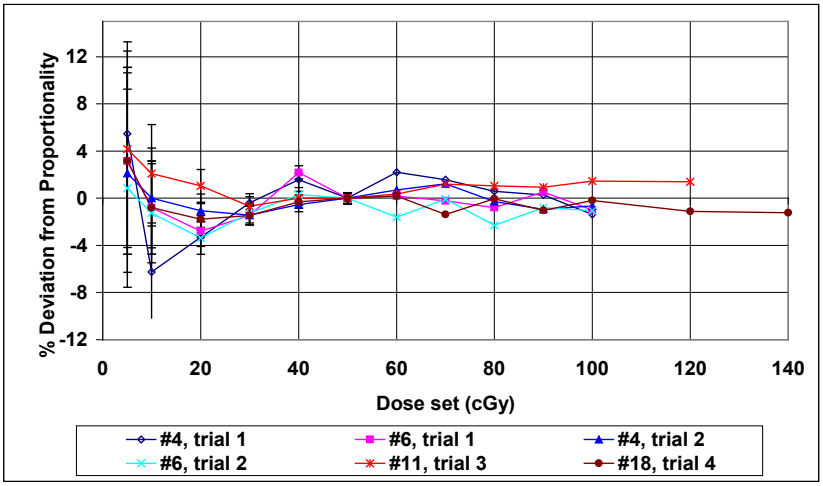

(b)

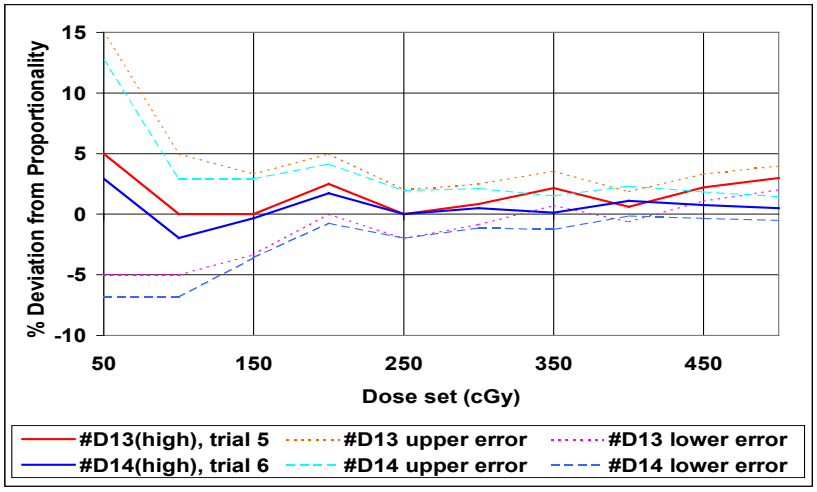

Figure 5.5 Percentage deviations from proportionality for (a) single sensitivity and (b) dual (low dose) probes

Results for Trials 1 and 2 (probes #4 and #6) indicate slightly greater average variations when 2 – 2½ min were allowed between readings, than when the waiting period was 1 – 1½ min. The respective readings were 0.0% cf -0.1% for #4, and –0.1% cf –1.0% for #6. This indicates that no benefit is achieved in waiting longer than 1 – 1½ min between consecutive readings. Trials 3-6 indicated there was no significant reading order effect (as regards increasing or decreasing delivered doses), nor difference in response between the single and dual sensitivity probes. In summary, the MOSFETs showed good linearity with dose, except for very low doses as mentioned above, for doses of up to 140

cGy for the low dose probes, and 500 cGy for the high dose probes. It is therefore concluded that the minimum doses to be measured by the single and dual (high) probes should be 30 cGy and 100 cGy respectively.

5.3 *Drift response*

5.3.1 *Drift following an irradiation*

Figure 5.6 shows the typical post-irradiation drift curves of the MOSFETs used for this work. An initial rapid increase in ΔV_{th} is apparent, followed by a plateau, then a gradual decrease. These curves are characteristic of all MOSFETs and are the result of the continued build-up then discharge of interface states and other contributing factors mentioned in section 3.8. The difference in ΔV_{th} between sets 6, 7 and 8 is due to the greater accumulated dose (and hence less sensitivity) of the probe used for set 6.

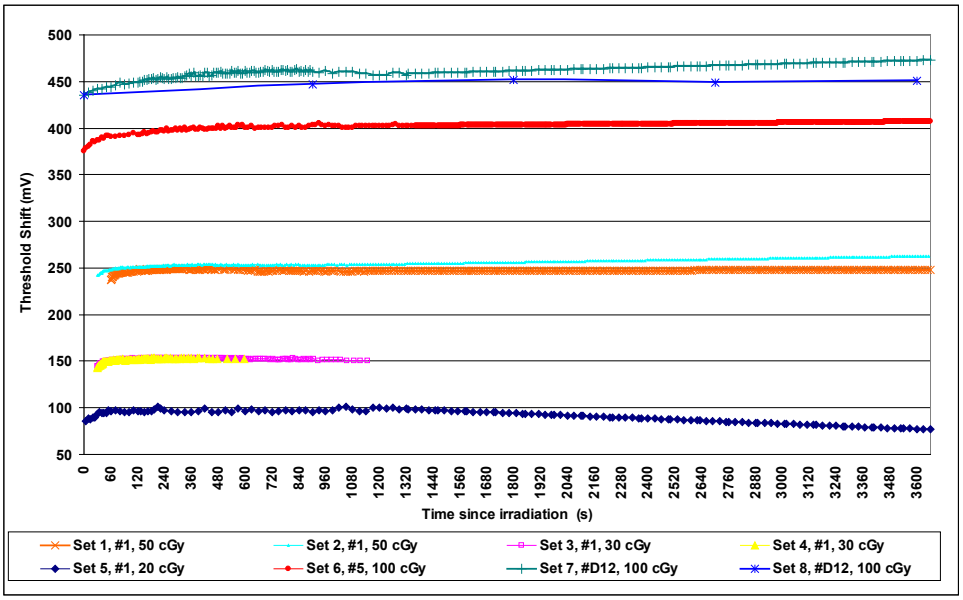

Figure 5.6 Drift up to 1 hour following single 4MV irradiations

The drift curves were analysed in terms of:

- time taken for the plateau to be reached;
- reproducibility within the plateau period; and
- maximum drift from the initial reading of ΔV_{th}

and any dependence of these factors on delivered and accumulated dose, or readout interval. Table 5 shows the results for each MOSFET.

Rdg Set	Accum Dose (Gy)	Dose (cGy)	Time after exposure when plateau reached (s)	Reproducibility within plateau period %	Maximum drift in ΔV_{th} as percentage of initial V_{th} %
1	13.3	50	192	1.3	5.9
2	13.8	50	284	1.2	5.4
3	14.1	30	108	1.4	5.5
4*	14.4	30	125	2.8	7.0
5	24.9	20	55	7.0	18.6
6	37.7	100	570	1.3	8.0
7	27.7	100	690	0.6	6.4
8	28.7	100	1800 (3^{rd} rdg)	0.9	3.9

** readings taken for only 10 minutes following irradiation*

Table 5 Characteristics of drift up to 1 hour following single 4 MV irradiations

The time taken for each plateau was dose-dependent, as expected, with the MOSFETs exposed to larger doses taking a longer time to reach a plateau, due to dose-dependence of the build-up of interface states. However, a comparison of the sets for which the same dose had been given shows a readout interval influence, in that the plateau was reached sooner for the sets with more frequent readings. This is probably a result of charge injected by the reader [74]. Reproducibility within the plateau period generally improved with increasing delivered dose, but this also depended on readout interval. The greatest statistical uncertainty due to smaller shifts for lesser doses is reflected in the results for set 5. Disregarding this set for statistical reasons, reproducibility within the plateau periods for the other sets was within 2.8%.

No relationship between delivered dose and maximum drift was apparent (again disregarding set 5), but there was a reading interval dependence, as indicated by comparison of the reading sets for the same delivered doses, where the greatest drifts occurred for the more frequently-read sets. (See Table 1, page 49 for reading intervals for the sets.)

To compare the drift curves for different delivered doses, data from reading sets 2, 3, 5, 6 and 7, for the period up to 20 minutes following irradiation, were graphed as a percentage drift from the initial reading of ΔV_{th} (figure 5.7).

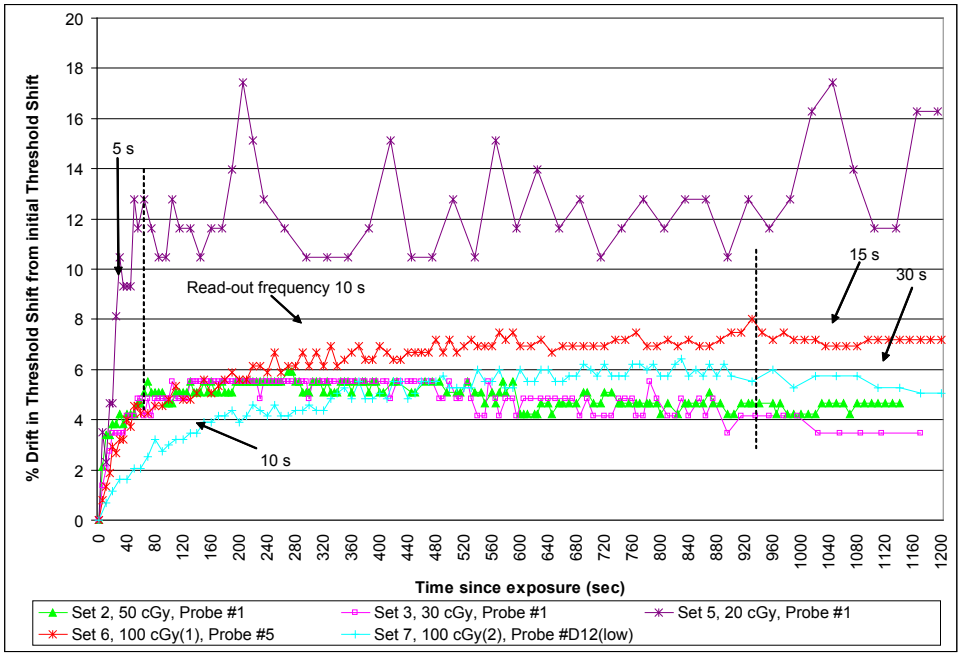

Figure 5.7 Drift up to 20 minutes following single 4MV irradiations

This graph confirms an apparent increased drift with increased frequency of taking readings, particularly for sets 6 and 7. Probe 6 had accumulated 10 Gy more than probe 7 at the time of the tests. A greater drift is apparent for set 6 than for set 7 during the first minute, and also after 15 minutes, during which periods the readings were taken more frequently for set 6. Between 1 and 15 minutes, when both probes were read at 10 s intervals, the drift trends were similar.

To understand these drift characteristics in more detail, in order to determine the most stable periods for dose determination, the data for the 8 sets were analysed for various time intervals since irradiation (e.g. 0 – 1 min, 1 – 5 min, 5 – 10 min etc.) to ascertain the periods of least and most drift,. The average drift for each time interval considered was defined as:

$$\left(\frac{\overline{\Delta V_{th,\,interval}}}{\Delta V_{th,\,immediate}} \right) * 100 \quad \text{.....(5.2)}$$

and the results are graphed in figure 5.8.

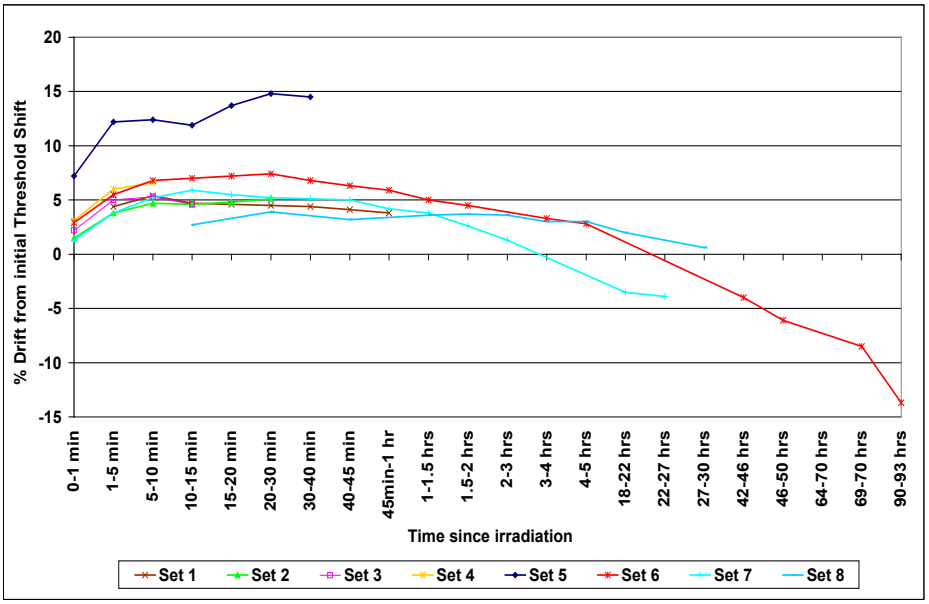

Figure 5.8 Average drift per time interval following single 4MV irradiation

The uncertainties are: 1.0%, 1.1%, 1.2%, 5.3%, 3.1%, 3.0%, 1.8% and 1.8% for sets 1-8 respectively.

From this figure, it can be seen that:

- all probes exhibited an initial rapid increase in response during the first 5 minutes after irradiation, of between 1.3% (set 7) and 7.2% (set 5) (excluding set 8, for which readings were taken every 15 min);
- for the 20 cGy dose, the greatest drift occurred at 15 – 20 minutes (14.8%), and the least when readings were taken at 15 minute intervals (< 4 % throughout the entire measurement period);
- the readings for most of the probes became stable by 10 minutes after irradiation;
- except for the 20 cGy dose, a relatively stable period existed up until about 1 hour after irradiation, when the drift decreased;
- overall, the least drift occurred when readings were taken at 15 minute intervals (set 8) until 1.5 hours after irradiation.

These results, particularly the rapid drift during the first 5 min after irradiation prompted further investigation of this clinically relevant period. In order to characterise any delivered or accumulated dose dependence of drift during this period, the data from four probes which had been exposed to a single 4MV irradiations of 20, 30, 50 or 100 cGy at various times during their lifetimes, and read out with varying intervals, were analysed. The data were divided into sets for "new" (< 20 Gy accumulated dose) and "old" probes (> 20 Gy accumulated dose), and were considered in terms of average drift (mV) for periods of 0 – 30s, 30 – 60s, 60 – 90s, 90 – 120s, 2 – 3 min, 3 – 4 min and 4 – 5 min (see Appendix E). The results, shown as percentage drift from initial ΔV_{th} for each time interval, are graphed in figures 5.9 (i) and (ii) where (a) is the combined drift from all sets, and (b) and (c) show the low and high accumulated dose probe data respectively.

The greatest drift occurred within the first 60 seconds after irradiation for all probes tested. After that period, drift stabilised to < 1% except for the 100 cGy irradiations, for which drift fell to below 1% during the 90-120 s interval. For the "new" probes, the drift was dose-dependent, with greater drift for greater delivered dose, however, this delivered dose dependence lessened for the "older" probes after the first 30 s. The drift for the "older" probes was greater than that for the "newer" probes.

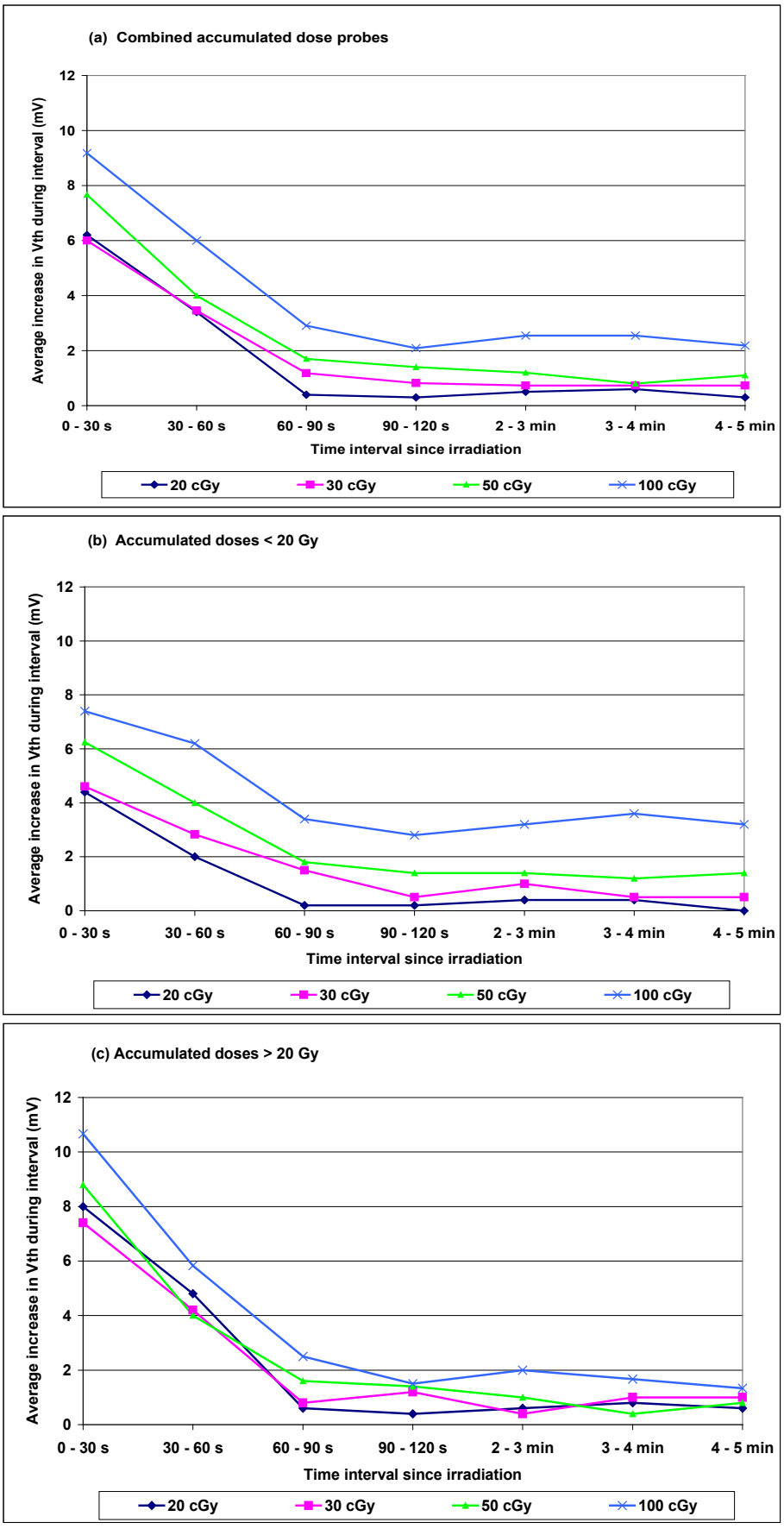

Figure 5.9 (i) Average drift (mV) during each time interval up to 5 minutes following single irradiations. (a) combined, (b) "new" and (c) "old" probes

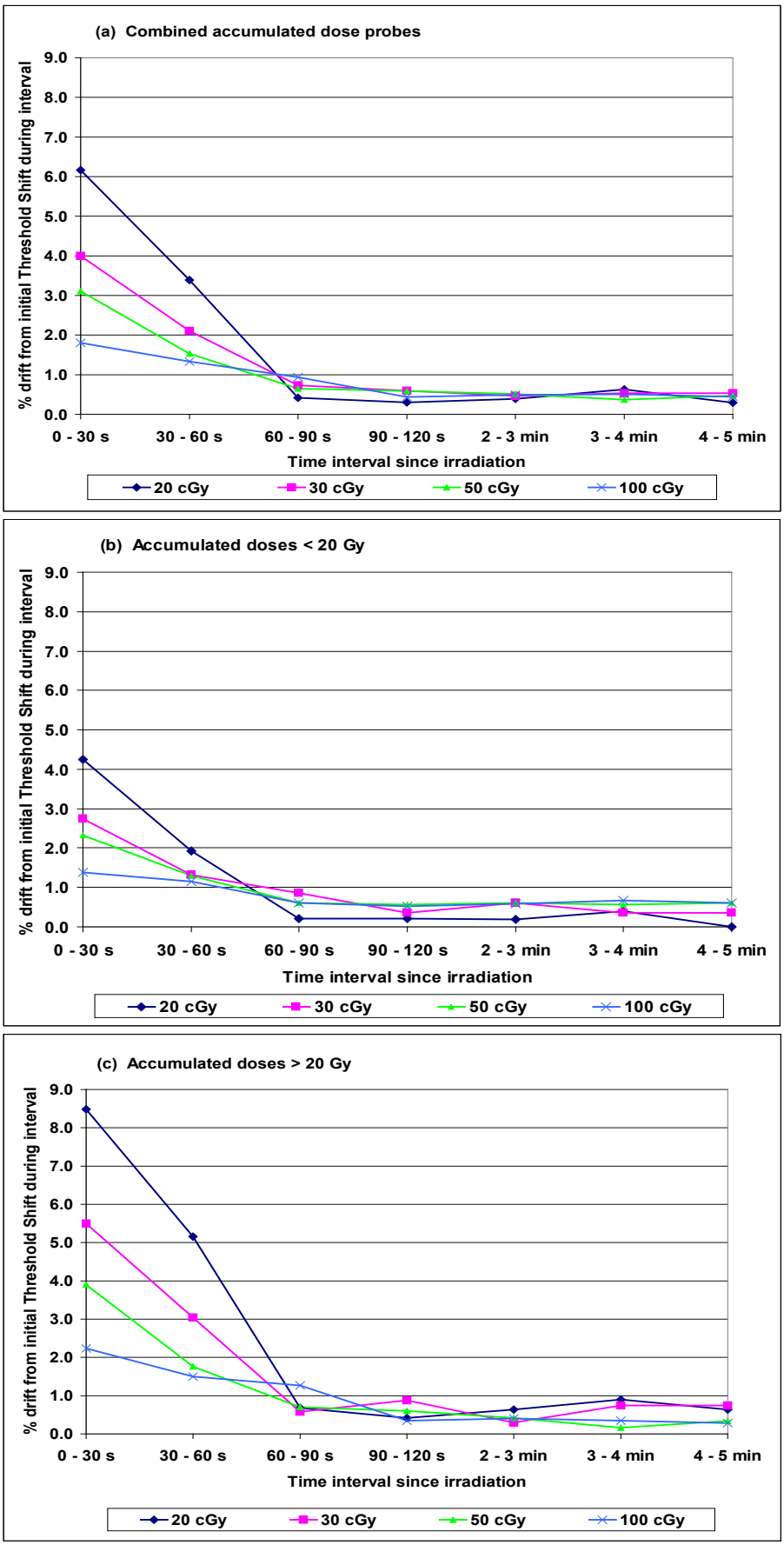

Figure 5.9 (ii) Drift during each interval as a percentage of initial Threshold Shift (data from figure 5.9 (i))

5.3.2 *Creep-up*

Figure 5.10 shows the results of creep-up effect measurements. The figure indicates creep-up continuing for at least 5 minutes after irradiation, with none of the second readings being similar to the immediate post-irradiation reading, as has been reported for the T&N MOSFETs.

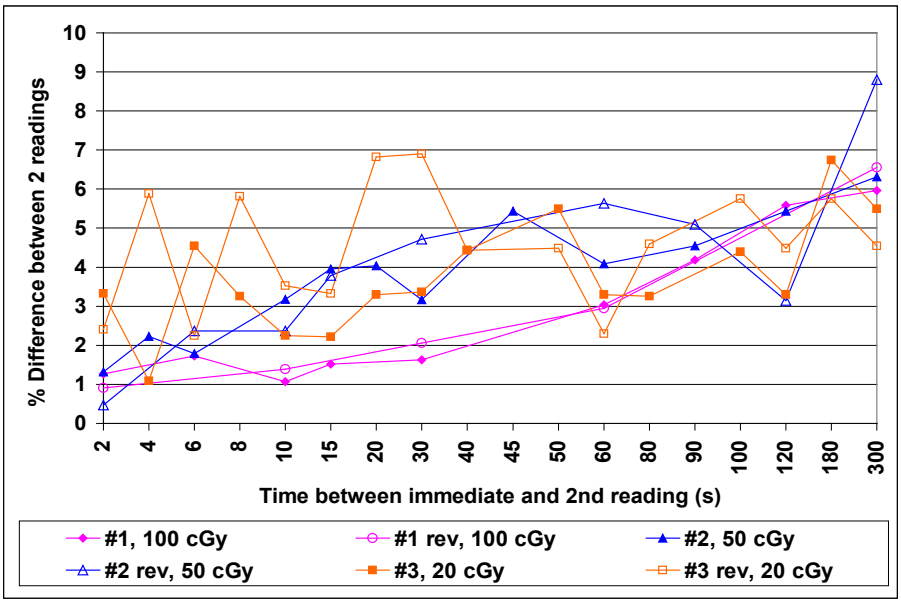

Figure 5.10 Creep-up up to 5 minutes following irradiation

The percentage difference in ΔV_{th} between first and second readings for all detectors generally increased as the time interval between the two readings increased. The minimum and maximum differences are shown in table 6, together with the reading interval at which these occurred.

Probe #	Accum. Dose (Gy)	*Dose* (cGy)	Difference in ΔV_{th} between immediate and 2nd readings				% Uncertainty ±
			Min. %	Reading interval between 2 rdgs (s)	Max. %	Reading interval between 2 rdgs (s)	
1	20.8	100	1.07	10	5.96	300	0.6
1 rev	21.8	100	0.91	2	6.55	300	0.6
2	24.8	50	1.32	2	6.31	300	1.2
2 rev	30.8	50	0.47	2	8.80	300	1.2
3	26.3	20	1.09	4	6.74	180	3.1
3 rev	29.5	20	2.25	6	6.90	30	3.1

Table 6 Creep-up effect. Minimum and maximum drift in ΔV_{th} between two post-irradiation readings, showing the time intervals of their occurrence

The two readings for the 100 cGy dose were the most consistent with each other, differing by less than 2% until the reading interval reached 30 s, then rising to a maximum difference when the interval between the readings was 5 minutes.

The average drift for probe 2 was less than 3% for intervals of less than 10 seconds between readings. Analysis of these results in terms of dose dependence is inconclusive, due to the differing accumulated doses of the probes at the time of the experiment, and the large uncertainty for the 20 cGy doses. It was apparent that system noise became a dominant factor at this low dose, despite the manufacturer's claim that doses as low as 10 cGy could be measured confidently. Although the drift generally appears to increase with decreasing delivered dose, this effect may also be the result of increasing accumulated dose. To confirm dose-dependence, it would be necessary to use probes having similar accumulated doses, however this was not possible due to the limited number of MOSFETs made available for this work. However, there is an increasing trend over the 5 minute interval for probes 1 and 2. This creep-up effect differs from that reported for T&N MOSFETs [62] where the second reading was similar to the initial reading when the interval between the readings was 1 minute (see figure 3.13, section 3.8.2).

5.3.3 Reading interval

To investigate this apparent effect found from the results shown in section 5.3.1, the data for the three 100 cGy sets (6, 7 and 8) were analysed up to 1 hour following irradiation. Figure 5.11 shows the variations in drift occasioned by different reading intervals. A greater drift can be seen for set 6 compared to set 7 when it was read out more frequently (first minute and after 15 minutes). Between 1 and 15 minutes, when both detectors were read out at 10 s intervals, the drifts for these two probes were similar. Much less drift is apparent for set 8 for which readings were taken every 15 minutes.

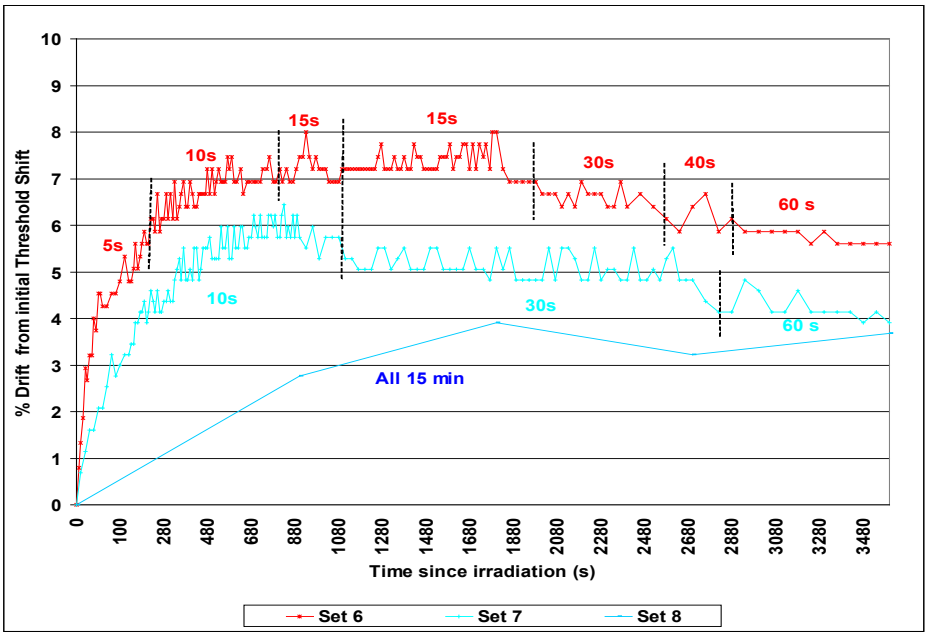

Figure 5.11 Drift up to 1 hour since 100 cGy irradiations of probe #5 (set 6) and #D12 (low) (sets 7 and 8), showing intervals of taking repeated readings

To ascertain the longer-term effect, these data were analysed up to 2.5 hours (7 & 8) or 1.5 hrs (set 6) following irradiation (figure 5.12).

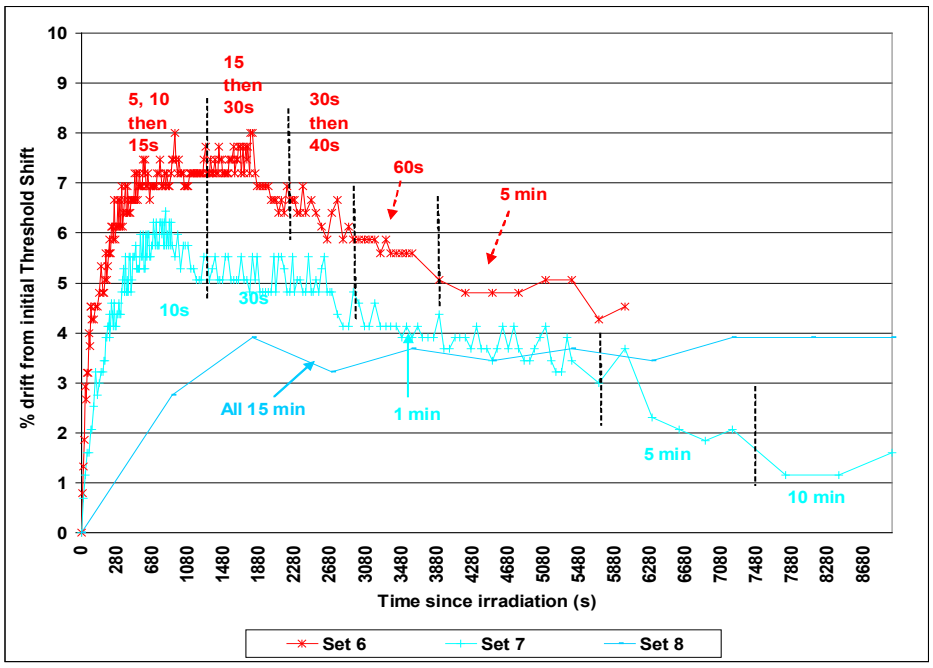

Figure 5.12 Drift up to 2.5 hours following 100 cGy irradiations

The drift curves for the sets show dissimilarities. Readings taken at 5 s - 10 min intervals resulted in up to 4% greater ΔV_{th} than when 15 minute readings were taken. Set 8 resulted in a maximum drift from initial ΔV_{th} of 3.9%, whereas that for set 7 was

6.4%, and it was 7.9% for set 6. The drift abatement behaviour for sets 7 and 8 is also quite different. The drift for set 7 had decreased to 1.61% after 2.5 hours, however the drift for set 8 was still at a plateau at 2.5 hours following irradiation. A continuation of readings the next day (between 18 and 27 hours after the irradiations) revealed ΔV_{th} for set 7 had fallen to 3.9% less than initial ΔV_{th} whereas for set 8, readings were 1.1% greater than initial ΔV_{th}.

A similar trend was observed for the 50 cGy data, but seemingly not for the 30 cGy data (see figure 5.13 (a) and (b)). For these graphs, the data from different sets were normalised to the same initial ΔV_{th} for comparison.

The graphs indicate a possible reading delay effect. Sets 1 and 2 readings were begun at differing times after the irradiation had ceased. As seen in figure 5.13(a), set 1 readings were commenced at 1 minute after irradiation and, although readings were taken only slightly more frequently during the first five minutes than set 2 (for which readings began after 30 seconds), a larger drift resulted. (The reductions in V_{th} after short breaks is due to thermal annealing.)

However, the opposite trend seemed to occur for the 30 cGy sets. For these sets (3 and 4), although set 4 readings were less frequent than for set 3, a greater drift occurred, in contrast to the results for 50 and 100 cGy sets. On closer examination of the data for the first minute following irradiation, it was observed that the initial drifts of sets 3 and 4 were similar during the first 41 seconds, when readings for both sets were taken at 1 s intervals. However, there was then a pause in readings for 8 s for set 3. During that pause, set 4 readings increased by 1.4%, and continued thereafter to produce an overall greater drift for set 4 (figure 5.14).

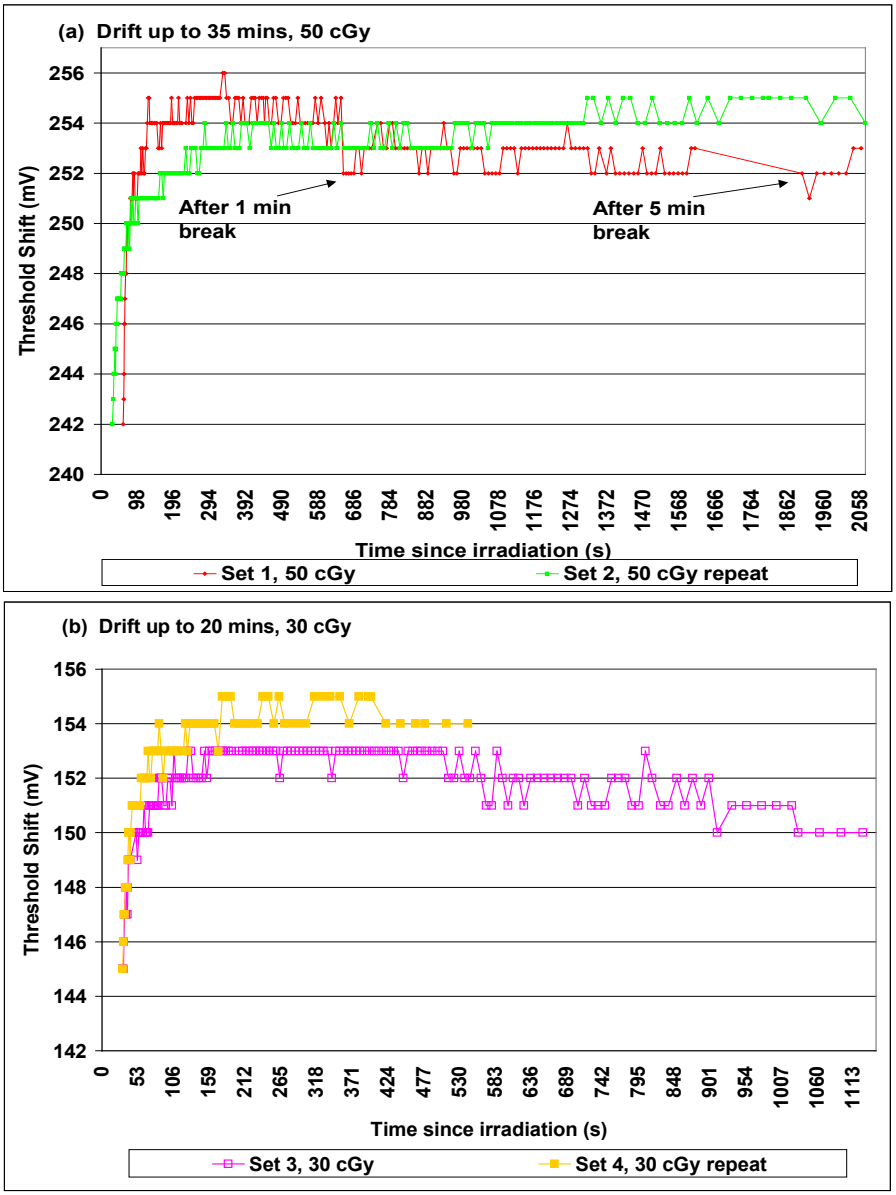

Figure 5.13 Drift following single irradiations of 4MV, normalised to same initial ΔV_{th}. (a) 50 cGy; (b) 30 cGy

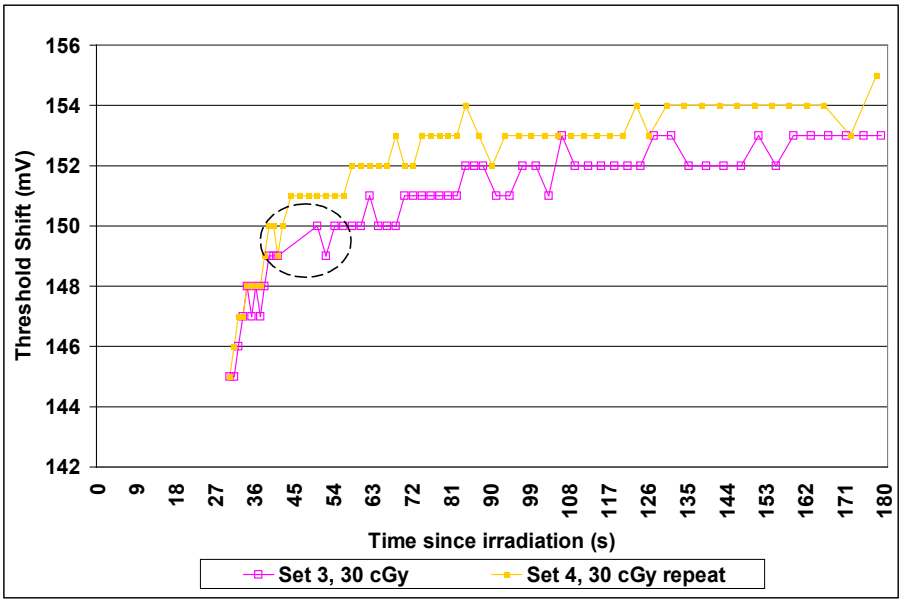

Figure 5.14 Enlargement of first 3 minutes following 30 cGy irradiations of 4MV (normalised to same initial shift)

This indicated that how often readings are taken during the first few seconds following an irradiation may have a strong influence on post-irradiation drift, and prompted further investigation, particularly into whether the effect was influenced by delivered and/or accumulated dose.

The results of the reading interval trials are shown in table 7. This table shows the drift (mV) from initial ΔV_{th} at 5 min after irradiation, for each measurement set. The results are graphed in figures 5.15 and 5.16 (a) and (b) for the "new" (less than 20 Gy accumulated dose) and "old" probe (greater than 20 Gy accumulated dose) respectively, showing drift at 5 min as a percentage of the initial ΔV_{th}.

Reading → Interval Set	***A***	***B***	***C***	***D***	***E***
Del. Dose (cGy)	***Drift from initial Threshold Shift (mV)*** (initial Threshold Shift in brackets)				
	"New" probe				
20	***5*** **(113)**	***8*** **(103)**	***8*** **(103)**	***9*** **(105)**	***8*** **(102)**
30	***10*** **(171)**	***12*** **(169)**	***11*** **(169)**	***12*** **(157)**	***13*** **(169)**
50	***15*** **(257)**	***21*** **(256)**	***not msrd***	***17*** ***(263)***	***19*** **(274)**
100	***24*** **(565)**	***33*** **(513)**	***31*** **(539)**	***33*** **(527)**	***32*** **(539)**
	"Old" probe				
20	***9*** **(86)**	***13*** **(92)**	***19*** **(92)**	***15*** **(92)**	***21*** **(92)**
30	***7*** **(145)**	***16*** **(129)**	***17*** **(136)**	***16*** **(136)**	***22*** **(133)**
50	***15*** **(228)**	***20*** **(224)**	***18*** **(225)**	***22*** **(228)**	***23*** **(220)**
100	***23*** **(448)**	***20*** **(435)**	***28*** **(450)**	***29*** **(449)**	***36*** **(445)**

Table 7 Reading interval results.
Drift (mV) in ΔV_{th} at 5 min following irradiation

Figure 5.16 (a) and (b) shows percentage drift from initial ΔV_{th} with delivered dose, for reading sets A-D.

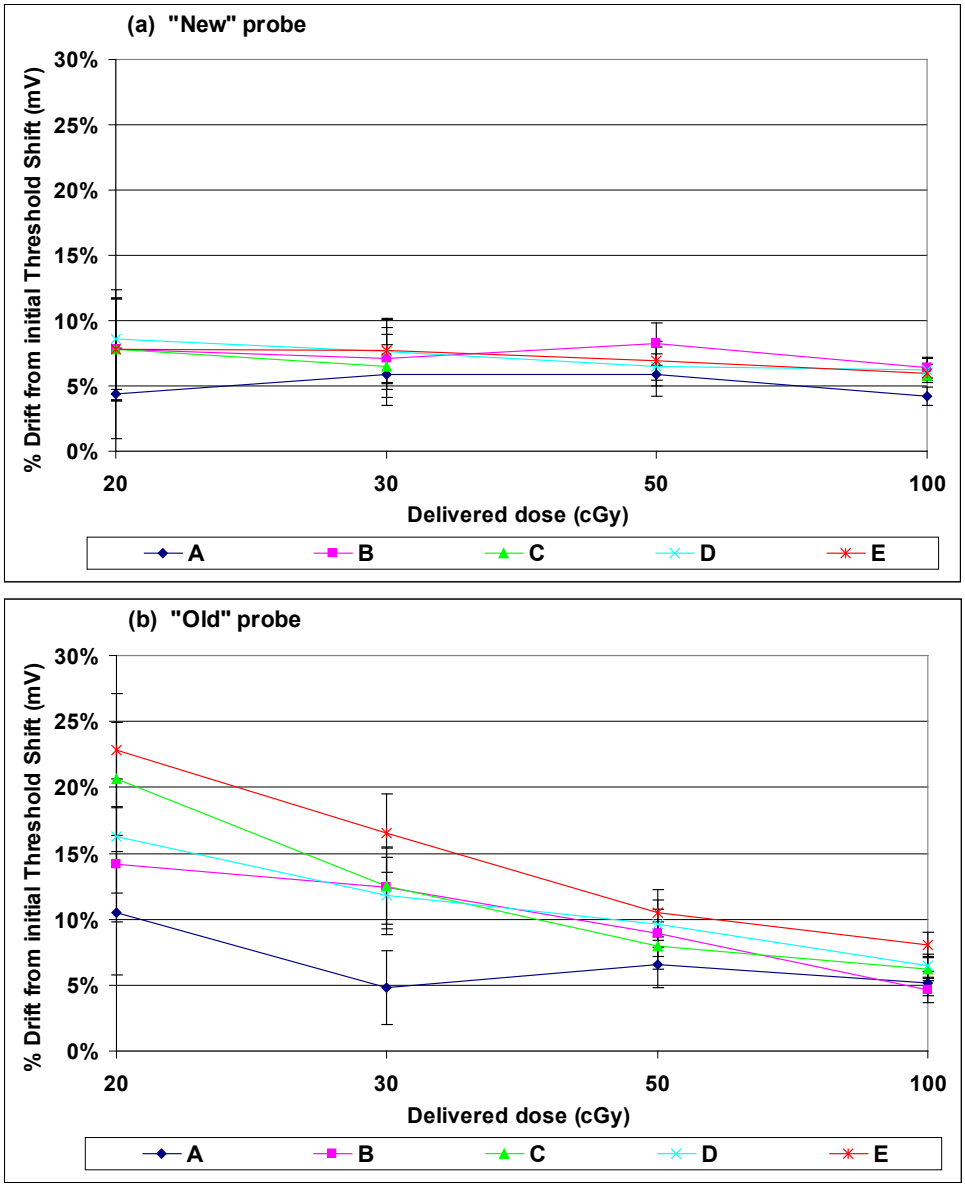

Figure 5.15 Drift at 5 minutes after single 4MV irradiations for Reading Interval Sets A – E (least → most frequent). Drift vs delivered dose

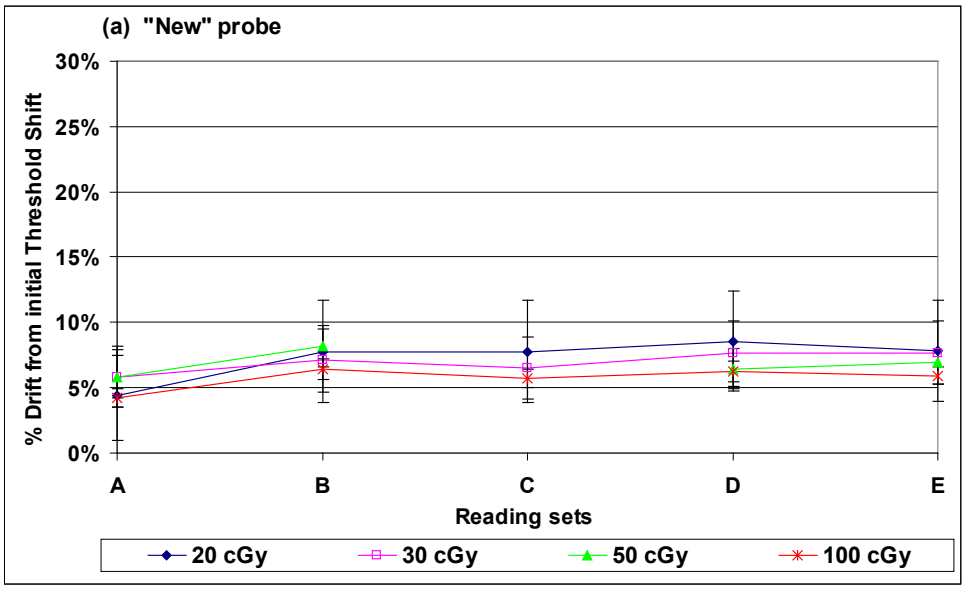

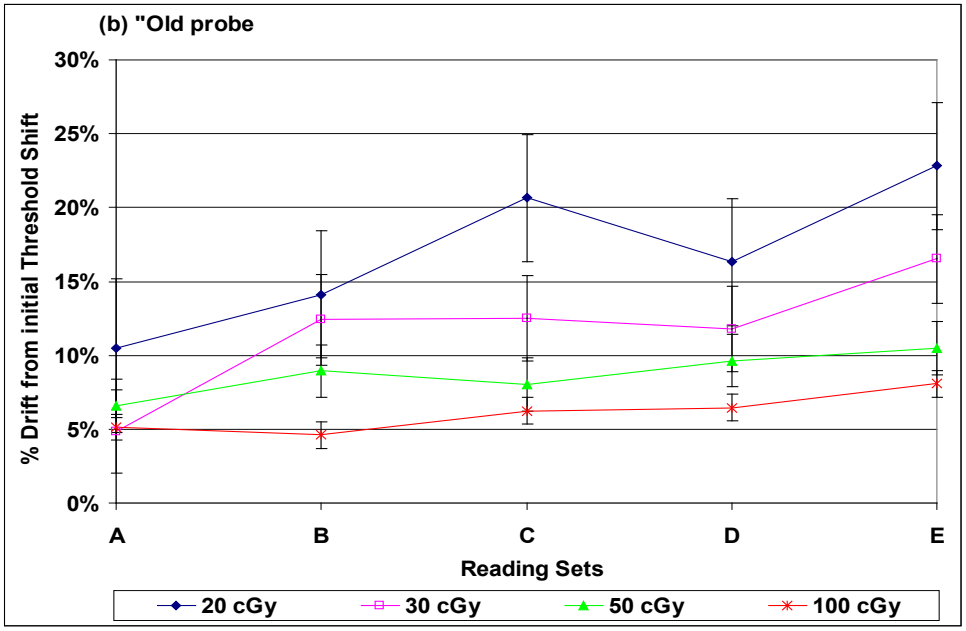

Figure 5.16 Drift at 5 minutes after single 4MV irradiations for Reading Interval Sets A – E. Drift vs Reading Set

These results show:

- an accumulated dose effect – the range of drift for the new probe was 4.2% – 8.6%, whilst for the old probe, it was 4.6% - 22.8%.

- delivered dose-dependence for the old probe but not for the new probe; and

- a small reading interval effect for the new probe and a more pronounced drift with reading frequency for the old probe.

The drift is a greater percentage of the initial shift for the old probe, due to the decreasing sensitivity with accumulated dose.

5.3.4 Reading Delay

In order to differentiate between the inherent reduction in sensitivity with accumulated dose, and the effects due to delays in taking readings, the measured data were first corrected for sensitivity reduction as described in Appendix A1. The data were then analysed to determine the drift due to delay in taking pre- or post-irradiation readings, and any delivered dose and/or accumulated dose dependence. Figure 5.17 is a graph of the data for several of the probes. Similar trends were found for the other probes.

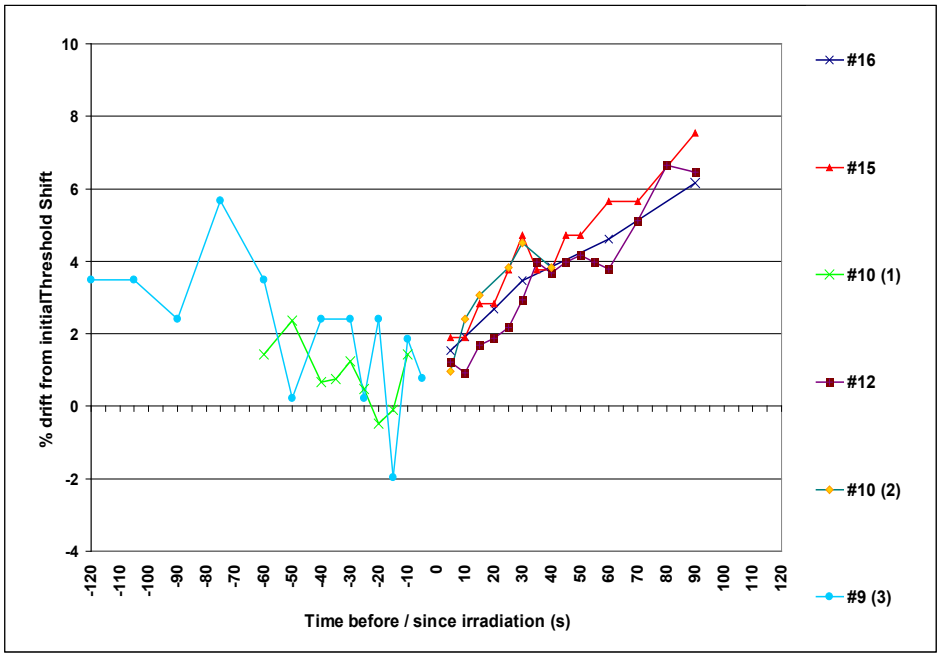

Figure 5.17 Reading delay response –data for several probes

The "negative times" on the x-axis indicate time between pre-irradiation reading and irradiation, and the positive times indicate time between irradiation and post-irradiation reading. It shows the percentage drift in ΔV_{th} from that measured immediately before/since irradiation (i.e. within 1 s of beam-on or beam-off). The left-hand data were obtained by read-out methodology (i), and the right-hand data by methods (ii) and (iii) on page 56.

A generally increasing drift in ΔV_{th} with delay of reading is evident. This drift is time-dependent, and is less for pre-irradiation delays than for post-irradiation delays, particularly for delays ≤ of 30 seconds. The pre-irradiation drift range for all probes is -2.9% to +3.9%, as compared to +0.6% to +8.4% for post-irradiation drift. By fitting linear equations to the data, the overall average drift per second delay (all probes) was 0.02% for pre-irradiation delays, and 0.06% for post-irradiation delays.

Table 8 shows the drift ranges with delivered and accumulated dose for delays up to 1 min pre- or post-irradiation.

Probe # (Trial)	Threshold Voltage (mV)	Delivered Dose (cGy)	Accumulated Dose (Gy)	Drift range (min-max) %	Pre- or Post-
16	8886	50	New probe	1.5 – 4.6	Post
9 (1)	8937	20	New probe	3.7 – 7.5	Post
15	9179	20	New probe	1.9 – 5.7	Post
10 (1)	9253	20	New probe	-0.5 – 2.4	Pre
12	9275	50	New probe	0.9 – 4.2	Post
11*	9319	20	New probe	1.0 – 4.5	Post
10 (2)	13340	20	7.4	-1.5 – 2.1	Pre
9 (2)	13367	20	8.2	-2.0 – 3.5	Pre
9 (3)	17266	20	16.0	-0.9 – 3.9	Pre
10 (3)	17734	20	14.2	3.1 – 8.4	Post
9 (4)	19310**	20	21.2	2.5 – 7.3	Post
D9	23133	20	29.0	0.6 – 2.6	Post
D8	23217	20	29.0	-2.9 – 1.7	Pre

* *Measurements taken only up to 40 s delay*

Table 8 Range of drift with delivered and accomulated dose

The drift indicated there may be some delivered dose dependence (although only two doses were trialled), being generally less for 50 cGy doses than for 20 cGy doses for the "new" probes tested. However, the large uncertainties for the 20 cGy dose results preclude a conclusion on this point, and this effect requires further investigation. The results for probe #9, exposed to 20 cGy at different stages of its lifetime, are graphed in Figure 5.18.

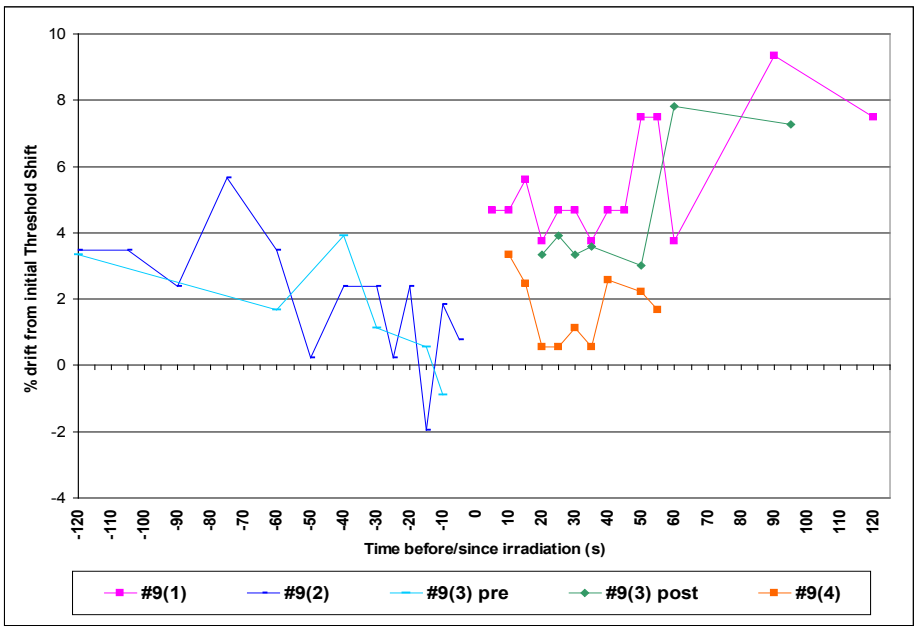

Figure 5.18 Reading delay response at various stages of probe #9's lifetime

Reduced drift is observed for reading method (iii) (page 56), which had a delay both pre- and post-irradiation (#9(3) in the figure), and readings appeared to be more consistent compared to the drift when this probe was new. Similar results over the lifetime of probe #10 were found.

5.3.5 *Discussion of drift response results*

The characteristic drift of ΔV_{th} with time after an irradiation is due to many complex processes, as previously described, and there is still some debate as to whether interface states or border traps are responsible for drift. However, it is generally believed that the initial rapid increase in ΔV_{th} is due to hole and H^+ transport towards the interface, and the subsequent build-up of interface states and/or border traps, which continues for several thousands of seconds. At later times, ΔV_{th} is reduced by electrons generated in the oxide or the Si recombining with some of the trapped holes, and the other processes mentioned in section 3.8. These processes are influenced by bias conditions during and following irradiation, the local electric field and temperature. The local electric field itself is modulated by the space charge (trapped holes). With increasing accumulated dose, the space charge

enhances the electric field near the Si interface and reduces it with respect to its initial value near the gate, as shown in figure 3.6.

The drift in ΔV_{th} with time has been shown in the current work to be a function of delivered and accumulated dose, reading frequency and reading delay. The average mV drift during each time interval since irradiation was dose-dependent for the "new" probes, but the dose-dependency was less for the "old" probes (see figure 5.9 (i)). Most drift occurred for all probes during the first 90 s after irradiation, after which drift stabilised to < 1% per measurement interval. The average drift during each interval up to 90 s was greater for the "old" probes than for the "new" probes, for all delivered doses. Also, there was a slight reading frequency effect for the "new" probes, but a more pronounced effect for the "old" probes. This drift may be explained as follows, in terms of interface state build-up and/or border trap discharging.

It is suggested that drift for "new" probes may be mainly due to the build-up and filling of positive oxide traps. However, with the filling of these traps with accumulated dose, the build-up of interface states and border traps and the discharge of electrons from the latter into the Si, may predominate. This would explain the greater drift (compared with drift when "new") and also the diminishing of dose-dependence with increasing accumulated dose, as explained hereunder.

For "new" probes, many oxide hole traps are available, so oxide hole trapping may predominate, and drift will be dose-dependent. However, as accumulated dose increases, the probability of oxide trapping reduces due to the diminishing number of available traps, and to the increasing positive space charge in the oxide close to the interface. This means that more holes may escape the oxide traps and reach the interface, where they are trapped in border or interface traps. The build-up of interface and border traps may therefore predominate for the "older" probes and, because in p-MOSFETs the interface states trap positive charge, which adds to

ΔV_{th} produced by oxide trapped holes, the drift will be greater during a specified time compared to the "new" probes.

In addition, as suggested by Savić , Radjenović and Pejović [77], the electrons associated with positive charge in border traps may tunnel across the interface to the Si, leaving uncompensated positive charges as shown in figure 3.5, which will increase ΔV_{th}. With the greater density of filled border traps with increasing accumulated dose, the drift will also increase. Also, due to the decreasing sensitivity over the lifetime of MOSFETs, the drift will be a greater percentage of the initial shift which reduces as accumulated dose increases.

The tunnelling of electrons from border traps can also explain the reading frequency effect. The Wollongong reader system maintains a constant positive gate bias (+5 V, R-type or +12 V, K-type) at all times except when readings are being taken, at which time the applied bias momentarily becomes negative. During this time, the interface potential barrier is lowered, increasing the probability of electron tunnelling, and creating more uncompensated positive charges. This may explain the greater drift for more frequent readings. The reading frequency effect will be less pronounced for "new" probes, for which oxide trapping, rather than border traps, may predominate.

The drift during pre- and post-irradiation delays can also be related to the build-up of interface states and/or discharge of border traps as explained above. Figure 5.19 (a) shows that when there is a pre-irradiation delay, the continuing drift from the previous irradiation contributes to the measured ΔV_{th}. This contribution will depend on the elapsed time since the previous irradiation, the accumulated dose and the dose delivered during that previous irradiation, as shown in table 4. When the delay is post-irradiation (figure 5. 19 (b)), the drift is due predominantly to the current irradiation. Appendix F shows that the rate of drift following irradiation is a maximum during the first 60 s, then stabilises at

less than 1% of ΔV_{th} by 120 s. Therefore, even allowing a 2 min break between successive irradiations, the drift from the previous irradiation will contribute to measurements of ΔV_{th} by up to 1% per minute if there is a pre-irradiation delay. Post-irradiation delay drift will be greater than the pre-irradiation delay drift, as shown by the results in this work.

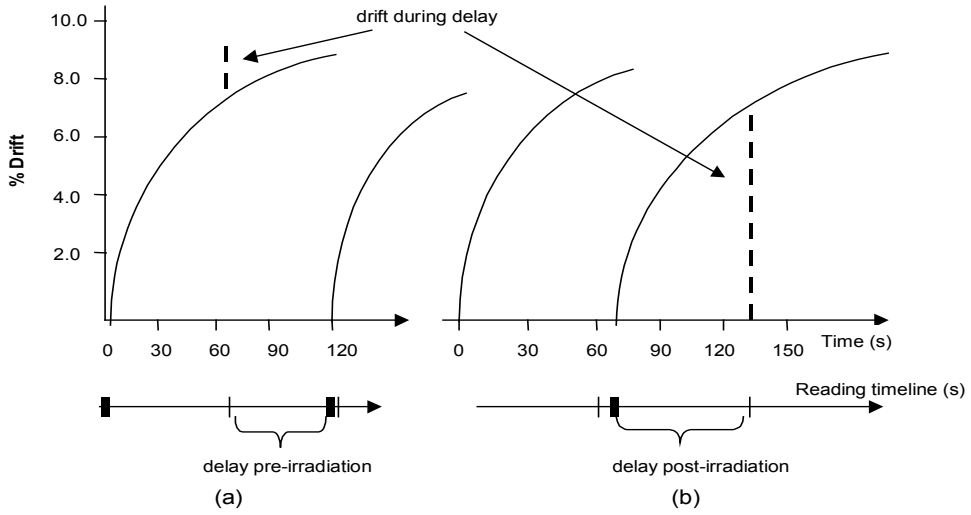

Figure 5.19 Drift in ΔV_{th} during pre- or post-irradiation delays. (a) The drift from the previous irradiation contributes to the ΔV_{th} measurement. (b) The measured drift is due mainly to the current irradiation, during the most rapid interface build-up/border trap period

To be used for IVD purposes, it is necessary that readings obtained are reliable and consistent, and the abovementioned problems with drift must be minimised. This may be achieved by consistency between calibration and treatment reading procedures, and by ensuring that pre- and post-irradiation readings are made by the same method in both instances. See section 7.1 for further recommendations for readout methods.

5.4 Angular dependence

The results of angular dependence measurements are graphed in figure 5.20, which shows variation in ΔV_{th} as a percentage of ΔV_{th} for incident beam angle of 0^{o}. A set-up error of $\pm 2^{o}$ is estimated and ±5% error is estimated for ΔV_{th} variation. The direction of rotation of the phantom did not impact on the results.

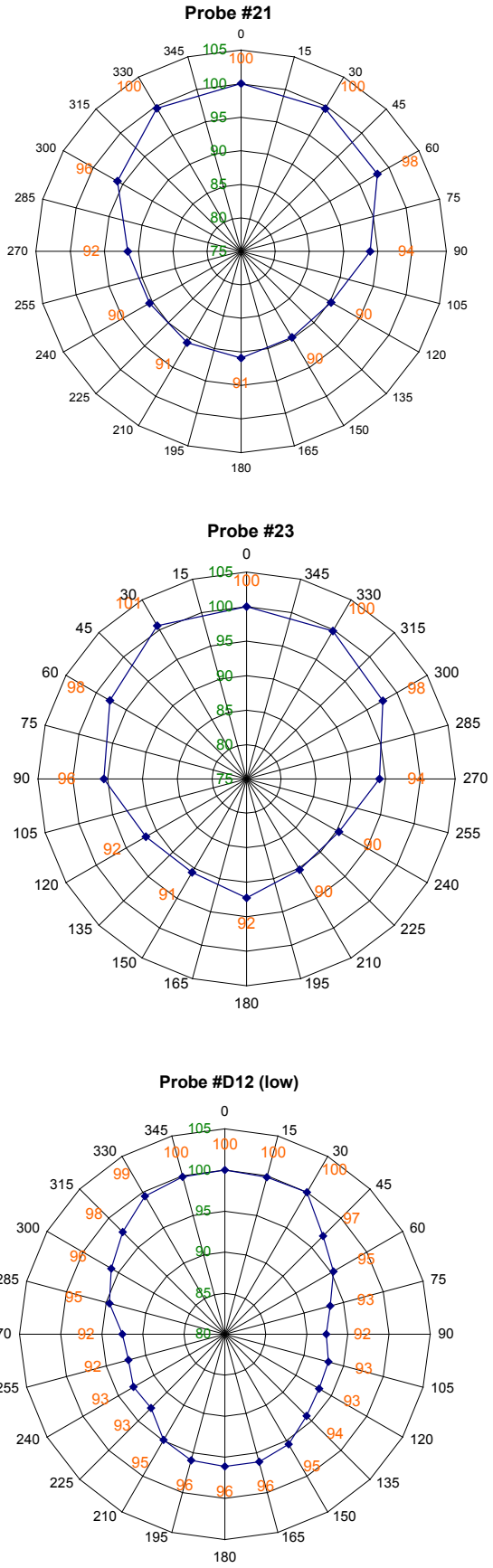

Figure 5.20 Variation in ΔV_{th} as a function of angle of radiation incidence as a percentage of ΔV_{th} with epoxy bubble facing the beam

Overall, for all probes, the range of variation was +1% at 30° angle, to -10% at angles of 120°, 150°, 210° and 240°. For all probes, greater sensitivity was measured with the epoxy bubble facing towards the beam ("top hemisphere"), rather than away from it ("lower hemisphere"), where "top hemisphere" encompasses the angles between 90° – 0° - 270° respective to the beam. This is in part because the top hemisphere contains the oxide in which the dose is deposited. When the epoxy bubble faces away from the beam (90° – 180° – 270°), the beam must firstly pass through the substrate before reaching the oxide, and is attenuated and backscattered.

As can be seen from figure 5.21, silicon, with a density of 2.33 g/cm^3, absorbs most of the keV photons from the beam. The other components of the probe will also attenuate the beam to some extent, depending on their mass energy absorption coefficient, μ_{en}/ρ, where :

μ_{en}/ρ = $\mu/\rho\ (\bar{E}_{ab}/hf)$ (cm^2/g).....*(5.3)*

and μ = fraction of photons which interact in distance Δx

ρ = density of material, cm^3/g

$\bar{E}_{ab}$ = average energy absorbed per interaction, J

f = radiation frequency, s^{-1}

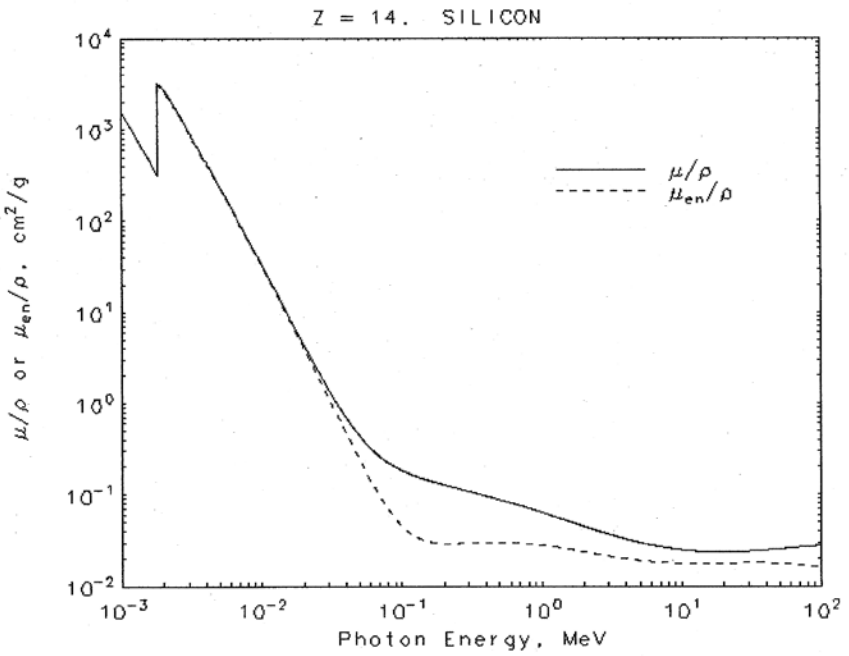

Figure 5.21 Mass attenuation coefficient for silicon
(www.physics.nist.gov /PhysRefData/XrayMassCoef/cover.html)

Attenuation will also be greater when the beam travels a greater path-length to reach the oxide (since Δx is greater), which occurs for oblique angles of incidence, as can be seen in figure 5.22, and is clearly reflected in Figure 5.20 for angles of incidence between 105^{o} – 150^{o} and 210^{o} – 255^{o}.

The epoxy insulator filters low energy photons, and although at the energies used in this work most scatter would be in the forward direction, the TO-5 gold-plated Kovar substrate backscatters electrons [47], hence It is possible that this scatter also contributes to the reduction in sensitivity at oblique angles.

Each individual probe's substrate and epoxy dimensions are unique, so angular dependence will also be unique, however the results indicate reproducible variations, which could be accounted for by the use of correction factors.

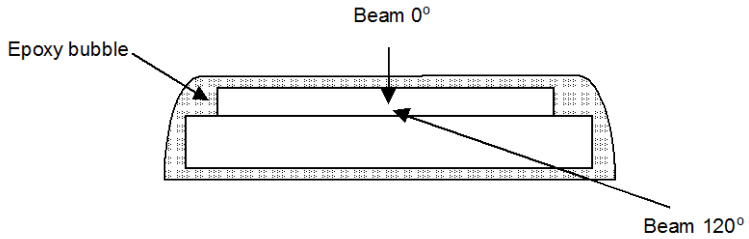

Figure 5.22 Beam attenuation depends on the angle of incidence of the beam in relation to the sensitive area of the MOSFET

Alternatively, the probes could always be used with the substrate placed onto the patient, with the epoxy bubble facing towards the beam, then only the top hemisphere results need to be considered. For the top hemisphere, the greatest variation was -8% at 90 ° and 270 °. Disregarding the readings for 270^{o} and 90^{o} (when the beam is side-on to the probe), the greatest variation for the top hemisphere was -7% at an angle of 75 °. In terms of uncertainty in dose, this translates to 3.5%. These results are comparable with those of Scalchi and Francescon [1] and Chuang *et al* [64].

6. SUMMARY AND CONCLUSIONS

Using a reader system and associated hardware developed by the Centre for Medical Radiation Physics, University of Wollongong, 37 MOSFET probes (REM Oxford (UK)) were investigated for sensitivity to radiation (including accumulated dose effect and saturation), linearity with dose, angular dependence and drift effects. Single (high) sensitivity and dual (high and low) sensitivity probes were used. Readings of V_{th} were taken in the manual, on-line mode, through an Interface Unit. Radiation doses of 20, 30, 50 or 100 cGy (high sensitivity probes), and 50 – 500 cGy (low sensitivity probes) were delivered using 4MV or 6MV beams from medical linear accelerators. Probes were placed in solid water® at depth of maximum dose, except for angular dependence measurements, when a custom-made phantom was used.

The average sensitivity reduction over the lifetime of the probes was found to be 22.37% with a standard deviation of 0.63%. The sensitivity of all probes decreased with accumulated dose in a reproducible manner, represented by an average sensitivity drift equation (equation 5.1):

$$y = 3 \times 10^{-9} x^2 - 0.0002x + C \quad \text{.....6.1}$$

where y is sensitivity (mV/cGy), x is V_{th} pre-irradiation, and C is initial sensitivity. Sensitivity is the Calibration Factor (CF) from which dose can be determined from measurements of ΔV_{th} (equation 3.5):

$$D = \frac{\Delta V_{th}}{CF} \quad \text{.....6.2}$$

For sets of repeated irradiations, the reduction in sensitivity with accumulated dose can be corrected for by the use of drift equations over the measurement period (Appendix A). Saturation occurred for the high sensitivity probes at an approximate V_{th} of 26.5 V, or 40 Gy accumulated dose.

The average deviation from linearity for 4 single sensitivity probes was within 1.6% for doses between 5 and 140 cGy, and within 3.8% for 2 dual probes (low sensitivity), for doses between 50 and 500 cGy.

Post-irradiation drift in ΔV_{th} with time is a common characteristic of MOSFETs. It was found to be influenced by reading frequency, reading delays, delivered and accumulated dose. The most rapid drift occurred within the first 5 minutes of irradiation (1.3 – 7.2%), and stabilised by 10 minutes between 3% and 7%. During the first 5 minutes, post-irradiation drift increased with delivered dose, and was greater for probes having accumulated dose of > 20 Gy (2.0 – 16.2% compared with 1.2 – 7.4% for < 20 Gy probes).

Creep-up of the Wollongong MOSFETs was found to be different to that reported for T&N MOSFETs. For two post-irradiation readings – one taken immediately and a second at a later time - there were no signs of the second reading becoming similar to the immediate reading within 5 minutes following irradiation. The percentage drift in ΔV_{th} between the two readings generally increased as the time interval between the two readings increased, by up to 8.8%.

The reading methodology was found to be a critical factor, with delays in pre- or post-irradiation readings, or taking frequent repeated readings of V_{th} during the first few seconds and minutes following an irradiation, having a significant effect on response drift. The increased drift with more frequent readings was greater for probes with > 20 Gy. For these probes, up until 5 minutes after irradiation, the percentage drift generally increased with frequency of readings. The range of drift at 5 minutes compared to initial ΔV_{th} was 5.3 – 22.8% for these probes. However, for probes with accumulated dose of < 20 Gy, the drift range was 4.7 – 9.5%. These results reflect the decreasing sensitivity with accumulated dose, since then the drift occasioned by a particular dose is a greater percentage of initial ΔV_{th}.

For delays of up to 2 minutes in taking the pre-irradiation reading, if the probe has recently been exposed, the drift from previous exposures may contribute to ΔV_{th}. Drifts of up to 5.7% compared to reading immediately before irradiation were measured. The drift was greater for a post-irradiation delay, since the most rapid drift occurs within the first 60 s. The maximum post-irradiation drift was 9.3% (although this was measured for 20 cGy doses, for which the uncertainty was ± 3.9%).

The abovementioned drift characteristics are believed to be linked to the decreasing number of oxide traps with increasing radiation exposure, with a preferential build-up of interface traps as accumulated dose increases, or the tunnelling of electrons from border traps into the Si, leaving behind uncompensated positive charges. It is believed that the frequency effect is caused by the changed bias conditions during read-out which lower the potential barrier at the interface, increasing the probability of electron tunnelling, leaving unaccompanied positive charges in border and/or interface traps and thus increasing V_{th}.

The orientation of the epoxy bubble in relation to the radiation beam affected the response in a reproducible manner for the 3 probes tested. ΔV_{th} varied by up to 10% for orientations other than the epoxy bubble facing directly towards the beam. Greater sensitivity was measured with the bubble, rather than the substrate side, facing the beam, due to attenuation by the Si. In this orientation, the greatest variation was –7% at 75^{o}, or 3.5% uncertainty in dose. This level of uncertainty could be achieved by a use regime whereby the probes were always used with the epoxy bubble always facing the beam wherever possible, or an appropriate correction factor applied in cases where this is not feasible.

The MOSFETs showed acceptable linearity with dose for the dose ranges investigated. They exhibited reproducible reduction in sensitivity with accumulated dose and angular dependence, which could be accounted for in dose determination from readings of V_{th}. With consistent calibration and clinical reading methodologies, and the application of correction factors, indications are that they could be used successfully for IVD.

7. RECOMMENDATIONS AND FUTURE WORK

7.1 Recommendations

The following recommendations are made regarding the use of MOSFETs:

(a) There must be consistency between the taking of readings for calibration purposes, and in the clinical situation. The raw readings must be corrected for response variations when treatment conditions are at variance with calibration conditions.

(b) Readings of V_{th} should be taken *immediately* (≤ 1 s) before and after irradiation, for both calibration and IVD, to avoid drift effects due to delays.

(c) Sensitivity drift equations can be used to determine *in vivo* dose from readings of ΔV_{th}, following MOSFET calibration. Each MOSFET is unique, and must be calibrated individually prior to use, to determine its initial sensitivity, *C*. This can be used to determine the sensitivity drift equation from which dose is determined, as follows:

$$D = \frac{\Delta V_{th}}{CF}$$

where *CF* = sensitivity.
Sensitivity is given by: $3 \times 10^{-9} x^2 - 0.0002x + C$ where x is V_{th}.

(d) There is no apparent optimum time to allow between consecutive readings, but rapid repeated readings following a single exposure should be avoided.

(e) Further research should be performed to investigate appropriate reading intervals for taking measurements *during* irradiation (e.g. for TBI), and the use of the automatic reading mode.

(f) The single and dual (high sensitivity) probes should not be used for V_{th} above 26 V, or 40 Gy accumulated dose, above which saturation occurs.

(g) The single sensitivity probes should not be used to measure doses of less than 30 cGy, and the dual sensitivity probes used in the high sensitivity mode, should not be used for less than 100 cGy doses.

(h) The sensitivity drift equation over the measurement period should be used to correct data obtained during protracted measurement sets of repeated irradiations, for sensitivity reduction with accumulated dose. For sets where V_{th} changes by less than 5V, linear equations can be fitted to the data, whereas quadratic equations give the best fit for changes of > 5V.

7.2 Future Work

The following matters should be investigated before the MOSFETs can be used clinically:

- *Surface response*

  For skin dose IVD, the MOSFETs would be placed onto the patient's surface without buildup, so their response under these conditions should be examined. In addition, the use of buildup caps could be investigated to provide appropriate buildup conditions for internal dose determinations.

- *Use of automatic mode for continuous readings during irradiation*

  Determine an optimum frequency for taking repeated readings, such as for total body irradiations, taking into account the accumulated dose of the probes.

- *Energy dependence*

  Determine suitability of use of MOSFETs with superficial and orthovoltage X-ray beams.

- *Temperature dependence*

  Investigate variations in response with temperature, particularly in the range of human body temperatures, and determine an appropriate calibration and reading procedure to account for response variations.

- *Greater range of linearity*

  Investigate linearity for doses higher than those used in this work, particularly using the dual sensitivity (high dose) probes.

- *Lifetime of dual sensitivity (high dose) probes*

  Determine saturation V_{th} for these probes.

- *Beam modifiers and field size dependence*

  Investigate any field size effects, and response variations with beam modifiers such as photon wedges.

- *Annealing*

  It may be possible to anneal the saturated MOSFET probes for re-use. This would involve investigating various temperature and heating time combinations which would result in the release of trapped electrons and holes, in an attempt to restore them to their pre-irradiation state. It would then be necessary to re-investigate their characteristics.

- *Angular dependence* for orientations other than those investigated in the current work, e.g. along cable axis

- *Calibration against secondary standard ion chambers,* prior to use for IVD, in accordance with ACPSEM recommendations [88]

CORRECTION METHODS FOR SENSITIVITY REDUCTION WITH ACCUMULATED DOSE

A1 Drift response

In characterising reading delay response (section 5.3), many repeated exposures were made, with read-outs at random time intervals prior to or following the exposures. Over the course of these measurement sets, the inherent reduction of sensitivity with accumulated dose became significant, in that the data reflected not only the effects of reading delay, but also of reduced sensitivity. It was therefore necessary to account for this sensitivity drift prior to analysing the data for reading delay response.

It was initially envisaged that the ΔV_{th} or sensitivity drift equations which had previously been ascertained (section 5.1) could be used for this purpose. It was first considered that, assuming the measured data conformed to the drift equation, the data could be corrected using the "distance from a point to a line" method, as follows.

For example, the average ΔV_{th} drift equation for 50 cGy doses had been determined to be of the form $Ax^2 - Bx + C$:

$$\Delta V_{th} = 1 \times 10^{-7} x^2 - 0.0083x + 318.16 \quad \text{.....(1)}$$

where $x = V_{th}$, which increases (greater negative voltage) with accumulated dose. The distance between each data point and the drift line was firstly obtained, then each point was shifted to a position that same distance from the line of constant ΔV_{th}, as shown in fig A1-1.

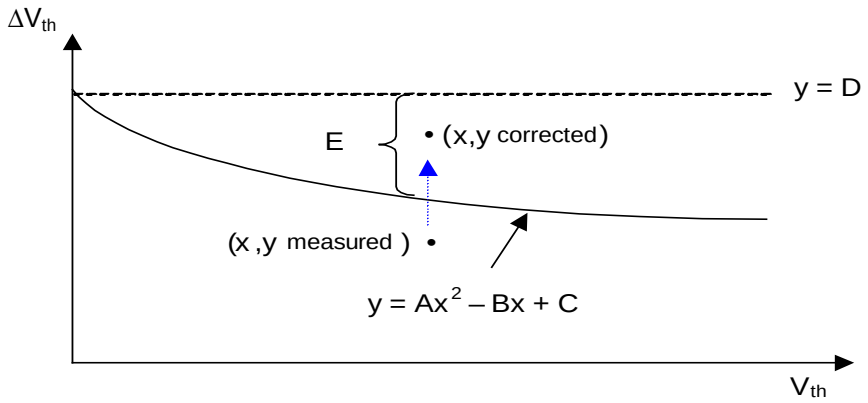

Figure A1-1 Method of correction for change of sensitivity with accumulated dose

However, on applying the average ΔV_{th} drift equation to the measured data, the required correction was not achieved. Nor was it achieved using the average sensitivity drift equation, nor linear trendlines for ΔV_{th} and sensitivity rather than quadratic equations, as can be seen in figure A1-2.

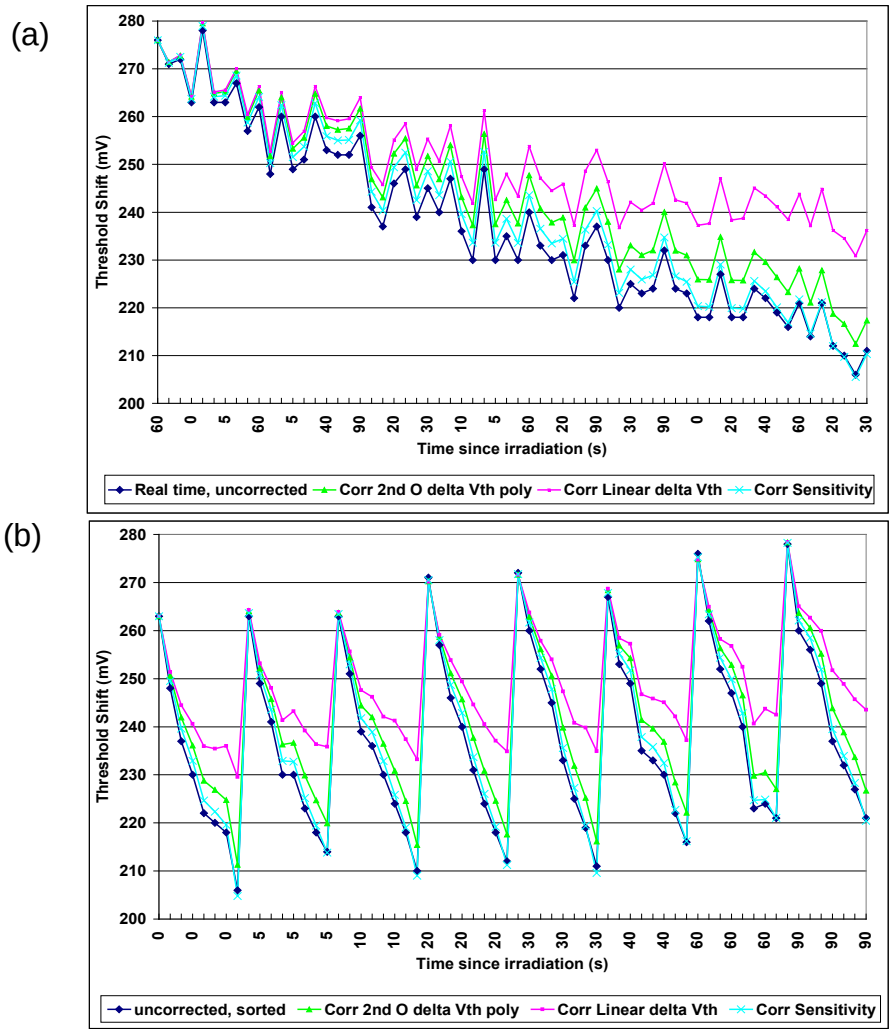

Figure A1-2 Threshold Shift measurements, real-time data. Readings taken at random times after repeated irradiations of 50 cGy, 4MV. (a) Data corrected for sensitivity drift using average drift equations previously obtained for ΔV_{th} and sensitivity. (b) Data from (a) sorted into ascending time order

The dark blue graph in figure A1-2 (a) shows the real-time data, obtained from repeated irradiations of one probe from "new" until saturation, with doses of 50 cGy from a 4MV linac beam. After each irradiation, read-out was delayed for a random period between 0 and 90 seconds, as shown on the x-axis of the figure, to investigate any read-out delay response. At least 8 measurements for each time interval were made throughout the probe's lifetime. During the set of measurements, ΔV_{th} changed from 276 mV to 211 mV, a reduction of 23.5%. The same data, sorted into

ascending time order, as shown in figure A1-2 (b) indicates a possible reading delay effect, however it can be seen that the application of the average quadratic ΔV_{th} and sensitivity drift equations did not correct for the sensitivity change, nor did the linear ΔV_{th} drift equation.

The reason for this became apparent on consideration of a plot of ΔV_{th} vs V_{th} showing the data for various time intervals between irradiation and read-out (figure A1-3). It was observed that there was a general upward shift of the curve with increasing delay of read-out. This means that, since the ΔV_{th} and sensitivity drift equations had been obtained for *immediate* read-outs, their use for *delayed* read-outs was not effective nor appropriate.

This problem was overcome by the use the sensitivity drift equation for the *measurement period* rather than the drift equations which had been obtained previously with *immediate* read-outs. This "measurement interval drift equation" then related to *all* of the measurement intervals, not only those where the read-out was taken *immediately* following irradiation. For measurement periods over the lifetime of the probes, quadratic equations were found to give the best fit to the measured data.

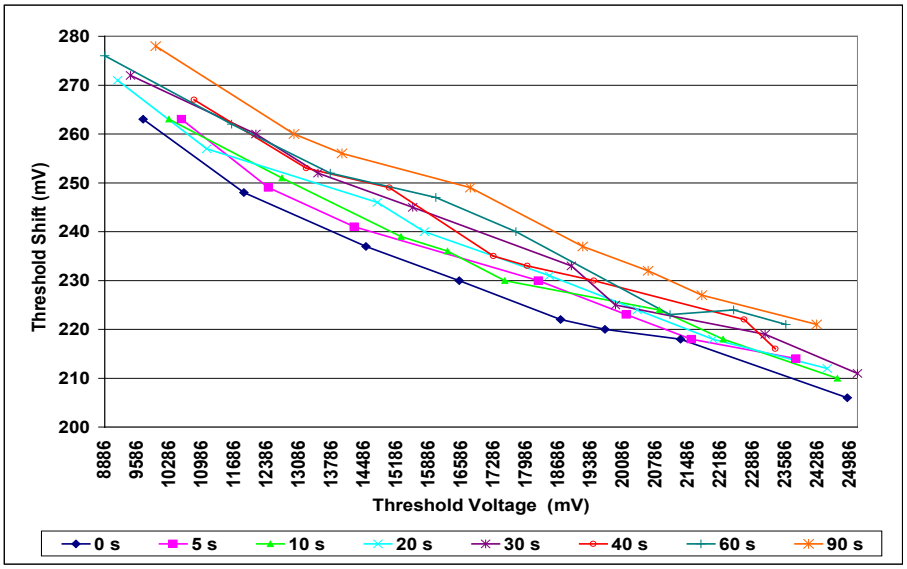

Figure A1-3 Various time intervals since irradiations, uncorrected for sensitivity reduction

Figure A1-4 is an example of the correction method of sensitivity drift correction using the ΔV_{th} and the measurement interval drift equations. The calculations (using arbitrary data) for this method are tabled in Table

9 which shows the results using the different drift equations. The measurement interval drift equation achieves the required correction of the data.

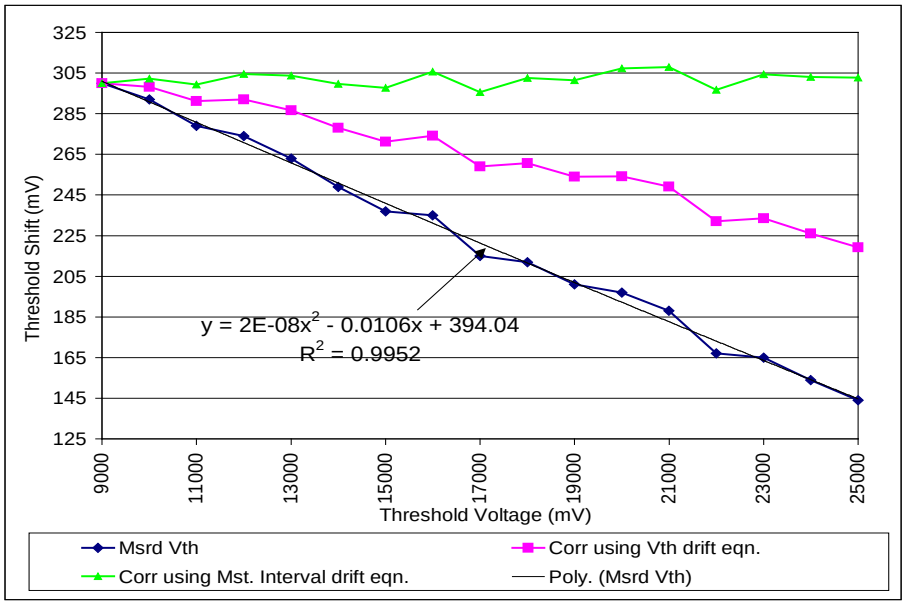

Figure A1-4 Example of correction to eliminate effect of sensitivity drift due to accumulated dose (arbitrary data)

ΔV_{th} drift equation:
Threshold Shift = $1 \times 10^{-7} x^2 - 0.0081 x + 318.16$
where A = 0.0000001
B = 0.0081
(measured intercept) C = 318.16
(theoretical intercept) D = 253.36

Measurement interval drift equation:
Threshold Shift = $2 \times 10^{-8} x^2 - 0.0106 x + 394.04$
A = 0.00000002
B = 0.0106
C = 394.04
D = 300.26

Using ΔV_{th} drift equation:

THRESHOLD VOLTAGE (V) (x)	MEASURED THRESHOLD SHIFT (mV) (y)	Ax^2	Bx	THEORETICAL Y (on Constancy line $Ax^2 - Bx + C$)	THEORETICAL INTERCEPT MINUS THEORETICAL Y (D - [Ax^2 - Bx + C]) (E)	CORRECTED THRESHOLD SHIFT ± 2mV (E + y)
9000	300	8	73	**253.36**	0.00	300.00
10000	292	10	81	247.16	6.20	298.20
11000	279	12	89	241.16	12.20	291.20
12000	274	14	97	235.36	18.00	292.00
13000	263	17	105	229.76	23.60	286.60
14000	249	20	113	224.36	29.00	278.00
15000	237	23	122	219.16	34.20	271.20
16000	235	26	130	214.16	39.20	274.20
17000	215	29	138	209.36	44.00	259.00
18000	212	32	146	204.76	48.60	260.60
19000	201	36	154	200.36	53.00	254.00
20000	197	40	162	196.16	57.20	254.20
21000	188	44	170	192.16	61.20	249.20
22000	167	48	178	188.36	65.00	232.00
23000	165	53	186	184.76	68.60	233.60
24000	154	58	194	181.36	72.00	226.00
25000	144	63	203	178.16	75.20	219.20

Using Measurement interval drift equation:

THRESHOLD VOLTAGE (V) (x)	MEASURED THRESHOLD SHIFT (mV) (y)	Ax^2	Bx	THEORETICAL Y (on Constancy line $Ax^2 - Bx + C$)	THEORETICAL INTERCEPT MINUS THEORETICAL Y (D - [Ax^2 - Bx + C]) (E)	*CORRECTED* THRESHOLD SHIFT ± 2mV (E + y)
9000	300	2	95	**300.26**	0.00	300.00
10000	292	2	106	290.04	10.22	302.22
11000	279	2	117	279.86	20.40	299.40
12000	274	3	127	269.72	30.54	304.54
13000	263	3	138	259.62	40.64	303.64
14000	249	4	148	249.56	50.70	299.70
15000	237	5	159	239.54	60.72	297.72
16000	235	5	170	229.56	70.70	305.70
17000	215	6	180	219.62	80.64	295.64
18000	212	6	191	209.72	90.54	302.54
19000	201	7	201	199.86	100.40	301.40
20000	197	8	212	190.04	110.22	307.22
21000	188	9	223	180.26	120.00	308.00
22000	167	10	233	170.52	129.74	296.74
23000	165	11	244	160.82	139.44	304.44
24000	154	12	254	151.16	149.10	303.10
25000	144	13	265	141.54	158.72	302.72

Table 9 Example of calculations used for sensitivity drift correction

A2 Linearity

The correction method outlined in A1 above was not appropriate for measurements taken to test for linearity, since different *delivered doses* were being given in each measurement set. Fig A2-1 is typical of the uncorrected raw data.

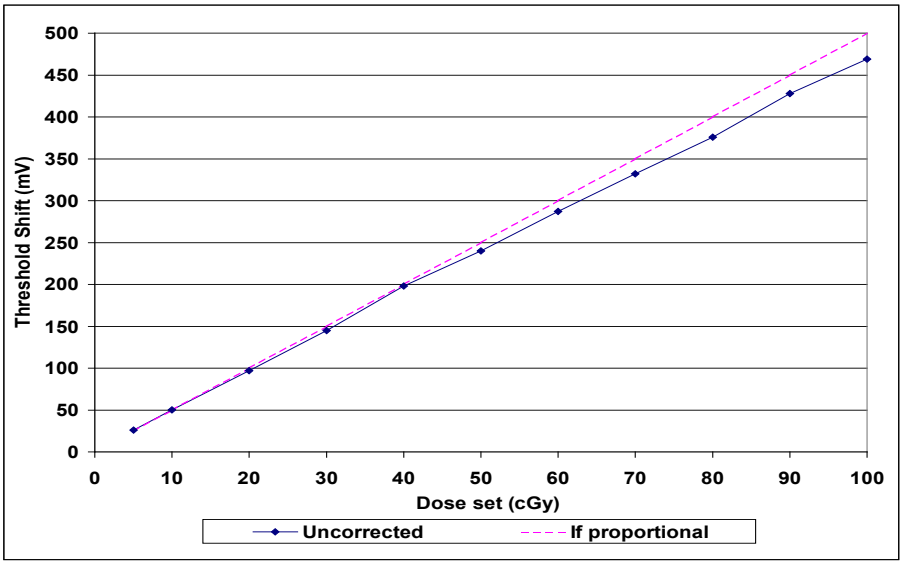

Figure A2-1 Uncorrected data to investigate linearity

Sub-proportionality is indicated, however, these data also reflect the decreased sensitivity over the measurement period, which must be eliminated before analysis for linearity.

To correct for the sensitivity reduction, four methods were trialled using 2 probes (1 each of high and low sensitivity) in an endeavour to determine an optimum method. These involved taking 2 consecutive reading sets, and averaging the results. Different orders of doses were investigated, to determine whether this factor was significant. The methods of reading were as follows:

1. 2 sets from low to high doses;
2. A set from low to high doses, and then from high to low doses;
3. As for 1. above, corrected using the sensitivity drift equation over the measurement interval;
4. As for 2. above, corrected using the sensitivity drift equation over the measurement interval.

The results were considered as a percentage difference from the ΔV_{th} obtained for the 50 cGy or 250 cGy delivered doses (high or low sensitivity probes respectively). Examples of these methods are shown in figure A2-2. Methods 3 and 4 are similar to the method described in A1 however, since delivered dose was a variable, the readings of ΔV_{th} were first converted to sensitivity as follows:

(a) The raw "as read" ΔV_{th} data were divided by dose set, to obtain sensitivity in mV/cGy.

(b) The sensitivity data were graphed against dose set, and trendlines were fitted to obtain the sensitivity drift equation over the measurement interval. Quadratic equations were found to give the best fit in most cases.

(c) The distance between the trendline and the line "sensitivity = constant" (the normalisation point, D) was ascertained and added to each data point. The constant selected was 50 cGy for the low sensitivity probes, or 250 cGy for the high sensitivity probes. (It had previously been ascertained that the first data point proved unreliable for normalisation purposes, due to the greater statistical effect of the ± 2 mV uncertainty in readings, in view of the relatively small shifts involved.)

(d) The data were re-converted to ΔV_{th} and the two sets were averaged. The maximum difference between the sets was 4%.

(e) Deviations from proportionality were then determined.

Average percentage variations from proportionality, with standard deviations, were as follows:

Method	Average % Difference from Proportionality	Standard Deviation %
1	-1.0	2.3
2	1.4	2.0
3	-0.6	0.9
4	1.5	1.3

These results indicate similar average variations from proportionality, but Methods 3 and 4 achieve less standard deviation.

EXAMPLE OF CORRECTION FOR SENSITIVITY DRIFT DURING CHECKS FOR LINEARITY
probe #18 (high sensitivity)

Method 1
2 reading sets: from low to high doses

DOSE SET (cGy)	MEASURED THRESHOLD SHIFT (mV) (y) 1st set	2nd set	AVERAGE OF 2 SETS	IF PROP'L	% DIFF'CE FROM PROP'Y
0					
5	26		25	24	4.2
10	50		49	48	1.0
20	101		96	96	0.0
30	148		144	144	-0.3
40	199		192	192	0.0
50	247		240	240	0.0
60	299		288	288	-0.2
70	341		329	336	-2.2
80	397		380	384	-1.2
90	434		420	432	-2.8
100	485		470	480	-2.2
110					
120	574		553	576	-4.0
130					
140	659		640	672	-4.8
5		24		Avge:	-1.0
10		47		St. Dev:	2.3
20		91			
30		139			
40		185			
50		233			
60		276			
70		316			
80		362			
90		406			
100		454			
110					
120		532			
130					
140		620			

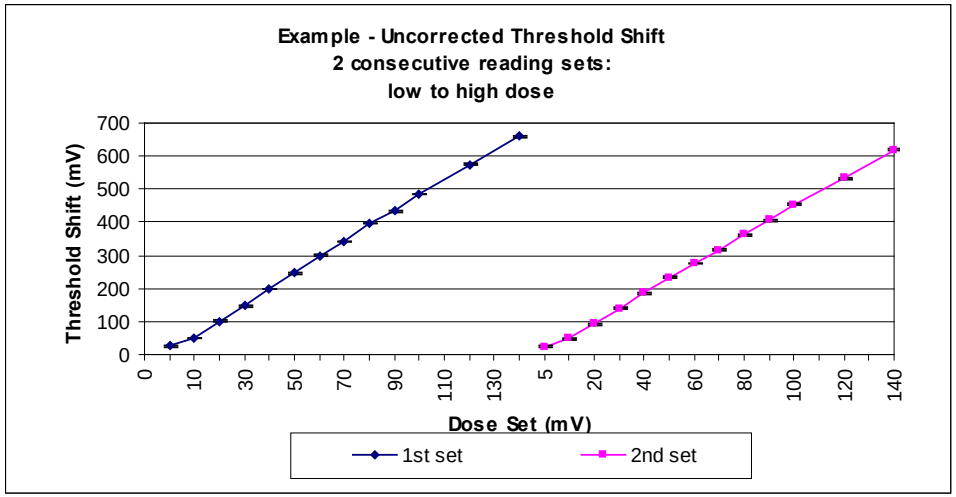

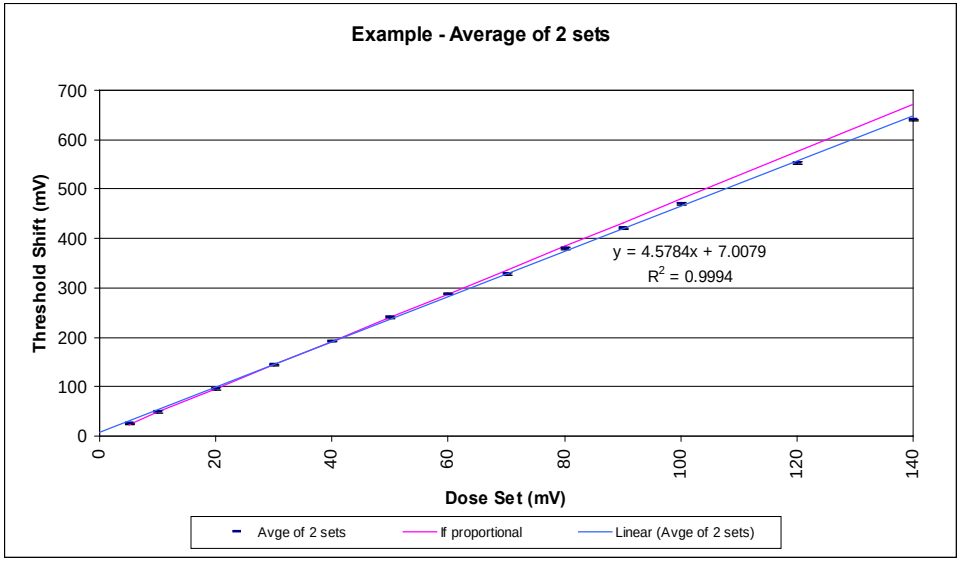

Figure A2-2 (a) Correction of linearity data for sensitivity drift with accumulated dose – Method 1

EXAMPLE OF CORRECTION FOR SENSITIVITY DRIFT DURING CHECKS FOR LINEARITY

probe #D13 (low sensitivity)

Method 2

2 reading sets: from low to high doses, then from high to low doses

DOSE SET (cGy)	MEASURED THRESHOLD SHIFT (mV) (y) 1st set	2nd set	AVERAGE OF 2 SETS	IF PROP'L	% DIFF'CE FROM PROP'Y
0					
50	21		20	19	6.4
100	40		38	38	1.1
150	59		57	56	1.1
200	80		78	75	3.1
250	97		94	94	0.0
300	116		113	113	0.2
350	136		133	132	1.1
400	152		149	150	-0.9
450	175		171	169	0.8
500	190		191	188	1.3
500		191		Avge:	1.4
450		166		St. Dev:	2.0
400		146			
350		130			
300		110			
250		91			
200		75			
150		55			
100		36			
50		19			
0					

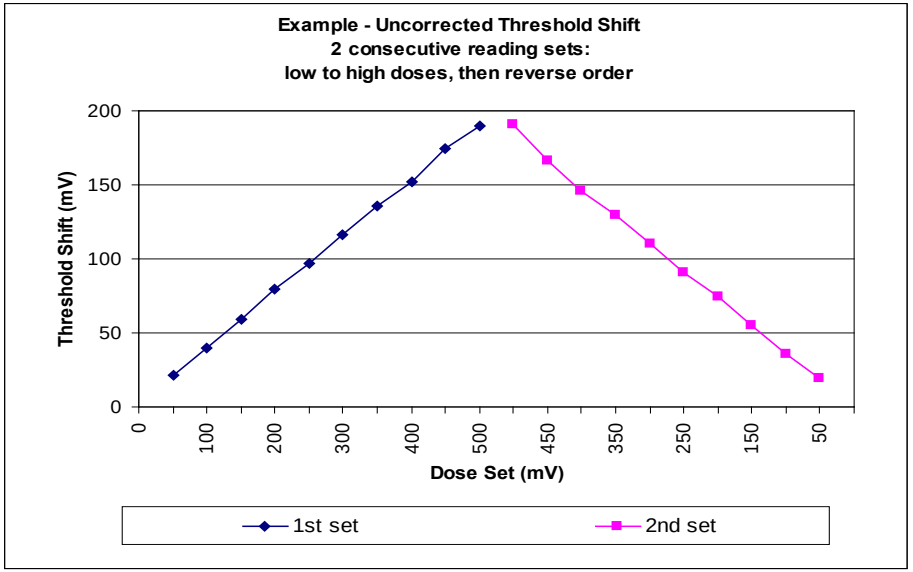

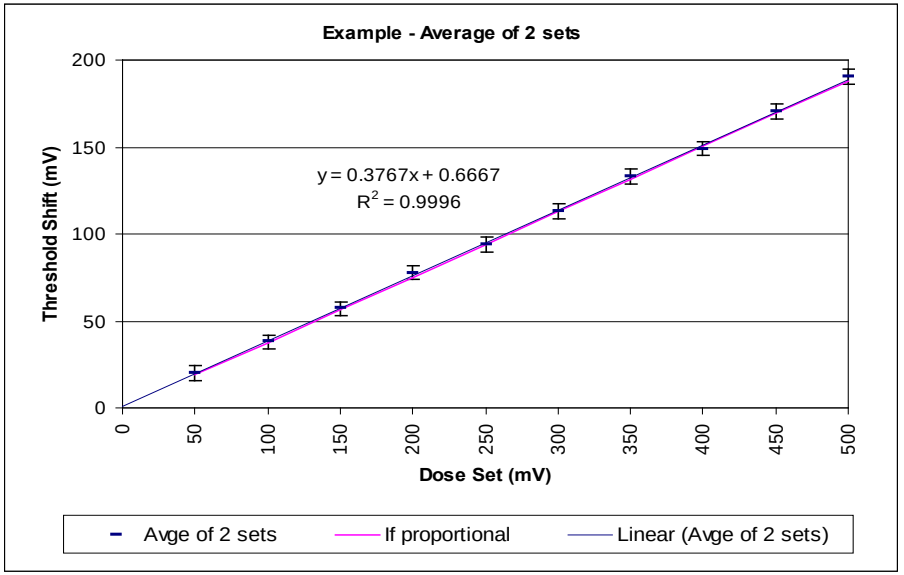

Figure A2-2 (b) Correction of linearity data for sensitivity drift with accumulated dose – Method 2

EXAMPLE OF CORRECTION FOR SENSITIVITY DRIFT DURING CHECKS FOR LINEARITY

Probe #18 (high sensitivity) — Corrected using sensitivity drift equation over measuring interval

Method 3
2 reading sets: low to high doses
Corrected using sensitivity drift equation

A	0.0002	
B	0.0261	
C	5.1132	
D	5.06	(normalised to 10 cGy data point)

Dose Set (cGy)	Measured Shift (mV)		Sensitivity mV/cGy	"X"	X^2	$A * X^2$	B*X	E AX^2-BX+C	F = D - E	F + Sens'y	Converted back to TS	Average of 2 sets	If prop'l	% Diff'ce
5	26		5.20	1	1	0.00	0.03	5.09	-0.03	5.17	26	26	25	1.6
10	50		5.00	2	4	0.00	0.05	5.06	0.00	5.00	50	50	50	-0.9
20	101		5.05	3	9	0.00	0.08	5.04	0.02	5.07	101	99	101	-1.4
30	148		4.93	4	16	0.00	0.10	5.01	0.05	4.98	149	149	151	-1.3
40	199		4.98	5	25	0.01	0.13	4.99	0.07	5.05	202	200	202	-0.6
50	247		4.94	6	36	0.01	0.16	4.96	0.10	5.04	252	252	252	-0.1
60	299		4.98	7	49	0.01	0.18	4.94	0.12	5.10	306	303	302	0.1
70	341		4.87	8	64	0.01	0.21	4.92	0.14	5.01	351	348	353	-1.4
80	397	Trial 1	4.96	9	81	0.02	0.23	4.89	0.17	5.13	410	403	403	0.0
90	434		4.82	10	100	0.02	0.26	4.87	0.19	5.01	451	448	454	-1.2
100	485		4.85	11	121	0.02	0.29	4.85	0.21	5.06	506	503	504	-0.2
110														
120	574		4.78	13	169	0.03	0.34	4.81	0.25	5.04	604	598	605	-1.2
130														
140	659		4.71	15	225	0.05	0.39	4.77	0.29	5.00	700	696	706	-1.3
													Avge:	-0.6
													St. Dev:	0.9
5	24		4.80	14	196	0.04	0.37	4.79	0.27	5.07	25			
10	47		4.70	15	225	0.05	0.39	4.77	0.29	4.99	50			
20	91		4.55	16	256	0.05	0.42	4.75	0.31	4.86	97			
30	139		4.63	17	289	0.06	0.44	4.73	0.33	4.97	149			
40	185		4.63	18	324	0.06	0.47	4.71	0.35	4.98	199			
50	233		4.66	19	361	0.07	0.50	4.69	0.37	5.03	252			
60	276		4.60	20	400	0.08	0.52	4.67	0.39	4.99	299			
70	316	Trial 2	4.51	21	441	0.09	0.55	4.65	0.41	4.92	344			
80	362		4.53	22	484	0.10	0.57	4.64	0.42	4.95	396			
90	406		4.51	23	529	0.11	0.60	4.62	0.44	4.95	446			
100	454		4.54	24	576	0.12	0.63	4.60	0.46	5.00	500			
110														
120	532		4.43	26	676	0.14	0.68	4.57	0.49	4.92	591			
130														
140	620		4.43	28	784	0.16	0.73	4.54	0.52	4.95	693			

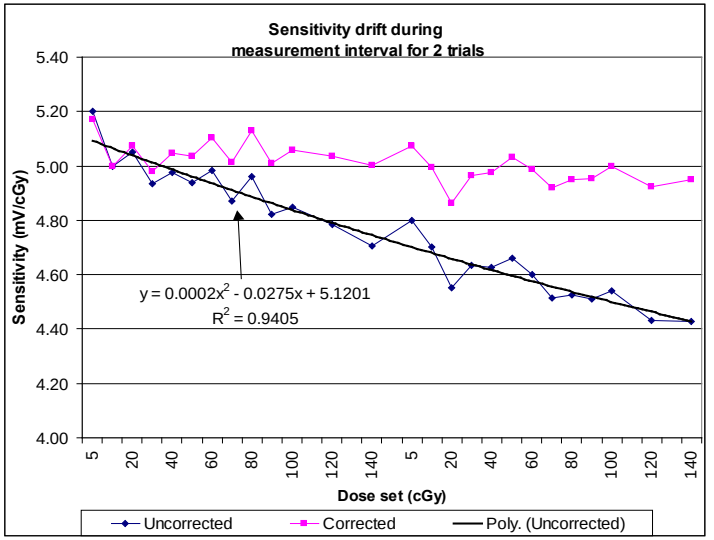

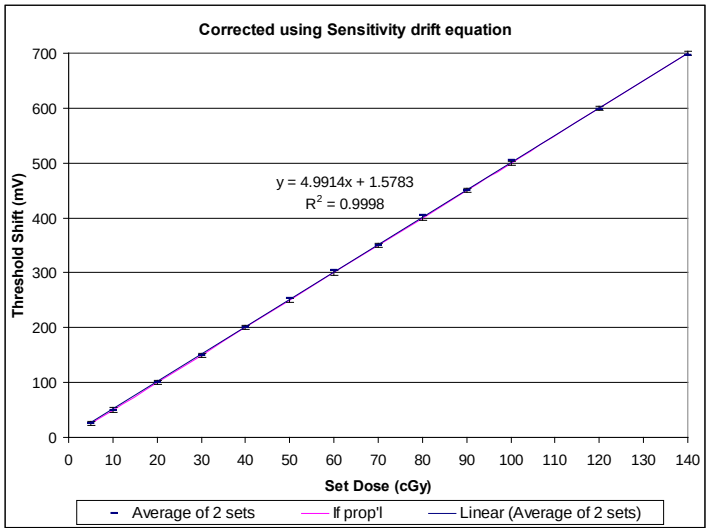

Figure A2-2 (c) Correction of linearity data for sensitivity drift with accumulated dose – Method 3

EXAMPLE OF CORRECTION FOR SENSITIVITY DRIFT DURING CHECKS FOR LINEARITY
Probe #D13 (low sensitivity)

Method 4
2 reading sets: low to high doses, then high to low
Corrected using sensitivity drift equation

A	0.0002	
B	0.0057	
C	0.4167	
D	0.41	(normalised to 10 cGy data point)

Dose set (cGy)	Threshold Shift (mV) +/- 4mV		Sensitivity mV/cGy	X	X^2	A * X^2	B*X	E AX^2-BX+C	F = D - E	F + Sens'y	Converted back to TS	Average of 2 sets +/- 4mV	If prop'l	% Diff'ce
50	21		0.42	1	1	0.00	0.01	0.41	0.00	0.42	21	21	20	3.3
100	40		0.40	2	4	0.00	0.01	0.41	0.00	0.40	40	40	40	0.0
150	59		0.39	3	9	0.00	0.02	0.40	0.01	0.40	60	60	60	0.0
200	80		0.40	4	16	0.00	0.02	0.40	0.01	0.41	83	82	80	2.5
250	97	Trial 1	0.39	5	25	0.01	0.03	0.39	0.02	0.40	101	100	100	0.3
300	116		0.39	6	36	0.01	0.03	0.39	0.02	0.41	122	121	120	0.9
350	136		0.39	7	49	0.01	0.04	0.39	0.02	0.41	144	143	140	2.2
400	152		0.38	8	64	0.01	0.05	0.38	0.03	0.41	162	161	160	0.6
450	175		0.39	9	81	0.02	0.05	0.38	0.03	0.42	188	184	180	2.4
500	190		0.38	10	100	0.02	0.06	0.38	0.03	0.41	205	206	200	3.0
500	191		0.38	11	121	0.02	0.06	0.38	0.03	0.41	207		Avge:	1.5
450	166		0.37	12	144	0.03	0.07	0.38	0.03	0.40	181		St. Dev:	1.3
400	146		0.37	13	169	0.03	0.07	0.38	0.03	0.40	159			
350	130		0.37	14	196	0.04	0.08	0.38	0.03	0.41	142			
300	110		0.37	15	225	0.05	0.09	0.38	0.03	0.40	120			
250	91	Trial 2	0.36	16	256	0.05	0.09	0.38	0.03	0.40	99			
200	75		0.38	17	289	0.06	0.10	0.38	0.03	0.41	81			
150	55		0.37	18	324	0.06	0.10	0.38	0.03	0.40	60			
100	36		0.36	19	361	0.07	0.11	0.38	0.03	0.39	39			
50	19		0.38	20	400	0.08	0.11	0.38	0.03	0.41	20			

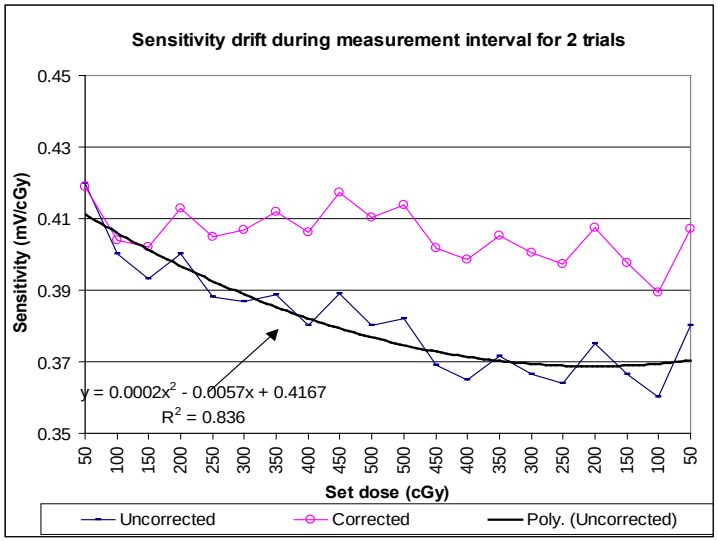

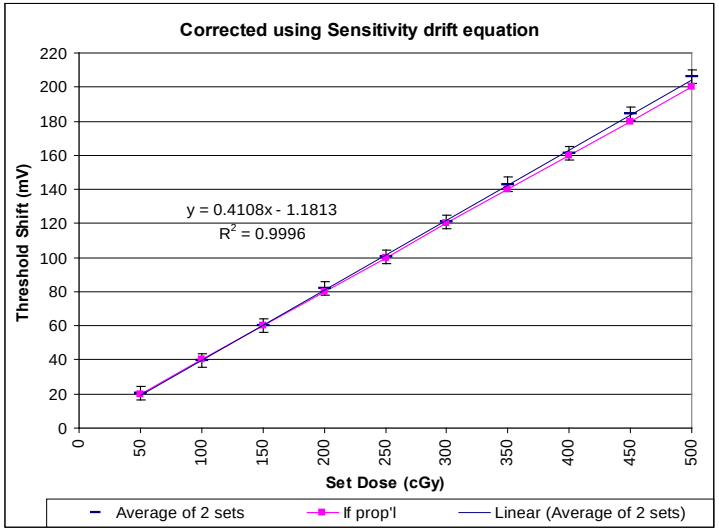

Figure A2-2 (d) Correction of linearity data for sensitivity drift with accumulated dose – Method 4

A3 Angular dependence

Figures. A3-1 and A3-2 show the steps involved in data correction for sensitivity reduction with accumulated dose over the course of the measurement interval. The raw data (figure A3-2(a)) are uncorrected measurements of ΔV_{th} for two consecutive rotations. These data were then plotted as a continuous graph of ΔV_{th} vs angle (figure A3-1), the drift equation was obtained (as shown on the graph) and used to correct for accumulated dose, as described in A1 above. The resulting data are shown in A3-2(b). Then, the results were normalised to the result for 0^o angle (100% defined at 0^o as the ΔV_{th} with the epoxy bubble facing towards the beam) (A3-2(c)). Finally, the two sets were averaged to achieve the final graph A3-2(d). The maximum difference between the two sets was < 6%.

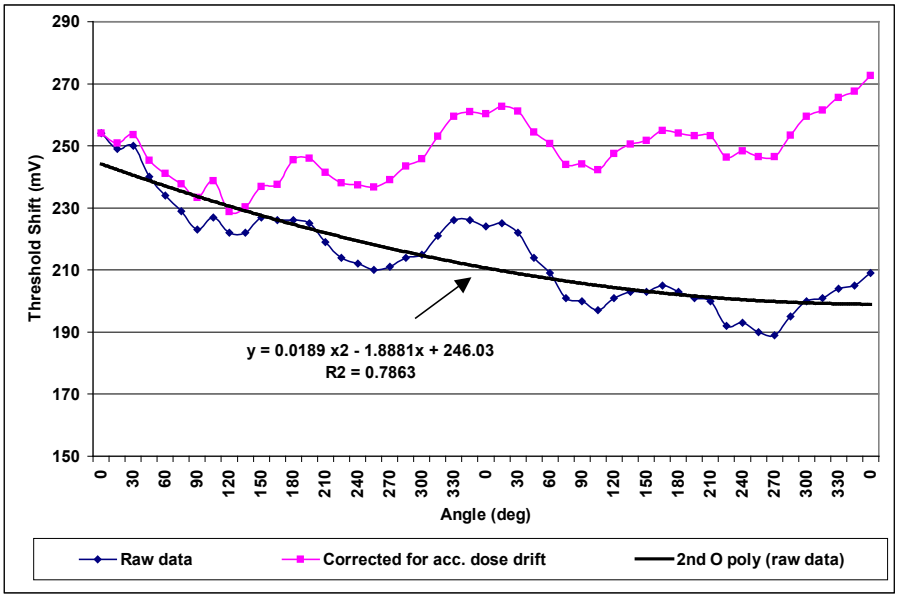

Figure A3-1 Example of accumulated dose drift equation correction for angular dependence measurements

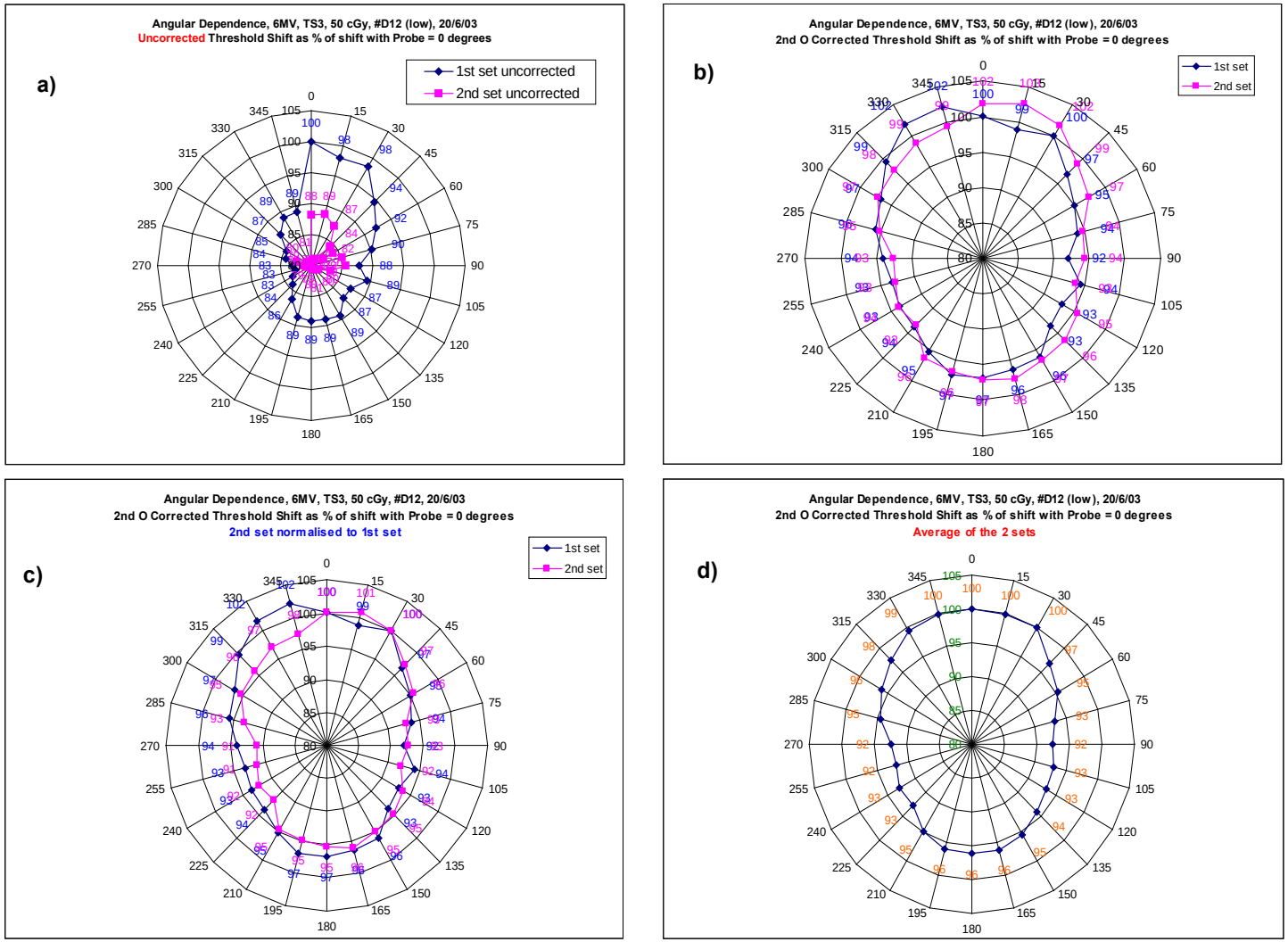

Figure A3-2 Steps for correction for sensitivity reduction with accumulated dose.
(a) uncorrected data; (b) data corrected with drift equation over the measurement interval;
(b) (c) second set normalised to first set; (d) average of two sets.

GLOSSARY OF TERMS

Absorbed dose, Gy	The amount of energy deposited in a medium. The SI unit for absorbed dose is the Gray (Gy) where 1 Gy = 1 joule/kg.
Accumulated dose	Total dose (Gy) delivered to a MOSFET.
Angular dependence	Effect on ΔV_{th} of different orientations of MOSFETs to the incident radiation beam.
Bandgap	The difference in energies between the valence and conduction bands in an atom.
Border traps	Defects in SiO_2 between 0.2-2 nm from the interface with Si in which charge may be trapped.
CMRP	Centre for Medical Radiation Physics, The University of Wollongong, New South Wales, Australia.
Creep-up	Response drift between two post-irradiation readings of a MOSFET, i.e. different readings of ΔV_{th} for the same radiation exposure, depending on the difference in time between the radiation and the readings being taken. Also known as “fade”, “drift” and “annealing”.
Drift curve	Graph of ΔV_{th} vs ln(time).
Epoxy bubble	The protective coating covering the MOSFET.
Fermi level	Energy level in an atom for which there are equal densities of filled shells above and below it.
Flatband voltage	Applied gate voltage which yields a flat energy band in a semiconductor. It equals the difference between the work-functions of the metal and the semi-conductor minus terms expressing the voltage across the SiO_2 due to charge at the interface with the Si substrate and in the oxide.
Gate voltage, V_g	The bias voltage between the substrate and the aluminium gate in a MOSFET.
In vivo dosimetry (IVD)	Real-time measurement of absorbed dose received during a treatment.
Interface traps	Defects at < 0.2 nm of the Si/SiO_2 interface which increase the density of energy levels within the bandgap, close to the valence or conduction band.

Inversion layer	In n-type Si, inversion occurs at the interface between the substrate and the SiO_2 layer when a negative gate bias is applied. This voltage repels electrons from, and holes to, the interface, producing a positively charged channel. This region of the substrate, having been "inverted" from n-type to p-type is called the "inversion layer".
Ionising radiation	High energy radiation which, on interaction with an atom, can remove electrons from their orbits. This causes the atom to become charged or ionized.
MOSFET	Metal Oxide Semiconductor Field Effect Transistor comprising silicon substrate with source and drain terminals, SiO_2 sensitive region and aluminium gate. They may be operated in different modes, depending on the bias voltage between the substrate and the gate, called "gate voltage". Semiconductors doped with extra electrons are called "donors" or "n-type", whilst those with extra holes are called "acceptors" or "p-type".
"New" probe	MOSFET having less than 20 Gy accumulated dose
"Old" probe	MOSFET having greater than 20 Gy accumulated dose
Reading delay	A delay between irradiation and either the pre-irradiation reading or the post-irradiation reading.
Reading interval effect	Effect on ΔV_{th} of repeated post-irradiation readings made at varying time intervals.
Saturation	Occurs in a MOSFET when all available charge traps have been filled and the gate charge density equals the trapped charge density.
Semiconductor	Materials in which, under certain conditions (e.g. heating) electrons in the valence band are able to surmount the bandgap and enter the conduction band and carry negative charge throughout the lattice structure. The vacancy left in the valence band can similarly carry positive charge.
Sensitive region	The sensitive (or "active") region of a MOSFET is the SiO_2 layer.
Sensitivity, mV/cGy	A measure of the response of a dosimeter to radiation, defined as ΔV_{th}*/dose.*
Threshold shift, ΔV_{th}	The difference in readings of V_{th} (mV) prior to and following irradiation of a MOSFET.
Threshold voltage, V_{th}	In relation to MOSFETs, V_{th} is the gate voltage at which a specified constant current flows between source and drain.
Work function	Voltage required to extract an electron from the Fermi level to the vacuum level (outside the atom).

APPENDIX C

SUMMARY OF RESULTS OF MEASUREMENTS OF ΔVth AND SENSITIVITY OVER LIFETIME OF PROBES

SENSITIVITY is defined as (ΔV_{th} per dose) vs V_{th} ($\propto$ accumulated dose)

Probe #	Beam Energy MV	Dose cGy	% Reduction in ΔV_{th} / Sensitivity over lifetime (± 1%)	Linear trendline equations ("x" = V_{th}, mV)		2nd O polynomial nominal trendline equations ("x" = V_{th}, mV)		Comments
				ΔV_{th}	Sensitivity	ΔV_{th}	Sensitivity	
7	4	50	22.2	$-3.6\times10^{-3}\ x + 295.20$	$-7\times10^{-5}\ x + 5.9045$	$1\times10^{-7}\ x^2 - 7.6\times10^{-3}\ x + 327.89$	$2\times10^{-9}\ x^2 - 2\times10^{-4}\ x + 6.5599$	
8	4	50	22.1	$-3.7\times10^{-3}\ x + 295.69$	$-7\times10^{-5}\ x + 5.9139$	$1\times10^{-7}\ x^2 - 8.4\times10^{-3}\ x + 334.39$	$3\times10^{-9}\ x^2 - 2\times10^{-4}\ x + 6.6879$	
13	4	20	22.2	$-1.6\times10^{-3}\ x + 118.94$	$-8\times10^{-5}\ x + 5.9472$	$7\times10^{-8}\ x^2 - 4.0\times10^{-3}\ x + 137.88$	$4\times10^{-9}\ x^2 - 2\times10^{-4}\ x + 6.8940$	used to ~ 24V
14	4	20	23.6	$-1.5\times10^{-3}\ x + 118.59$	$-8\times10^{-5}\ x + 5.9309$	$6\times10^{-8}\ x^2 - 3.7\times10^{-3}\ x + 135.07$	$3\times10^{-9}\ x^2 - 2\times10^{-4}\ x + 6.7584$	used to ~ 24V
19	6	20	22.6	$-1.4\times10^{-3}\ x + 114.81$	$-7\times10^{-5}\ x + 5.7362$	$6\times10^{-8}\ x^2 - 3.5\times10^{-3}\ x + 132.27$	$3\times10^{-9}\ x^2 - 2\times10^{-4}\ x + 6.6208$	used to ~ 26.5V
22	6	50	22.7	$-3.5\times10^{-3}\ x + 278.32$	$-7\times10^{-5}\ x + 5.5664$	$1\times10^{-7}\ x^2 - 8.3\times10^{-3}\ x + 318.16$	$3\times10^{-9}\ x^2 - 2\times10^{-4}\ x + 6.3632$	
D7(low)	4	50	21.7	$-3.8\times10^{-3}\ x + 301.93$	$-8\times10^{-5}\ x + 6.0386$	$2\times10^{-7}\ x^2 - 10.4\times10^{-3}\ x + 354.66$	$4\times10^{-9}\ x^2 - 2\times10^{-4}\ x + 7.0932$	
D8(low)	4	50	21.8	$-4.1\times10^{-3}\ x + 305.21$	$-8\times10^{-5}\ x + 6.1041$	$1\times10^{-7}\ x^2 - 8.7\times10^{-3}\ x + 340.76$	$3\times10^{-9}\ x^2 - 2\times10^{-4}\ x + 6.8151$	
D9(low)	4	50	21.7	$-4.1\times10^{-3}\ x + 305.58$	$-8\times10^{-5}\ x + 6.1116$	$2\times10^{-7}\ x^2 - 9.1\times10^{-3}\ x + 343.99$	$3\times10^{-9}\ x^2 - 2\times10^{-4}\ x + 6.8798$	
D11(low)	6	50	23.1	$-3.5\times10^{-3}\ x + 281.77$	$-7\times10^{-5}\ x + 5.6354$	$1\times10^{-7}\ x^2 - 8.7\times10^{-3}\ x + 324.18$	$3\times10^{-9}\ x^2 - 2\times10^{-4}\ x + 6.4835$	
		Avge:	**22.37**	**Avge R^2 values: 0.954**		**Avge R^2 values: 0.980**		
		St Dev:	**0.63**					

LINEARITY / PROPORTIONALITY RESULTS

APPENDIX D

2nd O Sensitivity drift equation over measurement interval for Accumulated dose correction
4MV
Normalised to Shift for 50 cGy (or 250 cGy for dual (low dose) probes)

Dose Set cGy	Probe #	Date	As Read Shift (mV) +/- 2 mV	Corrected Shift (mV) +/- 2 mV	Upper error mV	Lower error mV	Shift If directly proportional mV	Deviation from proportion'y %	Upper error Deviation from proportion'y %	Lower error Deviation from proportion'y %	Average Deviation %	Max. Deviation %	Min. Deviation %	Max. Deviation (excl. 5, 10 & 20/50 cGy) %	Min. Deviation (excl. 5,10 & 20/50 cGy) %	Avge. Deviation (excl. 5,10 & 20/50 cGy) %
5	4	09/08/2002	28	27	29	25	26	5.5	13.3	-2.3						
10	Trial 1, probe 1		48	48	50	46	51	-6.3	-2.3	-10.2						
20	1 to 1-1/2 min		97	99	101	97	102	-3.3	-1.4	-5.3						
30	between readings		146	153	155	151	154	-0.4	0.9	-1.7						
40			196	208	210	206	205	1.6	2.5	0.6						
50			238	256	258	254	256	0.0	0.8	-0.8						
60			290	314	316	312	307	2.2	2.9	1.6						
70			335	364	366	362	358	1.6	2.1	1.0						
80			380	412	414	410	410	0.6	1.1	0.1						
90			429	462	464	460	461	0.3	0.7	-0.2						
100			474	505	507	503	512	-1.4	-1.0	-1.8	0.0	5.5	-6.3	2.2	-1.4	0.6
5	6	09/08/2002	26	26	28	24	25	3.2	11.1	-4.8						
10	Trial 1, probe 2		50	50	52	48	50	-0.8	3.2	-4.8						
20	1 to 1-1/2 min		97	98	100	96	101	-2.8	-0.8	-4.8						
30	between readings		145	149	151	147	151	-1.5	-0.1	-2.8						
40			198	206	208	204	202	2.2	3.2	1.2						
50			240	252	254	250	252	0.0	0.8	-0.8						
60			287	303	305	301	302	0.2	0.9	-0.5						
70			332	352	354	350	353	-0.2	0.3	-0.8						
80			376	400	402	398	403	-0.8	-0.3	-1.3						
90			428	456	458	454	454	0.5	1.0	0.1						
100			469	499	501	497	504	-1.0	-0.6	-1.4	-0.1	3.2	-2.8	2.2	-1.5	-0.1
5	4	09/08/2002	24	24	26	22	24	2.1	10.6	-6.4						
10	Trial 2, probe 1		47	47	49	45	47	0.0	4.3	-4.3						
20	2 to 2-1/2 min		92	93	95	91	94	-1.1	1.1	-3.2						
30	between readings		136	139	141	137	141	-1.4	0.0	-2.8						
40			182	187	189	185	188	-0.5	0.5	-1.6						
50			227	235	237	233	235	0.0	0.9	-0.9						
60			274	284	286	282	282	0.7	1.4	0.0						
70			320	333	335	331	329	1.2	1.8	0.6						
80			359	375	377	373	376	-0.3	0.3	-0.8						
90			401	419	421	417	423	-0.9	-0.5	-1.4						
100			448	467	469	465	470	-0.6	-0.2	-1.1	-0.1	2.1	-1.4	1.2	-1.4	-0.2
5	6	09/08/2002	24	24	26	22	24	0.8	9.2	-7.6						
10	Trial 2, probe 2		47	47	49	45	48	-1.3	2.9	-5.5						
20	2 to 2-1/2 min		91	92	94	90	95	-3.4	-1.3	-5.5						
30	between readings		139	141	143	139	143	-1.3	0.1	-2.7						
40			187	191	193	189	190	0.3	1.4	-0.7						
50			232	238	240	236	238	0.0	0.8	-0.8						
60			271	281	283	279	286	-1.6	-0.9	-2.3						
70			320	333	335	331	333	-0.1	0.5	-0.7						
80			355	372	374	370	381	-2.3	-1.8	-2.8						
90			404	425	427	423	428	-0.8	-0.3	-1.3						
100			445	471	473	469	476	-1.1	-0.6	-1.5	-1.0	0.8	-3.4	0.3	-2.3	-0.8
5	11	11/09/2003	24	25	27	23	24	4.2	12.5	-4.2						
10	(avge of 2 sets)		48	49	51	47	48	2.1	6.3	-2.1						
20	Trial 3		94	97	99	95	96	1.0	3.1	-1.0						
30			139	143	145	141	144	-0.7	0.7	-2.1						
40	low --> high		186	192	194	190	192	0.0	1.0	-1.0						
50	& reverse		233	240	242	238	240	0.0	0.8	-0.8						
60			280	289	291	287	288	0.3	1.0	-0.3						
70			329	340	342	338	336	1.2	1.8	0.6						
80			375	388	390	386	384	1.0	1.6	0.5						
90			421	436	438	434	432	0.9	1.4	0.5						
100			470	487	489	485	480	1.5	1.9	1.0						
110																
120			564	584	586	582	576	1.4	1.7	1.0	1.1	4.2	-0.7	1.5	-0.7	0.6
5	18	05/09/2003	25	26	28	24	25	3.2	11.1	-4.8						
10	(avge of 2 sets)		49	50	52	48	50	-0.8	3.2	-4.8						
20	Trial 4		96	99	101	97	101	-1.8	0.2	-3.8						
30			144	149	151	147	151	-1.5	-0.1	-2.8						
40	low --> high		192	201	203	199	202	-0.3	0.7	-1.3						
50	low --> high		240	252	254	250	252	0.0	0.8	-0.8						
60			288	303	305	301	302	0.2	0.9	-0.5						
70			329	348	350	346	353	-1.4	-0.8	-1.9						
80			380	403	405	401	403	0.0	0.4	-0.5						
90			420	449	451	447	454	-1.0	-0.6	-1.5						
100			470	503	505	501	504	-0.2	0.2	-0.6						
110																
120			553	598	600	596	605	-1.1	-0.8	-1.5						
130																
140			640	697	699	695	706	-1.2	-0.9	-1.5	-0.5	3.2	-1.8	0.2	-1.5	-0.7
50	D13(high)	05/09/2003	20	21	23	19	20	5.0	15.0	-5.0						
100	(avge of 2 sets)		38	40	42	38	40	0.0	5.0	-5.0						
150	Trial 5		57	60	62	58	60	0.0	3.3	-3.3						
200			78	82	84	80	80	2.5	5.0	0.0						
250	low --> high		94	100	102	98	100	0.0	2.0	-2.0						
300	& reverse		113	121	123	119	120	0.8	2.5	-0.8						
350			133	143	145	141	140	2.1	3.6	0.7						
400			149	161	163	159	160	0.6	1.9	-0.6						
450			171	184	186	182	180	2.2	3.3	1.1						
500			191	206	208	204	200	3.0	4.0	2.0	1.6	5.0	0.0	3.0	0.0	1.3
50	D14(high)	05/09/2003	20	21	23	19	20	2.9	12.7	-6.9						
100	(avge of 2 sets)		38	40	42	38	41	-2.0	2.9	-6.9						
150	Trial 6		58	61	63	59	61	-0.3	2.9	-3.6						
200			78	83	85	81	82	1.7	4.2	-0.7						
250	low --> high		96	102	104	100	102	0.0	2.0	-2.0						
300	& reverse		116	123	125	121	122	0.5	2.1	-1.1						
350			134	143	145	141	143	0.1	1.5	-1.3						
400			155	165	167	163	163	1.1	2.3	-0.1						
450			173	185	187	183	184	0.8	1.9	-0.3						
500			193	205	207	203	204	0.5	1.5	-0.5	0.5	2.9	-2.0	1.7	-2.0	0.3
											Overall	Avge	max	min	max	min	Avge
										Variation from Proportionality:	0.2	5.5	-6.3	3.0	-2.3	0.1
										St. Dev:	1.8	1.5	1.9	1.0	0.7	1.1

LOW DOSE PROBES			
Dose Set cGy	Avge of Shifts +/- 2 mV	Dose set as fraction of 50 cGy dose	If prop'l
5	25	0.1	25
10	49	0.2	49
20	96	0.4	98
30	146	0.6	148
40	198	0.8	197
50	246	1	246
60	296	1.2	295
70	345	1.4	344
80	392	1.6	394
90	441	1.8	443
100	489	2	492
110			
120	591	2.4	590
130			

HIGH DOSE PROBES			
Dose Set cGy	Avge of Shifts +/- 2 mV	Dose set as fraction of 250 cGy dose	If prop'l
50	21	0.2	21
100	40	0.4	40
150	61	0.6	61
200	83	0.8	83
250	101	1.0	101
300	122	1.2	122
350	143	1.4	143
400	163	1.6	163
450	185	1.8	185
500	206	2.0	206

Avge variation high dose probes:	**1.1 +/- 0.8%**
Avge variation low dose probes:	**-0.1 +/- 0.7%**
OVERALL AVERAGE VARIATION:	**0.2%**
Overall St. Dev:	**1.8%**

DRIFT RESULTS

APPENDIX E

Drift up to 5 min following irradiation Probes 1, 5, D12 (low) and D15 (low)

Single 4 MV irradiations

Divided into Threshold Shift < 20 Gy and >20 Gy

		Time after irradiation:	0 - 30 s	30 - 60 s	60 - 90 s	90 - 120 s	2 - 3 min	3 - 4 min	4 - 5 min
Date	Dose (MU)	Accum. Dose (Gy)	Probe #	Increase during period (mV)						
6/11/03	100	1.9	D15 (low)	4	7	3	2	3	3	3
6/11/03	100	2.9	D15 (low)	8	6	4	2	4	3	3
6/11/03	100	3.9	D15 (low)	8	7	3	3	3	4	3
6/11/03	100	4.9	D15 (low)	8	6	4	3	3	4	3
10/11/03	100	8.5	D15 (low)	9	6	3	4	3	4	4
	Avge for low acc dose:			7.4	6.4	3.4	2.8	3.2	3.6	3.2
20-22/10/03	100	27.7	D12 (low)	5	3	4	2	3	2	0
15/7/02	100	37.7	5	7	8	2	2	1	2	2
6/11/03	100	32.8	D12 (low)	11	6	2	2	2	2	2
10/11/03	100	35.0	D12 (low)	9	7	2	2	1	1	1
10/11/03	100	36.5	D12 (low)	14	8	4	1	2	2	2
10/11/03	100	37.5	D12 (low)	13	7	2	1	1	1	1
	Avge for high acc dose			9.8	6.5	2.7	1.7	1.7	1.7	1.3
			Max.	14.0	8.0	4.0	4.0	4.0	4.0	4.0
			Min.	4.0	3.0	2.0	1.0	1.0	1.0	0.0
			St Dev	3.0	1.4	0.9	0.9	1.0	1.1	1.2
			AVGE :	8.7	6.5	3.0	2.2	2.4	2.5	2.2
6/11/03	50	1.4	D15 (low)	7	4	1	2	1	2	1
10/11/03	50	7.0	D15 (low)	8	3	2	1	1	1	1
10/11/03	50	7.5	D15 (low)	4	4	1	1	2	1	2
10/11/03	50	8.0	D15 (low)	6	3	2	2	2	2	2
	Avge for low acc dose:			6.3	3.5	1.5	1.5	1.5	1.5	1.5
6/11/03	50	30.8	D12 (low)	9	3	1	1	1	1	1
6/11/03	50	31.3	D12 (low)	7	4	1	1	3	1	1
6/11/03	50	31.8	D12 (low)	4	4	2	2	0	0	2
6/11/03	50	32.3	D12 (low)	11	5	1	2	1	0	0
10/11/03	50	35.0	D12 (low)	13	4	3	1	0	0	0
	Avge for high acc dose			8.8	4.0	1.6	1.4	1.0	0.4	0.8
			Max.	13.0	5.0	3.0	2.0	3.0	2.0	2.0
			Min.	4.0	3.0	1.0	1.0	0.0	0.0	0.0
			St Dev	3.0	0.7	0.7	0.5	1.0	0.8	0.8
			AVGE:	7.7	3.8	1.6	1.4	1.2	0.9	1.1
6/11/03	30	0.2	D15 (low)	5	2	2	0	1	0	1
6/11/03	30	0.5	D15 (low)	5	2	1	1	0	2	0
6/11/03	30	0.8	D15 (low)	5	2	1	1	2	0	1
6/11/03	30	1.1	D15 (low)	2	3	1	1	1	1	1
10/11/03	30	6.7	D15 (low)	6	2	2	0	1	0	0
	Avge for low acc dose:			4.6	2.2	1.4	0.6	1.0	0.6	0.6
6/11/03	30	30.5	D12 (low)	12	3	1	1	0	0	0
10/11/03	30	33.8	D12 (low)	1	6	1	2	0	1	0
10/11/03	30	34.1	D12 (low)	6	5	0	2	0	0	3
10/11/03	30	34.4	D12 (low)	6	2	1	1	1	2	2
10/11/03	30	34.7	D12 (low)	12	5	1	0	1	2	0
	Avge for high acc dose			7.4	4.2	0.8	1.2	0.4	1.0	1.0
			Max.	12.0	6.0	2.0	2.0	2.0	2.0	3.0
			Min.	1.0	2.0	0.0	0.0	0.0	0.0	0.0
			St Dev	3.6	1.5	0.6	0.7	0.7	0.9	1.0
			AVGE:	6.0	3.2	1.1	0.9	0.7	0.8	0.8
6/11/03	20	0.0	D15 (low)	2	2	0	0	1	0	0
10/11/03	20	5.9	D15 (low)	7	3	0	0	0	0	0
10/11/03	20	6.1	D15 (low)	5	2	0	1	0	0	0
10/11/03	20	6.3	D15 (low)	4	2	1	0	0	1	0
10/11/03	20	6.5	D15 (low)	4	1	0	0	1	1	0
	Avge for low acc dose:			4.4	2.0	0.2	0.2	0.4	0.4	0.0
26/6/02	20	24.7	1	3	6	1	0	0	3	0
6/11/03	20	29.7	D12 (low)	10	5	0	1	1	1	1
6/11/03	20	29.9	D12 (low)	5	4	0	0	2	0	1
6/11/03	20	30.1	D12 (low)	11	4	2	1	0	0	1
6/11/03	20	30.3	D12 (low)	11	5	0	0	0	0	0
	Avge for high acc dose			8.0	4.8	0.6	0.4	0.6	0.8	0.6
			Max.	11.0	6.0	2.0	1.0	2.0	3.0	1.0
			Min.	2.0	1.0	0.0	0.0	0.0	0.0	0.0
			St Dev	3.4	1.6	0.7	0.5	0.7	1.0	0.5
			AVGE:	6.2	3.4	0.4	0.3	0.5	0.6	0.3

REFERENCES

[1] P. Scalchi and P. Francescon, "Calibration of a MOSFET detection system for 6MV *in vivo* dosimetry," Int. J. Radiat. Oncol. Biol. Phys. **40**(4), 987-993 (1998).

[2] M. Essers and B.J. Mijnheer, "*In vivo* dosimetry during external photon beam radiotherapy," Int. J. Radiat. Oncol. Biol. Phys. **43**(2), 245-259 (1999).

[3] J.H. Lanson, M. Essers, G.J. Meijer, A.W.H. Minken, G.J. Uiterwaal and B.J. Mijnheer, "In vivo dosimetry during conformal radiotherapy – Requirements for and findings of a routine procedure," Radiother. Oncol. **52**(1), 51-59 (1999).

[4] Th. Loncol, J.L. Greffe, S. Vynckier and P. Scalliet, "Entrance and exit dose measurements with semiconductors and thermoluminescent dosemeters: a comparison of methods and in vivo results," Radiother. Oncol. **41**, 179-187 (1996).

[5] P. Francescon, S. Cora, C. Cavedon, P. Scalchi, S. Reccanello and F. Colombo, "Use of a new type of radiochromic film, a new parallel-plate micro-chamber, MOSFETs and TLD 800 microcubes in the dosimetry of small beams," Med. Phys. **25**(4), 503-511 (1998).

[6] G.I. Kaplan, A.B. Rosenfeld, B.J. Allen, J.T. Booth, M.G. Carolan and A. Holmes-Siedle, "Improved spatial resolution by MOSFET dosimetry of an x-ray microbeam," Med. Phys. **27**(1), 239-244 (2000).

[7] D.J. Peet and M.D. Pryor, "Evaluation of a MOSFET radiation sensor for the measurement of entrance surface dose in diagnostic radiology," Br. J. Radiol. **72,** 562-568 (1999).

[8] G.F. Derbenwick and H.H. Sander, "CMOS hardness prediction for low-dose-rate environments," IEEE Trans. Nucl. Sci. NS-**24**(6), 2244-2247 (1977).

[9] P. Scalchi, P. Francescon and G. Terrin, "MOSFET dosimetry for 6MV radiotherapy beams," Presentation, ESTRO, Nice 1997.

[10] T. Cheung, P.K.N. Yu and M.J. Butson, "Low-dose measurement with a MOSFET in high-energy radiotherapy applications," Radiat. Meas. ***39,*** 91-94 (2005).

[11] D.J. Gladstone, X.Q. Lu, J.L. Humm, H.F. Bowman and L.M. Chin, "A miniature MOSFET radiation dosimeter probe," Med. Phys. **21**(11), 1721-1728 (1994).

[12] P.S. Winokur and H.E. Boesch Jr, "Annealing of MOS capacitors with implications for test procedures to determine radiation hardness," IEEE Trans. Nucl. Sci. NS-**28**(6), 4088-4094 (1981).

[13] P.S. Winokur, K.G. Kerris and L. Harper, "Predicting CMOS inverter response in nuclear and space environments," IEEE Trans. Nucl. Sci. NS-**30**(6), 4326-4332 (1983).

[14] J.R. Schwank, P.S. Winokur, P.J. McWhorter, F.W. Sexton, P.V. Dressendorfer and D.C. Turpin, "Physical mechanisms contributing to device rebound," IEEE Trans. Nucl. Sci. NS-**31**(6), 1434-1438 (1984).

[15] W.J. Dennehy, G.J. Brucker and A.G. Holmes-Siedle, "A radiation-induced instability in silicon MOS transistors," IEEE Trans. Nucl. Sci. NS-**13**(6), 273-281 (1966).

[16] E.H. Nicollian and J.R. Brews, "MOS (Metal Oxide Semiconductor) Physics and Technology*,"* John Wiley & Sons (1982).

[17] B. Van Zeghbroeck, "Principles of Semiconductor Devices" Ch 7 MOS Field Effect Transistors, University of Colorado at Boulder, USA, on **http://ecee.colorado.edu/~bart/book/**, accessed 2007.

[18] H.E. Boesch Jr. and J.M. McGarrity, , "Charge yield and dose effects in MOS capacitors at 80K," IEEE Trans. Nucl. Sci. NS-**23**(6), 1520-1525 (1976).

[19] J. Benedetto and H. Boesch Jr, "The Relationship between Co-60 and 10 keV X-ray damage in MOS devices," IEEE Trans. Nucl. Sci. NS-**33**(6), 1318 (1986).

[20] W.J. Dennehy, A.G. Holmes-Siedle and K.H. Zaininger, "Process techniques and radiation effects in metal-insulator semiconductor structures," IEEE Trans. Nucl. Sci. NS-**14**(6), 276-283 (1967).

[21] J.E. Whitefield, H.D. Southward and R.J. Maier, "Total dose effects on surface state density, carrier concentration and mobility in MOS layers," IEEE Trans. Nucl. Sci. NS-**23** 6), 1549-1551 1976.

[22] R. Freeman and A. Holmes-Siedle, "A simple model for predicting radiation effects in MOS devices," IEEE Trans. Nucl. Sci. NS-**25**(6), 1216-1225 (1978).

[23 A. Holmes-Siedle, "The space-charge dosimeter," Nucl. Instrum. Meth. **121,** 169-179 (1974).

[24] L. Adams and A. Holmes-Siedle, "The development of an MOS dosimetry unit for use in space," IEEE Trans. Nucl. Sci. NS-**25**(6), 1607-1612 (1978).

[25] K.Y. Quach, J. Morales, M.J. Butson, A.B. Rosenfeld and P.E. Metcalfe, "Measurement of radiotherapy x-ray skin dose on a chest wall phantom," Med. Phys. **27**(7), 1676-80 (2000).

[26] S.L. Dong, T.C. Chu, J.S. Lee, G.Y. Lan, T.H. Wu, Y.H. Yeh and J.J. Hwang, "Estimation of mean-glandular dose from monitoring breast entrance skin air kerma using a high sensitivity metal-oxide-semiconductor field effect transister (MOSFET) dosimeter system in mammography," Appl. Radiat. Isotopes **57,** 791-799 (2002).

[27] E. Bräuer-Krisch, A. Bravin, M. Lerch, A. Rosenfeld, J. Stepanek, M. Di Michiel and J.A. Laissue, "MOSFET dosimetry for microbeam radiation therapy at the European Synchrotron Radiation Facility," Med. Phys. **30**(4), 583-589 (2003).

[28] A.B. Rosenfeld, G.I. Kaplan, T. Kron, B.J.K. Allen, A. Dilmanian, I. Orion, B. Ren, M.L.F. Lerch and A. Holmes-Siedle, "MOSFET dosimetry of an x-ray microbeam," IEEE Trans. Nucl. Sci. NS-**46**(6), 1774-1780 (1999).

[29] C.G. Rowbottom and D.A. Jaffray, "Characteristics and performance of a micro-MOSFET: An "imageable" dosimeter for image-guided radiotherapy," Med. Phys. **31**(3), 609-615 (2004).

[30] A.O. Jones and M.T. Kleiman, "Patient setup and verification for intensity-modulated radiation therapy (IMRT)," Med. Dosim. **28**(3), 175-183 (2003).

[31] C.F. Chuang, L.J. Verhey and P. Xia, "Investigation of the use of MOSFET for clinical IMRT dosimetric verification," Med. Phys. **29**(6), 1109-1115 (2002).

[32] H. Scher and M. Lax, "Stochastic transport in a disordered solid. I. Theory," Phys. Rev. B **7**(10), 4491-4502 (1973).

[33] F.E.N.G. Zhe Chuan (Editor), "Semiconductor Interfaces, Microstructures and Devices".Ch 10 pp 230, IOP Publishing (1993).

[34] M.L. Reed and J.D. Plummer, "Chemistry of Si-SiO_2 interface trap annealing," J. Appl. Phys. **63**(12), 5776-5793 (1988).

[35] A. Kalnitsky, J.P. Ellul, E.H. Poindexter, P.J. Caplan, R.A. Lux and A.R. Boothroyd, "Rechargeable E' centres in silicon-implanted SiO_2 films," J. Appl. Phys. **67**(12), 7359-7367 (1990).

[36] G.J. Gerardi, E.H. Poindexter, P.J. Caplan and N.M. Johnson, "Interface traps and Pb centres in oxidised (100) silicon wafers," Appl. Phys. Lett. **49**(6), 348-350 (1986).

[37] M.E. Zvanut, F.J. Feigl, W.B. Fowler, J.K. Rudra, P.J. Caplan, E.H. Poindexter and J.D. Zook, "Rechargeable E' centres in sputter-deposited silicon dioxide films," Appl. Phys. Lett. **54**(21), 2118-2220 (1989).

[38] M. Pejović, A. Jakšić and G. Ristić, "The behaviour of radiation-induced gate-oxide defects in MOSFETs during annealing at 140^{o} C," J. Non-crystalline solids **240,** 182-192 (1998).

[39] W.D. Zhang, J.F. Zhang, M. Lalor, D. Burton, G. Groeseneken and R. Degraeve, "On the mechanism of electron trap generation in gate oxides," Microelectronic Engineering **59**, 89-94 (2001).

[40] D.M. Fleetwood, P.S. Winokur, R.A. Reber Jnr, T.L. Meisenheimer, J.R. Schwank, M.R. Shaneyfelt and L.C. Riewe, "Effects of oxide traps, interface traps and "border traps" on metal-oxide-semiconductor devices," J. Appl. Phys. **73**(10), 5058-5074 (1993).

[41] M. Grattarola and G. Massobrio, "Bioelectronics Handbook – MOSFETs, Biosensors and Neurons," McGraw-Hill (1998).

[42] C. Ehringfeld, S. Schmidt, K. Poljanc, C. Kirisits, H. Aiginger and D. Georg, "Application of commercial MOSFET detectors for *in vivo* dosimetry in the therapeutic x-ray range from 80 kV to 250 kV," Phys. Med. Biol. **50,** 289-303 (2005).

[43] Thomson & Nielsen Electronics Ltd, Technical Note No. 1, "Dose reproducibility assessment for the Thomson and Nielsen electronic dosimetry systems" (1995).

[44] Thomson & Nielsen Electronics Ltd, Technical Note No. 3, "Reproducibility using Model TN-RD-19 high sensitivity bias supply" (1995).

[45] S.M. Sze, "Physics of Semiconductor Devices," John Wiley & Sons (1981).

[46] M. Soubra, J. Cygler and G. Mackay, "Evaluation of a dual bias dual metal-oxide-semiconductor field effect transistor detector as radiation dosimeter," Med. Phys. **21**(4), 567-572 (1994).

[47] T. Kron, L. Duggan, T. Smith, A. Rosenfeld, M. Butson, G. Kaplan, S. Howlett and K. Hyodo, "Dose response of various radiation detectors to synchotron radiation," Phys. Med. Biol. **43**(11), 3235-3259 (1988).

[48] P.S. Winokur and H.E. Boesch Jr, "Interface state generation in radiation-hard oxides," IEEE Trans. Nucl. Sci. NS-**27**(6), 1647-1657 (1980).

[49] P.G. Litovchenko, L.I. Barabash, A.B. Rosenfeld, V.I. Khivrich, O.S. Zinets, V.I. Kuts, I.A. Marusan, V.I. Petrov, G.F. Sluchenkov, G.N. Koval, V.I. Fominych, L.F. Belovodskiy, A.I. Dumik and V. Ya. Kiblik, "MOS Structure for emergency gamma and proton dosimetry," Radiat. Prot. Dosim. **33**, 179-182 (1990).

[50] C.R.M. Grovenor, "Microelectronics Materials," Adam Hilger, Briston and Philadelphia (1989).

[51] H.E. Boesch Jr and T.L. Taylor, "Charge and interface state generation in field oxides," IEEE Trans. Nucl. Sci. NS-**31**(6), 1273-1279 (1984).

[52] G. Ensell, A. Holmes-Siedle and L. Adams, "Thick oxide p-MOSFET dosimeters for high energy radiation," Nucl. Instr. Meth. Phys. Res. A **269,** 655-658 (1988).

[53] D.B. Brown and N.S. Saks, "Time dependence of radiation-induced interface trap formation in metal-oxide-semiconductor devices as a function of oxide thickness and applied field," J. Appl. Phys. **70**(7), 3734-3747 (1991).

[54] P. Halvorsen and S. Parker, "Mixed-beam 3D conformal therapy: Dosimetric verification," Poster Paper, AAPM 1999

[55] S.L. Dong, T.C. Chu, G.Y. Lan, T.H. Wu, Y.C. Lin and J.S. Lee, "Characterisation of high-sensitivity metal-oxide-semiconductor dosimeters system and LiF:Mg, Cu, P thermoluminescence dosimeters for use in diagnostic radiology," Appl. Radiat. Isotopes **57,** 883-891 (2002).

[56] T. Cheung, M.J. Butson and P.K.N. Yu, "MOSFET dosimetry *in-vivo* at superficial and orthovoltage x-ray energies," Australas. Phys. Eng. Sci. Med. **26**(2), 82-84 (2003).

[57] Thomson & Nielsen Electronics Ltd, Technical Note No. 4, "Introduction to the MOSFET dosimeter" (1996).

[58] C.R. Edwards, S. Green, J.E. Palethorpe and P.J. Mountford, "The response of a MOSFET, p-type semiconductor and LiF TLD to quasi-monoenergetic X-rays," Phys. Med. Biol. **42**(12), 2383-2391 1997).

[59] T. Cheung, M.J. Butson and P.K.N. Yu, "Effects of temperature variation on MOSFET dosimetry," Phys. Med. Biol. **49,** N191-N196 (2004).

[60] H.E. Boesch Jr, F.B. McLean, J.M. Benedetto and J.M. McGarrity, "Saturation of threshold voltage shift in MOSFETs at high total dose," IEEE Trans. Nucl. Sci. NS-**33**(6), 1191-1197 (1986).

[61] R.C. Hughes, D. Huffman, J.V. Snelling, T.E. Zipperian, A.J. Ricco, C.A. Kelsey, "Miniature radiation dosemeter for in vivo radiation measurements," Int. J. Radiat. Oncol. Biol. Phys. **14,** 963-967 (1988).

[62] R. Ramani, S. Russell and P. O'Brien, "Clinical dosimetry using MOSFETs," Int. J. Radiat. Oncol. Biol. Phys. **37**(4), 959-964 (1997).

[63] I. Thomson, "MOSFETs in medical physics – Applications in IMRT, brachytherapy and IORT," Presentation, AIFM Meeting, Italy, 2002

[64] C.F. Chuang, L.J. Verhey and P. Xia, "Investigation of the use of MOSFET for clinical IMRT dosimetric verification," Med. Phys. **29**(6), 1109-1115 (2002).

[65] M.J. Butson, A. Rozenfeld, J.N. Mathur, M. Carolan, T.P.Y. Wong and P.E. Metcalfe, "A new radiotherapy surface dose detector: The MOSFET," Med. Phys. **23**(5), 655-658 (1996).

[66] A.B. Rosenfeld, "MOSFET dosimetry on modern radiation oncology modalities," Radiat. Prot. Dosim. **101**(1-4), 393-398 (2002).

[67] C. Sharland and D. Smith, "Applications of MOS dosimeters," Presentation, IEE Colloquium on Modern Methods of Detecting and Measuring Ionising Radiations, London, Nov 6 1992.

[68] G. Trujillo, "Evaluation of the TN-RD-50 patient dosimetry system MOSFET-based," Paper (unpublished) August 1998.

[69] R. Ramaseshan, T. Lam, G. Perkins, R. Heaton and M. Islam, "In vivo dosimetry for IMRT using MOSET dosimeter," Poster paper and presentation, AAPM 2002.

[70] D.J. Gladstone and L.M. Chin, "Automated data collection and analysis system for MOSFET radiation detectors," Med. Phys. **18**(3), 542-548 (1991).

[71] D.A. Neamen, "Modeling of MOS radiation and post irradiation effects," IEEE Trans. Nucl. Sci. NS-**31**(6), 1439-1444 (1984).

[72] D.M. Fleetwood, "Long-term annealing study of midgap interface-trap charge neutrality," Appl. Phys. Lett. **60**(23), 2883-2885 (1992).

[73] A. Holmes-Siedle and L. Adams, "The mechanisms of small instabilities in irradiated MOS transistors," IEEE Trans. Nucl. Sci. NS-**30**(6), 4135-4140 (1983).

[74] M.V. Fischetti, R. Gastaldi, F. Maggioni and A. Modelli, "Slow and fast states induced by hot electrons at Si-SiO_2 interface," J. Appl. Phys. **53**(4), 3136-3144 (1982).

[75] F.B. McLean, "A framework for understanding radiation-induced interface states in SiO_2 MOS structures," IEEE Trans. Nucl. Sci. NS-**27**(6), 1651-1657 (1980).

[76] M. Aslam, "Electron self-trapping in SiO_2," J. Appl. Phys. **62**(1), 159-162 (1987).

[77] Z. Savić, B. Radjenović and M. Pejović, "The contribution of border traps to the threshold voltage shift in pMOS dosimetric transistors," IEEE Trans. Nucl. Sci. NS-**42**(4), 1445-1453 (1995).

[78] M.W. Bower and D.E. Hintenlang, "The characterization of a commercial MOSFET dosimeter system for use in diagnostic x-ray," Health Phys. **75**, 197-204 (1998).

[79] R.J. Meiler and M.B. Podgorsak, "Characterisation of the response of commercial diode detectors used for *in vivo* dosimetry," Med. Dosim. **22**(1), 31-37 (1997).

[80] G. Rikner and E. Grusell, “Patient dose measurements in photon fields by means of silicon semiconductor detectors,” Med. Phys. **14**(5), 870-873 (1987).

[81] A.B. Rosenfeld, M.G. Carolan, G.I. Kaplan, B.J. Allen and V.I. Khivrich, “MOSFET dosimeters: The role of encapsulation on dosimetric characteristics in mixed gamma-neutron and megavoltage x-ray fields,” IEEE Trans. Nucl. Sci. NS-**42**(6), 1870-1877 (1995).

[82] A. Wu, A. Maitz, K. Shortt, G. Mackay, I. Thomson, M. Johnson, J. Washick, L. Lunsford and S. Kalnicki, “Performance of a new dosimetry system with MOSFET sensor for radiosurgery applications,” Med. Phys. **21**(6), 368 (1994).

[83] P. Halvorsen and S. Parker, “Dosimetric evaluation of a new design MOSFET detector,” Poster paper, AAPM 1999.

[84] J.N. Roshau and D.E. Hintenlang, “Characterisation of the angular response of an “isotropic” MOSFET dosimeter,” Health Phys. **84**(3), 376 (2003).

[85] A.B. Rosenfeld, M.L.F. Lerch, T. Kron, E. Brauer-Krisch, A. Bravin, A. Holmes-Siedle and B.J. Allen, “Feasibility study of on-line, high-spatial-resolution MOSFET dosimetry in static and pulsed x-ray radiation fields,” IEEE Trans. Nucl. Sci. NS-**48**(6), 2061-2068 (2001).

[86] “Clinical MOSFET semiconductor dosimetry system”, Instruction Manual, Centre for Medical Radiation Physics, University of Wollongong, Australia 2001

[87] C.A. Betty, K.G. Girija and R. Lal, “Relaxation of operational amplifier parameters after pulsed electron beam irradiation,” Microelectronics Reliability **39,** 1485-1495 (1999).

[88] M. Millar, J. Cramb, R. Das, T. Ackerly, G. Brown and D. Webb, “Section 8.6. Position Paper – *Recommendations for the Safe Use of External Beams and Sealed Brachytherapy Sources in Radiation Oncology,*” Australas. Phys. Eng. Sci. Med. **20**(3), 16 (1997).

[89] A. Holmes-Siedle and L. Adams, “Handbook of Radiation Effects”, 2nd edn, Oxford University Press, pp 87, 89 and 139 (2002).

[90] J.A. Felix, J.R. Schwank, C.R. Cirba, R.D. Schrimpf, M.R. Shaneyfelt, D.M. Fleetwood and P.E. Dodd, “Influence of total dose radiation on the electrical characteristics of SOI MOSFETs,” Microelectronic Engineering **72,** 332-341 (2004).

[ICRU50] “Prescribing, Recording and Reporting Photon Beam Therapy,“ Report 50 of International Commission on Radiation Units and Measurements, Washington, 1987